ABSTRACT

Fried, Andrew. Rheological and Compositional Characterization of the Impacts of Recycling Agents and Extenders on Recycled Asphalt Blends. (Under the direction of Dr. Cassie Castorena)

Recycling agents (RAs) and extenders have recently been a topic of growing interest in the asphalt pavement industry. These products provide a potential method to increase the amount of recycled materials, including reclaimed asphalt pavement (RAP) and recycled asphalt shingles (RAS), used in new asphalt mixtures. The use of recycled asphalt materials decreases the amount of virgin binder required for creating new roadways. A primary goal of increasing the amount of recycled material is ensuring that the performance of the pavement is not negatively impacted. The overarching goal of this dissertation is to advance the understanding of RAs and extenders on the rheology and composition of recycled binder blends, by building on the existing body of literature through the following objectives; (1) Evaluate RA and extender dosage selection procedures to restore the intended high-temperature climatic grade of binder blends, (2) Develop practical methods to construct asphalt binder master curves and calculate master curve model coefficients that are amenable for specification, (3) Evaluate the effects of RAs and extenders on binder blends under dosage selection procedures to restore the high- and low-temperature performance grade of binder blends according to available rheological indicators of durability, (4) Identify correlations between alternative rheological indicators of durability and between the results of a given parameter at different long-term age levels, (5) Classify a set of RAs and extenders as softeners, replenishers, or emulsifiers based on their impacts on the rheology and composition of recycled binder blends.

The universality of slopes for additive dosage selection to restore the high-temperature grade of the blended binder system were evaluated. The results indicate that different additive types yield different slopes of the blended system high-temperature grade versus additive content. The results also show that uncertainty should be accounted for when establishing a dosage selection procedure to ensure that the blended binder grade does not fall below the desired value. Two alternative approaches were identified to account for the uncertainty: (1) dosage selection according to the lower bound of a confidence interval or (2) target a higher continuous high-temperature than the minimum accepted based on measured uncertainty. The rutting resistance of mixtures prepared using additive dosages intended to restore the high-temperature grade all passed recommended Hamburg Wheel-Track criteria.

To properly evaluate the changes that each additive had on a binder's rheology, it was important to establish a procedure that provided reproducible, consistent master curves. A method for constructing master curves was created, named pairwise interpolation, to determine the time-temperature shift factors using a free shifting approach. The results for this method of construction were contrasted with master curves constructed using the Gordon-Shaw method and findings showcased that both methods provided very similar results while the pairwise interpolation method is more easily implemented without sophisticated software. Practical methods to calculate the Christensen Anderson (CA) model parameters were compared. A method to calculate the model parameters using linear regression yielded acceptable model accuracy.

The master curves construction and model procedures were used to determine several rheological parameters and contrast the performance of recycled binder blends against 'control binders' that are those binders that would be specified for use with mixtures that do not contain RAP. Rheological parameters calculated from standard performance grading tests were also considered. The ability of softer virgin binders, RAs, and extenders to restore the rheology of RAP binders to that of control binders were all evaluated. Two procedures for RA dosage selection are examined: 1) dose to restore the intended high-temperature grade and 2) dose to restore the intended low-temperature grade. A broad range of point parameters and rheological parameters that measure the balance of relaxation and stiffness characteristics were examined at two long-term age levels. The results of recycled binder blends were compared to the control virgin binders statistically using Dunnett's test. Using softer virgin binders generally resulted in blended binder performance-graded properties that were similar to or better than the control. However, these softer binder systems often exhibited other rheological properties that were inferior to the control. The rheological characteristics of the RA blends varied with the RA type and dosage. RAs derived from triglycerides and fatty acids and tall oils generally yielded more favorable rheological characteristics than those derived from aromatic extracts. In addition, a vacuum gas oil (VGO) extender achieved similar blend rheological characteristics to RAs but extenders containing re-refined engine oil bottoms (REOB) generally yielded a poor balance of stiffness and relaxation characteristics. Rheological balance parameters were generally weakly correlated, suggesting they provide unique insight regarding the rheological behavior of binders.

Based on the rheological outcomes, the triglyceride and fatty acid and the vacuum gas oil extender were identified to emulsify or replenish recycled binder blends whereas extenders containing REOB were found to only soften and not restore rheological balance between stiffness and relaxation properties. Compositional analysis using X-ray Fluorescence (XRF), Saturates, Aromatics, Resins, Asphaltenes (SARA), and Fourier Transform Infrared spectroscopy (FTIR) was used to further classify additives based on their mechanism for modifying rheology. Each method provided unique information to classify each additive as an emulsifier, softener, or replenisher. Triglyceride and fatty acid additives increase the resins content of recycled binder blends due to including polar oxygen-containing functional groups. Resins peptize asphaltenes and therefore, triglyceride and fatty acid additives function as emulsifiers. The vacuum gas oil extender evaluated increased the aromatics content of recycled binder blends and did not exhibit clear evidence of oxygen-containing chemical functional groups in FTIR. Consequently, VGO acts a replenisher, replacing aromatics lost to oxidation in the RAP. The extenders containing REOB increased the saturates content, decreased the colloidal stability of recycled binder blends, and contained heavy metals, which led them to function as softeners.

Rheological and Compositional Characterization of the Impacts of Recycling Agents and Extenders on Recycled Asphalt Blends

By
Andrew Fried

A proposal for a dissertation submitted to the Graduate Faculty of North Carolina State University

Civil Engineering

Raleigh, North Carolina
2023

Committee Members:

Cassie Castorena, Professor Chair of Advisory Committee	Shane Underwood, Professor
Y. Richard Kim, Professor	Lilian Hsiao, Associate Professor

BIOGRAPHY

Andrew Joseph Fried was born in Charlotte, North Carolina and grew up in Concord, North Carolina. He moved to Raleigh when he decided to go to North Carolina State University for Engineering. During the course of his undergraduate studies, he began working the materials laboratory under Dr. Cassie Castorena. While working in materials laboratory he assisted with projects in both transportation materials and geotechnical engineering. This is how he became involved in transportation materials. In December 2016 he finished his B.S. in Civil Engineering with a concentration in structures. In January 2017 he began a master's degree in the Civil Engineering department at NCSU. During his time working on his master's project, he gained experience coordinating trips out to the field with fellow graduate students and NCDOT. The project he worked on was concerning the effect of crack sealant on skid resistance in the wheel path. After two years of data collection and analysis he successfully defends his thesis titled "Impact of Crack Sealant on Pavement Skid Resistance" and received his master's in December 2018. Upon completion of this project, he decided to continue his academic career by working towards his PhD. Having remained at NCSU he worked on a several projects before shifting towards working on the recycling agent research project that would ultimately be the focus of his dissertation under the direction of Dr. Cassie Castorena.

ACKNOWLEDGMENTS

I would like to very plainly state I would not have reached this point without the support of countless people. I will do my best to name them all but am certain I will miss more than a few.

First, I have to thank my friends and my family. My parents have always taught me the value of education and having good people with you. My friends supported me and made sure I knew I always a team supporting me. These lessons and support have helped keep me on the path of higher education, even when some of the challenges seemed insurmountable. I could not have done any of this without your unconditional love and support.

Next I would like to extend my thanks NCDOT and VDOT. Their commitment to advancing research in the transportation field was instrumental in bringing this project to completion. The funding provided essential resources and allowed us to acquire material, additives, and testing that were necessary to explore new areas in the transportation field. They were also responsible for providing testing of samples using the BBR and XRF. Thank you for your support. I would also like to thank MTE for testing SARA samples.

I also cannot emphasis the importance of having a group of supportive people working alongside of you. Jaime Precadio and Saqib Gulzar. Your assistance with the numerous experiments, paper writing, asphalt blending, and overall dedication to the project always kept me motivated and with a goal on the horizon. You helped me make all the blends, test all the materials, and we ran the DSR 24/7 for I can't even remember how long. I will miss seeing you both in the lab and the late-night calls about where to find specific cans of binder. Dr. Haritha Malladi, Dr. Jing Ding, Dr. Boris Goenaga, Dr. Nooralhuda Saleh, Dr. Mayzan Isied, Dr. Alan Zeng, Dr. Douglas Mucelin, Dr. Nithin Sudarsanan, Dr. Narges Matini, Caro Carolina, Gabriel Duarte, Rafaella Fnseca da Costa, Kazuo Kuchiishi, Gabriel Xue, Deepika Karanam, Elizabeth Braswell and Ernie Song. Seeing all of you in the office and the lab always working hard and always coming together to support each other with your projects and sharing your worldview has helped me widen mine. I will forever be grateful that I got to meet all of you and for your help, feedback, and friendship.

I would like to thank the various professors who have helped guide me throughout this journey showed me that there is always more to learn. My committee members, Dr. Richard Kim and Dr. Lilian Hsiao, your insight has helped guide my dissertation to be the best possible

version it could be. There were numerous times I reached out with questions and you were always supportive and quick to help me find my footing. Dr. Underwood your unwavering presence even when traveling abroad was felt throughout the entirety of this dissertation, as you offered guidance, assisted in resolving test related challenges, contributed new data, and consistently provided valuable resources and connections to help ensure this dissertation could be the best possible version.

Next, I would like to thank Dr. Ilker Boz, and Dr. Jhony Habbouche. Over the course of working with the Virginia materials there were many times I came to you with questions about analysis and the best path forward. You were always supportive and answered my questions honestly and were crucial for helping me better understand where to take this research.

Finally, I would like to thank my direct advisor Dr. Cassie Castorena. I can confidently say that without your endless guidance, support, and friendship I never would have made it this far. You introduced me to the wild world of asphalt back in 2015 and started me down the path of research that led me to where I am today. I am so proud of the research I have accomplished under your guidance and blessed to call you my friend.

TABLE OF CONTENTS

LIST OF FIGURES ..... **IX**

LIST OF TABLES ..... **XIII**

CHAPTER 1 INTRODUCTION **1**

1.1 BACKGROUND 1
1.2 OBJECTIVES 3
1.3 DISSERTATION OUTLINE 3
1.4 REFERENCES 7

CHAPTER 2 LITERATURE REVIEW **8**

2.1 INTRODUCTION 8
2.2 ASPHALT BINDER COMPOSITION AND COMPOSITION WITH OXIDATIVE AGING 8
2.2.1 SARA Fractions *8*
2.2.2 XRF *11*
2.2.3 MDSC *11*
2.2.4 Flocculation Titrimetry *12*
2.2.5 FTIR *15*
2.2.6 Molecular Size Distribution *15*
2.3 IMPACTS OF AGING ON AAHSTO M 30 PERFORMANCE GRADES 16
2.4 ADDITIVE TYPES 16
2.4.1 Recycling Agents *16*
2.4.2 Extenders *18*
2.4.3 Composition of Additives Reported in the Literature *21*
2.5 BINDER PERFORMANCE CHARACTERIZATION CONCERNS 22
2.5.1 Cracking Resistance *23*
2.5.2 Long-term Aging *30*
2.6 NCHRP 09-58 FINDINGS 31
2.6.1 Dosage Selection *31*
2.6.2 Cracking and Aging Potential Evaluation *34*
2.7 SUMMARY OF KNOWLEDGE GAPS AND APPLICATIONS 35
2.8 REFERENCES 37

CHAPTER 3 EVALUATION OF RECYCLING AGENT AND EXTENDER DOSAGE SELECTION PROCEDURES TO RESTORE THE HIGH-TEMPERATURE CLIMATIC GRADE **44**

3.1 INTRODUCTION 44

3.2 Methodology and Materials 46
3.2.1 Virgin and Recycled Binder Characterization 47
3.2.2 Additive Dosage Selection 49
3.2.3 Blend Verification at a Selected Dose 51
3.2.4 Hamburg Mixture Testing for Rutting Evaluation 51
3.3 Results 52
3.3.1 Virgin and Recycled Binder AASHTO M 320 High-Temperature Grades 52
3.3.2 Dosage Selection 53
3.3.3 Comparison of the Different Methods 59
3.3.4 Verification Testing Results 61
3.3.5 Hamburg Wheel-Track Test Results 64
3.4 Conclusions and Recommendations 65
3.5 Acknowledgements 66
3.6 References 67

CHAPTER 4 PRACTICAL METHODS TO CONSTRUCT ASPHALT BINDER MASTER CURVES AND CALCULATE CHRISTENSEN-ANDERSON MODEL PARAMETERS 68

4.1 Introduction 68
4.2 Materials and Test Procedures 70
4.3 Test Analysis 72
4.3.1 Data Screening 72
4.3.2 Master Curve Construction 73
4.3.3 Shift Factor Model 75
4.3.4 Master Curve Model 76
4.3.5 Evaluation of the Master Curve Model Results 80
4.4 Results 81
4.4.1 Evaluation of the Pairwise Interpolation Approach for Constructing Master Curves 81
4.4.2 Evaluation of the CA Model Results 82
4.4.3 Comparison of the CA Model Results from the Shift Factors Determined using Pairwise Interpolation versus Gordon and Shaw 93
4.5 Conclusions and Recommendations 97
4.6 Validation 98
4.7 Acknowledgements 99
4.8 References 100

CHAPTER 5 EVALUATION OF ALTERNATIVE APPROACHES TO RESTORE THE RHEOLOGY OF RECYCLED ASPHALT BINDERS 102

5.1 Introduction 102

5.2 OBJECTIVES 103
5.3 MATERIALS AND METHODS 104
5.3.1 Materials 104
5.3.2 Blend Preparation and Conditioning Procedures 105
5.3.3 Test Methods 107
5.3.4 Statistical Analysis 108
5.4 RESULTS 109
5.4.1 Comparisons of the Blends to the Controls 109
5.4.2 Evaluation of the Blends Corresponding to the Virginia Mixtures 112
5.5 CONCLUSIONS 121
5.6 ACKNOWLEDGEMENTS 122
REFERENCES 123
5.7 123

CHAPTER 6 EFFECTS OF RECYCLING AGENTS AND EXTENDERS ON THE COMPOSITION OF RECYCLED BINDER BLENDS 126

6.1 INTRODUCTION 126
6.2 BACKGROUND 126
6.3 OBJECTIVES 127
6.4 MATERIALS 127
6.5 EXPERIMENTAL METHODS 128
8.5.1. SARA 128
6.5.1 Fourier Transform Infrared (FTIR) 129
6.5.2 X-ray Fluorescence (XRF) 130
6.6 RESULTS 131
6.6.1 Identification of Softeners versus and Replenishers from the Rheological Results 131
6.6.2 SARA Results 132
6.6.3 FTIR Results 136
6.6.4 XRF Results 141
6.7 DISCUSSION 142
6.8 CONCLUSIONS 144
6.9 ACKNOWLEDGEMENTS 145
6.10 REFERENCES 146

CHAPTER 7 CONCLUSIONS AND RECOMMENDATIONS 147

7.1 CONCLUSIONS 147
7.1.1 Evaluation of Recycling Agent and Extender Dosage Selection Procedures to Restore the High-Temperature Climatic Grade 147

7.1.2 Practical Methods to Construct Asphalt Binder Master Curves and Calculate Christensen-Anderson Model Parameters *148*
7.1.3 Evaluation of Alternative Approaches to Restore the Rheology of Recycled Asphalt Binders *149*
7.1.4 Effects of Recycling Agents and Extenders on the Composition of Recycled Binder Blends *150*
7.2 RECOMMENDATIONS 151
APPENDIX A - SARA METHOD EVALUATION **154**
APPENDIX B – FITTING STATISTICS OF CHAPTER 5 BINDER MASTER CURVES **157**
APPENDIX C - BLACK SPACE GRAPHS **159**

List of Figures

Figure 1. Microstructure hypotheses for colloidal structure of asphalt binders 9
Figure 2. AFT analysis (Chandio et al. 2015)..... 13
Figure 3. Flocculation rate vs concentration (Chandio et al. 2015)..... 15
Figure 4. National survey results of laboratory tests used in practice to characterize the properties of asphalt binders modified by recycling agents (Epps Martin et al. 2020). 18
Figure 5. Relationship between RAP/RAS replacement and ΔT_c (Asphalt Institute 2019) 25
Figure 6. Rejuvenator dosage for aromatic extract (Epps-Martin et al. 2020) 33
Figure 7. Recycling agent dosages combined for tail oils, vegetable oils, and reacted bio-based oils (Epps-Martin et al. 2020) 33
Figure 8. (a) RAS lumps visible after blending in original state (b) No RAS lumps visible after RTFO aging 48
Figure 9. Dosage selection results for blends according to Method 1: (a) 64.RAP.R1, (b) 64.RAP.E1, (c) 58.RAP.E1, (d) 58.RAP.E2, (e) 64.RAS.R1, (f) 58.RAS.R1, (g) 64.RAS.R2. .. 55
Figure 10. Comparison of dosage selection according to Methods 1 and 2 for (a) 58.RAP.E1, (b) 58.RAP.E2, and 58.RAS.R1 57
Figure 11. Relationships between high-temperature grade change and additive content for (a) all blends containing R1 and (b) all blends containing E1 58
Figure 12. Slope of the continuous high-temperature grade change versus additive content based on the different methods evaluated 60
Figure 13. Selected doses according to the different methods evaluated 61
Figure 14. Continuous AASHTO M 320 high-temperature performance grades predicted based on the different dosage selection methods evaluated and measured via verification testing at the dosages selected according to Method 1..... 63
Figure 15. Confidence interval (CI) for Method 3 results of blends prepared using R1 64
Figure 16. Hamburg Wheel-track test results 65
Figure 17 Example of the effects of data screening for binder 4|O 73
Figure 18. Example of relationship used to determine ω_c for binder 4|O..... 77
Figure 19. Example relationship used to determine R in the LR method 78
Figure 20 Examples of trends of R values calculated according to Equation (6) with respect to $|G^*|$ 79

Figure 21. Comparison of log a_T values determined using the Gordon and Shaw and pairwise interpolation methods 82
Figure 22. *R* values 85
Figure 23. Master curves for binder 4|PAV-40: (a) |*G**| and (b) δ 86
Figure 24. Master curves for binder 8|PAV-20: (a) |*G**| and (b) δ 86
Figure 25. Comparison of the measured and predicted (a) |*G**| values for the Group A binders, (b) |G*| values for the Group B binders, (c) δ for the Group A binders, and (d) δ for the Group B binders. 88
Figure 26. Glover-Rowe values calculated at 15°C and 0.005 rad/s using the shift factor and CA models 93
Figure 27. Comparison of ω_c values calculated using PI and GS shift factors 94
Figure 28**.** Comparison of CA model predictions using pairwise PI and GS methods for: (a) |*G**| and (b) *Phase Angle* 95
Figure 29. Comparison between PI and GS shift factors on CA model predictions 96
Figure 30. Comparison of Glover-Rowe predictions at 15°C and 0.005 rad/s using the PI and GS shift factors 97
Figure 31. Low-temperature point parameters: (a) *S*(60) and (b) *m*(60). Colors convey Dunnett's test results: green, yellow, and red indicate better, equal, and worse results relative to 64-1, respectively. 110
Figure 32. Intermediate temperature point parameters: (a) $|G^*|sin\delta$, (b) $GR_{25°C}$, and (c) $GR_{15°C}$. Colors convey Dunnett's test results: green, yellow, and red indicate better, equal, and worse results relative to 64-1, respectively. 111
Figure 33. Rheological balance parameters: (a) R_{MC}, (b) $R_{09\text{-}59}$, (c) T_{45}, and (d) ΔT_c. Colors convey Dunnett's test results: green, yellow, and red indicate better, equal, and worse results relative to 64-1, respectively. 112
Figure 34. Low-temperature point parameters: (a) *S*(60) and (b) *m*(60). Colors convey Dunnett's test results: green, yellow, and red indicate better, equal, and worse results relative to 64-2, respectively. 114
Figure 35. Low-temperature point parameters: (a) *S*(60) and (b) *m*(60). Colors convey Dunnett's test results: green, yellow, and red indicate better, equal, and worse results relative to 64-3, respectively. 114

Figure 36. Intermediate temperature point parameters: (a) $|G^*|sin\delta$, (b) $GR_{25°C}$, and (c) $GR_{15°C}$. Colors convey Dunnett's test results: green, yellow, and red indicate better, equal, and worse results relative to 64-2, respectively. Gray indicates Dunnett's test could not be conducted due to unequal variance. 115
Figure 37. Intermediate temperature point parameters: (a) $|G^*|sin\delta$, (b) $GR_{25°C}$, and (c) $GR_{15°C}$. Colors convey Dunnett's test results: green, yellow, and red indicate better, equal, and worse results relative to 64-3, respectively. Gray indicates Dunnett's test could not be conducted due to unequal variance. 116
Figure 38. Rheological balance parameters: (a) R_{MC}, (b) $R_{09\text{-}59}$, (c) T_{45}, and (d) ΔT_c.. Colors convey Dunnett's test results: green, yellow, and red indicate better, equal, and worse results relative to 64-2, respectively. Gray indicates Dunnett's test could not be conducted due to unequal variance. 117
Figure 39. Rheological balance parameters: (a) (a) R_{MC}, (b) $R_{09\text{-}59}$, (c) T_{45}, and (d) ΔT_c.. Colors convey Dunnett's test results: green, yellow, and red indicate better, equal, and worse results relative to 64-3, respectively. Grey indicates Dunnett's test could not be conducted due to unequal variance. 118
Figure 40. Spearman's Rank Correlation Coefficient Values at the PAV-20 Age Level..... 119
Figure 41. Spearman's Rank Correlation Coefficient Values at the PAV-40 Age Level..... 119
Figure 42. Spearman's Correlation Coefficients Comparing PAV-20 to PAV-40..... 120
Figure 43. SARA results 134
Figure 44. FTIR Results for Additives and virgin binders 137
Figure 45. FTIR Results 1900cm^{-1} to 1500 cm^{-1} (a) RTFO (b) PAV-20 (c) PAV-40 138
Figure 46. Change in carbonyl and sulfoxide area compared to (a) log($GR_{15°C}$), (b) R_{MC} and change in carbonyl area (c) log($GR_{15°C}$), (d) R_{MC} 140
Figure 47. Binder Embrittlement Parameter (a) carbonyl area (b) carbonyl + sulfoxide area (c) BEP without FTIR spectra 141
Figure 48. XRF results for inorganic elements: (a) copper, (b) zinc, (c) calcium 142
Figure 49. Example of Saturates (X3), Aromatics (X4), and Resins (X5) 155
Figure 50. NCDOT all blends black space graph 159
Figure 51. NCDOT 58 blends black space graph 160
Figure 52. NCDOT 64-1 blends black space graph 160

Figure 53. VDOT 64-2 TO blends black space graph 161
Figure 54. VDOT 64-2 TF blends black space graph 161
Figure 55. VDOT 64-2 A and E blends black space graph 162
Figure 56. VDOT 64-3 TO blends black space graph 162
Figure 57. VDOT 64-3 TF blends black space graph 163
Figure 58. VDOT 64-3 TO and A blends black space graph 163

List of Tables

Table 1. Comparison of Virgin Binder to Recycled Materials (Epps-Martin et al. 2019) 16
Table 2. Types of Rejuvenators (NCAT 2014) 17
Table 3. SARA Results of Additives Reported by Hagshenas et al. (2020) 21
Table 4. Agencies and their selected parameter 25
Table 5. Summary of Binder Cracking Indicators 30
Table 6. Blends Evaluated 47
Table 7. Virgin and Recycled Binder AASHTO M 320 Continuous High-temperature Grades .. 53
Table 8. Slopes and Selected Additive Dosages 54
Table 9. Comparison between High-Temperature Grades Predicted by Methods 1 through 4 at the Dosages Selected According to Method 1 and Those Measured in Verification Testing 62
Table 10 Summary of the Asphalt Binders and Test Procedures 71
Table 11. Summary of the CA Model Parameters 84
Table 12. $|G^*|$ Model Fit Statistics Including All Data 90
Table 13. $|G^*|$ Model Fit Statistics Excluding $|G^*|$ values Below 10^5 Pa 90
Table 14. Phase Angle Model Fit Statistics Including All Data 91
Table 15. δ Model Fit Statistics Excluding Data Corresponding to $|G^*|$ values Below 10^5 Pa 92
Table 16. Summary of Model Differences 96
Table 17. Summary of the Binders and Blends Evaluated 106
Table 18. Summary of the NC Binders and Blends 128
Table 19. SARA Results 132
Table 20. Comparison of Estimate and Measurement of SARA Fractions for 58.RAP 133
Table 21. Change with Respect to Reference 58.R1 136
Table 22. Change with Respect to Reference 64-1.R1 136
Table 23. Comparison of NCSU and Outside Lab 156
Table 24. SARA NCSU Repeatability 156
Table 25. NCDOT and VDOT RMSE and MAPE 157

Chapter 1 Introduction

1.1 Background

Asphalt binder is one of the most vital materials in transportation infrastructure as it is the glue holding together the vast majority of roadway surfaces. Asphalt binder is a product of the crude oil refining process. Crude oil prices have risen drastically recently. Also, crude oil sources have become increasingly variable and improved efficiency in extracting gasoline and other light distillates has impacted the yield and properties of the asphalt binders, resulting in binders that are more difficult to work with. Measures to counteract these factors are needed to ensure the sustainability, durability, and cost effectiveness of asphalt pavement infrastructure.

Recycling is one very effective measure currently widely used to alleviate pressure to acquire new material as well as be a more environmentally friendly process to make use of existing infrastructure and reduce the needs for storage and landfilling of waste. Both reclaimed asphalt pavement (RAP) and recycled asphalt shingle (RAS) are commonly incorporated into asphalt mixtures. Recycled and reclaimed asphalt binders are oxidized and thus, harder and more susceptible to cracking than virgin binders. Therefore, the increased use of these materials increases the demand for softer virgin binders.

Potential measures to restore the properties of recycled binders and help achieve softer virgin binder grades are the use of recycling agents (RA) and extenders. RAs can come from a variety of sources. Common sources for these products include aromatic extracts, paraffinic oils, tall oils, and triglycerides and fatty acids. RAs are classified as products that can be used to increase the allowable amount of recycled material to be used in blend, which is accomplished by improving rheological characteristics such as softening and reducing brittleness. Extenders are products use to replace a portion of asphalt and often also used to soften the asphalt. Extenders can contain refined waste products such as recycled engine oil bottoms (REOB), and also be formulated from crude oil extracts, and plant based extracts. Extenders typically require a larger quantity to restore the same binder properties as a RA.

Presently, standards pertaining to the acceptance of RAs and extender products and establishment of their dosage are limited. There is a need for better understanding how to best quantify RA and extender effectiveness for restoring the rheological properties of recycled materials to enable improved specifications and more widespread adoption. In addition, a better

understanding of the impacts of the impacts of RAs and extenders on the chemical composition and compatibility of asphalts could potentially elucidate the mechanisms by which effectiveness is achieved.

Interest in RAs and their ability to improve high RAS and RAP content mixtures has translated into a recently completed national project, NCHRP Project 09-58 titled "Evaluating the Effects of Recycling Agents on Asphalt Mixtures with High RAS and RAP Binder Ratios" (Epps Martin et al. 2020). The project established a recommended RA dosage selection procedure and identified measures to classify RA products based on whether they function as softeners versus replenishers or emulsifiers. The project found that targeting restoration of high-temperature grade and low-temperature grade yielded different effects on performance (Epps Martin et al. 2020). Using a higher dosage also correlated to maintaining durability of binders are more extensive long-term aging while the lower doses did not. The report found that a number of rheological and compositional characteristics are important for a viable blend of virgin binder, recycled material, and RA. The NCHRP Project 09-58 proposed a simplified procedure to select RA dosages to achieve the intended high-temperature grade, which relies on the existence of class specific relationships between the blended system high-temperature grade and additive content. Further, the dosage selection procedure assumes complete recycled binder availability. There is general consensus that complete recycled binder availability is not achieved in practice, which may yield asphalt mixtures with poor rutting performance. Therefore, the dosage selection procedure merits further investigation to evaluate the universality of the slopes proposed in NCHRP Project 09-58 to both extenders and RAs and evaluate the rutting resistance of asphalt mixtures prepared using additive dosages selected to restore the high-temperature grade of the blended binder system. The NCHRP Project 09-58 project also identified that certain RA products function as softeners, which soften but do not restore the relaxation characteristics of recycled binders. In contrast, replenishers and emulsifiers restore both the modulus and relaxation characteristics of recycled binder systems. Further research is needed to understand the effects of RAs on composition that cause them function as softeners, replenishers, and emulsifiers.

It is also important to note that the AASHTO M 320 Performance-Graded (PG) specification was developed on the basis of unmodified, petroleum-based asphalts. Consequently, it has been demonstrated that the specification parameters and aging procedures

often fail to discriminate the performance of modified asphalt binders. This shortcoming has been overcome with respect to rutting resistance and corresponding high-temperature grading with the introduction of AASHTO M 332. However, the shortcomings of the current PG specification with respect to cracking performance have not been addressed. The characterization of binder cracking resistance requires an appropriate aging procedure to simulate long-term oxidative aging coupled with a test method and associated parameter to capture cracking resistance. Several alternative rheological parameters to characterize the cracking resistance of asphalt binders have been proposed which merit consideration when evaluating RA and extender modified binder systems. Some of these alternative methods rely on asphalt binder master curves. However, a standard procedure to construct asphalt binder master curves and fit a model to the master curve does not presently exist.

1.2 *Objectives*

The overarching goal of this dissertation is to advance the understanding of RAs and extenders on the rheology and composition of recycled binder blends. The specific objectives of this dissertation to accomplish this overarching goal are to:

1. Evaluate RA and extender dosage selection procedures to restore the intended high-temperature climatic grade of binder blends.
2. Develop practical methods to construct asphalt binder master curves and calculate master curve model coefficients that are amenable for specification.
3. Evaluate the effects of RAs and extenders on binder blends under dosage selection procedures to restore the high- and low-temperature performance grade of binder blends according to available rheological indicators of durability.
4. Identify correlations between alternative rheological indicators of durability and between the results of a given parameter at different long-term age levels.
5. Classify a set of RAs and extenders as softeners, replenishers, or emulsifiers on the basis of their impacts on the rheology and composition of recycled binder blends.

1.3 Dissertation Outline

This dissertation contains six chapters:

- **Chapter 1. Introduction:** This chapter contains the introduction, objectives, and outline of the dissertation.
- **Chapter 2. Literature Review:** This chapter covers a review of the literature pertaining to asphalt binder composition and the evolution of composition with oxidative aging, RA and extender additive types and their compositions, rheological indicators of asphalt binder cracking resistance, and RA dosage selection procedures. A summary of key insights and knowledge gaps is provided at the conclusion of the literature review.
- **Chapter 3. Evaluation of Recycling Agent and Extender Dosage Selection Procedures to Restore the High-temperature Climatic Grade:** This chapter addresses Objective 1. This chapter evaluates the universality of the slopes proposed in NCHRP Project 09-58 for RA dosage selection to both extenders and RAs and evaluates the rutting resistance of asphalt mixtures prepared using additive dosages selected to restore the high-temperature grade of the blended binder system. Four methods of selecting the additive dosages were evaluated. Several other graduate students supported this work, including Lei Gabriel Xue who conducted Hamburg Wheel Track Testing, and both Saqib Gulzar and Jaime Preciado who assisted in asphalt binder sample preparation and binder testing. This research was financially supported by the North Carolina Department of Transportation under NCDOT RP 2020-16. The work presented in this chapter is published in the *Transportation Research Record*, doi: 10.1177/03611981221074361
- **Chapter 4. Practical Methods to Construct Asphalt Binder Master Curves and Calculate Christensen-Anderson Model Parameters:** This chapter addresses Objective 2. A pairwise interpolation is established for free-shifting of isotherms that is readily implementable in Microsoft Excel. The chapter contrasts the results for determining shift factors using pairwise interpolation with those obtained using the RHEA software, which implements the Gordon and Shaw method. Practical methods to calculate the Christensen Anderson (CA) model cross over frequency and R parameters are compared and used to recommend a method for calculating CA model parameters. Graduate students Saqib Gulzar and Jaime Preciado assisted in testing the Group B binders and the Group A binder results were graciously shared by Dr. Akshay Gundla and Dr. Shane Underwood. Geoff Rowe and Sergio Raposo of Abatach, Inc. kindly shared RHEA software v2.1.2 with the authors. The work was financially support provided by NCDOT RP 2020-16.

The majority of the work presented in this chapter is published in the *Transportation Research Record*, doi: 10.1177/03611981231169274.

- **Chapter 5. Evaluation of Alternative Approaches to Restore the Rheology of Recycled Asphalt Binders:** This chapter addresses Objectives 3 and 4. covered the rheological impact of different additives. This chapter evaluates the ability of softer virgin binders, RAs, and extenders to restore the rheology of RAP binders to that of control binders. 'Control binders' are those binders that would be specified for use with mixtures that do not contain RAP. Two procedures for RA dosage selection are examined: 1) dose to restore the intended high-temperature grade and 2) dose to restore the intended low-temperature grade. A broad range of point parameters and rheological parameters that measure the balance of relaxation and stiffness characteristics are examined at two long-term age levels. The parameters for each blend were contrasted with a target performance of the virgin binder used in the blend and against a reference performance of a softer virgin binder and the RAP binder with no additive to replicate industry practice when working with a higher concentration of recycled material via Dunnett's test. Relationships between the different rheological parameters and age level are evaluated using Spearman's rank correlation coefficients. Graduate students Jaime Preciado and Saqib Gular assisted with data collection and sample preparation. Dr. Jhony Habbouche assisted with data collection. Dr. Ilker Boz kindly provided guidance on the statistical analysis. Testing and analysis was supported by NCDOT RP 2020-16 and VTRC Project 117566. The work presented in this chapter is currently undergoing Editorial Board review for publication in the *Transportation Research Record*.
- **Chapter 6. Effects of Recycling Agents and Extenders on the Composition of Recycled Binder Blends:** This chapter addresses Objective 5. The rheological results from Chapter 5 are used to classify the additives used in blends to restore the intended high-temperature climatic grade as softeners versus replenishers or emulsifiers. The effects of the additives on the composition of recycled binder blends is assessed through saturates, aromatics, resins, and asphaltenes (SARA), Fourier transform infrared spectroscopy (FTIR), and x-ray fluorescence (XRF). Each of these tests provided unique information for identifying how the additives alter asphalt binder composition and whether they function as a softener, emulsifier, or replenisher. The testing provided

insight into the rheological performance of the additives as well as provided different tools for detecting the additives in blends. Dr. Michael Elwardany kindly shared input on the SARA results and testing plan. Ronald Lichtenwalner from the NCDOT conducted the XRF testing.

- **Chapter 7. Conclusions and Recommendations:** The section presents the conclusions and recommendations drawn from the findings and results from this dissertation.

1.4 References

1. Epps Martin, A., Kasser, F., Mercado, E., Bajaj, A., Cucalon, L., Yin, F., Chowdhury, A., Epps, J., Glover, C., Hajj, E., Morian, N., Daniel, J., Oshone, M., Rastegar, R., Ogbo, C., King, G.The Effects of Recycling Agents on Asphalt Mixtures with High RAS and RAP Binder Ratios, *NCHRP Report 927*, National Academies, Washington, D.C., 2020.

Chapter 2 Literature Review

2.1 Introduction

The use of asphalt mixtures containing high Recycled Binder Replacement ratios (RBRs) is increasing. Recycled binders are oxidized and thus, harder and more susceptible to cracking than virgin binders. Consequently, the use of higher recycled content mixtures has prompted heightened interest in recycling agents and necessitated the use of asphalt extenders to produce softer virgin binder grades. Recycling agents include a wide-range of both softening agents and rejuvenators that are intended to restore the physical and chemical properties of aged asphalt binders (Epps Martin et al. 2020). Petroleum-based extender products have been in existence for a long time. Non-petroleum based products have been more recently introduced (e.g., bio-oils). This report consists of a review of relevant literature pertaining to the use of recycling agents and extenders, including changes to asphalt binders that are induced by oxidative aging, current recycling agent and extender products in use, performance concerns associated with the use of these products and shortcomings of the current specifications, potential means of improving binder characterization to enable screening of extenders and recycling agents, and dosage selection procedures (Epps Martin et al. 2020).

2.2 Asphalt Binder Composition and Composition with Oxidative Aging

2.2.1 SARA Fractions

Asphalt binder is regarded as a colloid, consisting of highly polar asphaltenes dispersed in a solvating maltene phase, consisting of saturates, aromatics, and resins. Saturates are the least polar, followed by aromatics, and then resins within the maltene phase. The resins serve to peptize the asphaltenes in the surrounding aromatics and saturates (Holleran et al. 2019). A visual example of the four fractionizations can be seen below Figure 1. The balance of the Saturates, Aromatics, Resins, and Asphaltenes (SARA) components affects the rheological properties of asphalt binders, though rheology cannot be tied to SARA composition alone (Sakib et al. 2020).

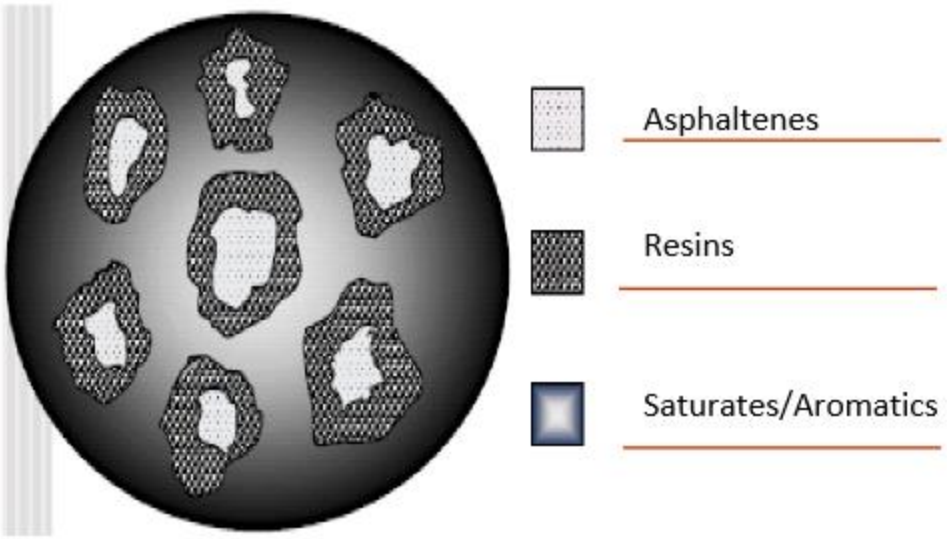

Figure 1. Microstructure hypotheses for colloidal structure of asphalt binders

Oxidative aging is a process that changes the microstructural and chemical composition of asphalt binders. Oxygen reacts with polar components of asphalt, converting polar aromatics and resins to asphaltenes (Petersen 2009). This is seen in Saturates, Aromatics, Resins, and Asphaltenes (SARA) fractionation as a loss of aromatics and resins, and a corresponding increase in asphaltenes. As binder ages the aromatics can convert into resins that subsequently can oxidize to form asphaltenes (Elkashef et al. 2020). With oxidation resins can convert into asphaltenes and thus more oxidized materials would expect to have higher asphaltene contents when compared to the maltene breakdown (Bhasin and Sakib 2018).The changes in SARA composition with aging can thus cause the asphaltenes to agglomerate, as the maltene phase is no longer providing adequate dispersing power, and consequently the viscosity and brittleness of the asphalt increases. Consequently, aging leads to hardening and embrittlement of asphalt binders, which leads to distinct behavior of recycled and virgin asphalts and the need for recycling agents and soft virgin binder grades to compensate.

Several researchers have postulated that restoring the chemical compatibility of the binder is important to ensure adequate long-term performance when using reclaimed materials. Chemical compatibility refers to the extent of microstructure in an asphalt binder. Microstructure can arise due to the formation of asphaltene clusters and/or the crystallization of waxes within the saturates phase. Binders with poor compatibility have been shown to be prone to oxidative age hardening (Petersen 2009). Thus, if a binder softens but does not restore compatibility, it may be prone to oxidation induced hardening.

One means of examining chemical compatibility is by using colloidal instability, measured by the Gaestel index (Kleizine 2019). The Gaestel index, also called the colloidal instability index (*CII*) can be calculated using Equation (1). As *CII* decreases, there tends to be an increase in the binder compatibility under the premise that having a high amount of resins and aromatics relative to asphaltenes and saturates helps prevents the formation of asphaltene clusters and crystallized wax formation (Kleiziene et al. 2019).

$$CII = \frac{(S_a + A_s)}{(R_e + A_r)} \times 100\% \quad \textbf{(1)}$$

where S_a is the concentration of saturates; A_r is the aromatics; R_e is the resins; A_s is the asphaltenes

The standard ASTM test for determining the SARA composition of asphalt binders is ASTM D4124. An alternative procedure was recently proposed by Bhasin and Sakib (2018). The first step in both procedures is separating the asphaltenes from the maltenes. For the ASTM method the filtration of the asphaltenes occurs by dissolving 2.0 g of asphalt binder in 200 mL of iso-octane and filtering using a 60 mL ASTM 10-15µL medium porosity funnel and attached filter ring. For the Bhasin and Sakib method, a .400 gram sample is dissolved in 40 mL of n-Heptane. After being dissolved in the n-Heptane the solution of binder and n-Heptane is separated into four syringes and run through a PTFE hydrophobic syringe filters with a 0.2µm filter size. The asphaltenes are trapped in the filter and what remains in the vial is the maltenes and n-Heptane.

The ASTM standard specifies the separation of the maltenes into its further three fractionizations by relying on solubility and thin layer chromatography. ASTM D4124 relies thin layer chromatography to separate the maltenes into the three components of saturates, aromatics, and resins. This method requires a long testing time per samples, long observation and supervision, and requires a large quantity of binder and solvent (Bhasin and Sakib 2018). Comparatively, the Bhasin and Sakib (2018) method developed by UT Austin, called the Solid Phase Extraction (SPE) method, requires a smaller quantity of binder and while there is a period for drying materials, it does not require constant operator supervision. It uses a 5 g silica gel cartridge with 20 mL capacity SPE in place of thin layer chromatography. Saturates are washed through the SPE cartridge with n-heptane, aromatics with toluene, and resins with dichloromethane and methanol (Bhasin and Sakib 2018). Many of the chemicals between the two

methods are comparable with both requiring n-Heptane, methanol, and toluene. However the ASTM method uses iso-octane and trichloroethylene for determining the aromatics and resins. When creating the SPE method, Bhasin and Sakib (2018)compared the maltene composition from 10 binder samples created to produce differing SARA composition. It was found that both the standard ASTM method and SPE method were able to identify samples that had artificially introduced higher saturates, aromatics, or resin contents. Due to the required materials and equipment for setup, the filter method developed by the team at UT Austin was utilized for this project. There are limits to relying on changes in SARA composition to interpret age induced hardening. The simple mass proportion changes in fractions measured do not fully capture the chemical reactions taking place (Petersen 2009).

2.2.2 XRF

X-Ray Fluorescence (XRF) is a method of analysis that measures the energy of fluorescent photons emitted from a sample after it has been hit with X-ray photons at 40 keV. 1.0 g of asphalt is placed on a polypropylene membrane and then another membrane is placed on top of the sample and spread evenly. Due to the compositional differences between binder and waste products such as REOB, the XRF is able to detect when REOB is added to a blend based on the presence of elements such as calcium, copper, and zinc that are present in REOB but not usually in virgin binder (Kaskow et al. 2018). A study by FHWA (2020) found that these elements are good indicators of REOB due to the high presence of these elements in different waste products.

2.2.3 MDSC

Modulated differential scanning calorimetry (MDSC) is a test that is used to perform thermal analysis to study thermoreversible aging in binders (Kovinich et al. 2021). MDSC measures the total heat flow, non-reversible heat flow, reversible heat capacity, and derivative reversible heat capacity to better understand phase transitions in binders. A study by Ding and Hesp (2021) found that binders dosed with a paraffin wax increased the heat flow of the blend, increasing with additional paraffin wax. This impact could lead to an increase in cracking susceptibility. Waxes present in asphalt binder can cause problems such as lack of cohesion and adhesion to aggregate. Currently in the United States there is no limit on the maximum allowable amount of wax to be present in a binder blend (Kovinich et al. 2021). However, there has been interest in addressing this problem as one common source of wax is REOB. Commonly evaluated

parameters with MDSC are glass transition temperature (T_g) and wax melting temperature. These can be used to better understand the effects of oxidation on binder as well as binder compatibility. A study by Sandrasagra (et al. 2023) found through use of MDSC that the addition of REOB lead to an increase in the aging process through changes in non-reversible heat flow curves. The ability to monitor these flows provides insight into how additives will affect a material blend as it undergoes aging based oxidation.

2.2.4 Flocculation Titrimetry

Flocculation titrimetry can be applied to measure the state of asphaltene peptization in asphalt binders to complement SARA analysis in understanding binder composition and the impacts of oxidative aging. Flocculation titrimetry measures the peptizability of the binder by measuring the flocculation behavior of asphaltenes in an asphalt placed in a solvent. The peptizability evaluates the ability of the maltenes to prevent the formation of asphaltene clusters. Thus, better peptization would generally indicate a higher compatibility and anticipated lower susceptibility to age hardening.

The automated flocculation titrimetry (AFT) is one method to measure peptizability parameters (Chandio et al. 2015, Yang et al. 2017). Alternatively, a more manual flocculation titrimetry (MFT) process can be used. The principles of determining peptization for AFT are the same as the MFT. Pauli (1996) found a relationship between MFT and the AFT results MFT is a modified version of the Heithaus Test. This test was created in 1962 by J. J. Heithaus in a paper titled "Measurement and Significance of Asphaltene Peptization" (Heithaus 1962). In the MFT experiment, the asphalt is dissolved in a solvent and titration of the sample is carried out using a precipitant to estimate the onset point of asphaltene flocculation. The asphalt is diluted by a solvent, toluene, using varying concentrations of solvent and titrated, n-Heptane, to determine the peptizability. At each dilution concentration, the flocculation ratio (*FR*) is measured. *FR* is the fraction of volume of solvent to the total volume of solvent-titrant mixture at flocculation onset point during titration. This can be seen visually by the onset of two distinct rings. In the literature, a distinct difference in grayscale intensity of 30 percent was measured using image processing within MATLAB (Sreeram et al. 2019). However, it has also be performed by visual inspection. The dilution concentration (*C*) is the ratio of the mass of the asphalt to the volume of titrant and solvent at the onset of flocculation. *FR* versus *C* is plotted and used to determine FR_{Max} and $C_{\min}$ as shown in Equations (**2**) and (**3**).

$$FR = \frac{V_S}{V_s + V_T} \quad \textbf{(2)}$$

$$C = \frac{W_a}{V_s + V_T} \quad \textbf{(3)}$$

where FR is the flocculation ratio; V_s is the volume of solvent; V_T is the volume of titrant; C is the concentration; and W_a is the weight of asphalt.

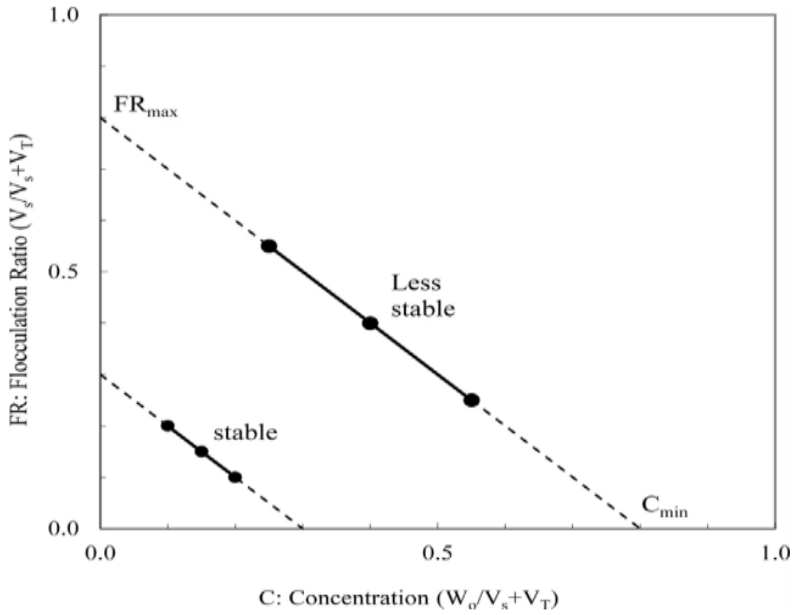

Figure 2. AFT analysis (Chandio et al. 2015)

Subsequently, the peptizability parameters are calculated using Equation (**4**) through Equation (**6**). Typically, the higher the P value the more peptized the binder (Chandio et al. 2015) while a lower P value indicates poorer expected performance with respect to cracking resistance and low temperature properties (Holleran et. al 2018). It has been seen in literature that P decreases with aging when a binder becomes less compatible Chakkoth et al. (2020). A higher P_a indicates the asphaltenes are more peptized. A higher P_o indicates higher solvation by the maltenes. The P is the overall state of peptization.

$$P = \frac{P_o}{1 - P_a} \quad \textbf{(4)}$$

$$P_a = 1 - FR_{Max} \quad \textbf{(5)}$$

$$P_o = FR_{Max} \times [(\frac{1}{C_{\min}}) + 1] \quad \textbf{(6)}$$

where *(P)* is the overall state of peptization; P_a is the asphaltene peptizability; (P_o) is the solvating power of maltenes; C_{min} is the minimum amount of concentration, FR_{Max} is the maximum flocculation ratio.

A study examining AFT in addition to SARA found that AFT was able to predict the agglomeration of the asphaltenes in a binder based on the polarity changes induced by the amount of resins in a binder (Holleran et al. 2019). This study also found that asphaltenes were of higher concentration in a RAP binder compared to a virgin binder evaluated and based on parameters from the AFT, the RAP material having a lower *P*, P_a, and P_o values, which correlated to a worse cracking performance for low temperature properties (Holleran et al. 2019). This report reiterated that a highly oxidized material such as RAP would have a low P_a value and that P_a has been reported to affect cracking resistance (Heithaus 1962).

A study by Chandio et al. (2015) found that changes in temperature can affect the flocculation rate (*FR*) versus concentration (*C*). The study observed that crude oil at 20°C could have flocculation rate of 0.15, while that same material at 95°C had a FR value of 0.74. The effect of temperature on FR can be seen in Figure 3. With each increase in temperature the slope of *FR* vs. *C* increases dramatically, which could present problems examining asphalt binder *FR* as the temperature sensitivity of the FR results. Across different materials, the rate of change with temperature is not constant which translated to some crude oils starting out with the best performance and changing its rank after increasing temperature.

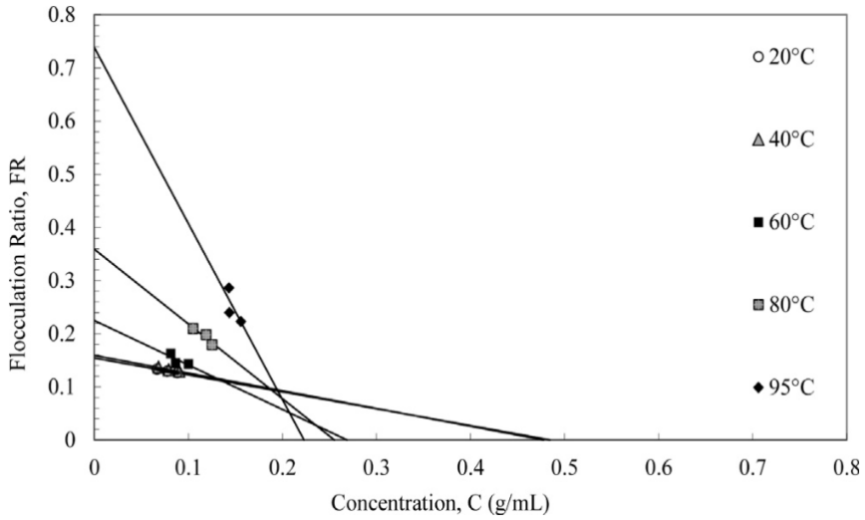

Figure 3. Flocculation rate vs concentration (Chandio et al. 2015)

2.2.5 FTIR

There are specific chemical functional groups that are form upon oxidative aging, including sulfoxides and carbonyls. Fourier transform infrared spectroscopy (FTIR) can be used to track the formation of carbonyls and sulfoxides at wavelengths of 1700 cm^{-1} and 1030 cm^{-1}, respectively. In addition to the sites for oxidation, additional species such vanadium containing components can shed light on the expected hardening susceptibility of a binder with aging. However, it should be noted that while some vanadium-containing molecules can catalyze oxidation, others do not (Petersen 2009). The spectra analysis also allows for the detection of specific additives such as triglycerides due to detecting peaks that are typically absent in virgin binder (Haghshenas et al. 2020).

2.2.6 Molecular Size Distribution

The molecular size distribution within asphalt binders also evolves with aging. As a binder ages, a greater number of large molecules are produced and thus, examining the proportion of large size molecules (LSM) is a proportion has been used to quantify the extent of aging in asphalt binders (Li 2020). The molecular size distribution in an asphalt binder can be characterized using Gel Permeation Chromatography (GPC). For example, Zhao et. al (2018) measured the molecular weight via GPC and divided molecules into two categories, molecular weight above 800 and molecular weight below 800 referred to in the paper as M800. The more aged a material the lower the ratio of M800, and it was found that using recycling agents had an overall

improved affect on the ratio of large molecule to smaller ones, with most recycling agents outperforming virgin binders in terms of molecular size breakdown.

2.3 Impacts of Aging on AAHSTO M 30 Performance Grades

The consequence of the chemical and microstructural on the AASHTO M 320 performance grades (PGs) of asphalt binders is evident by increases in the low and high temperature grades. Table 1 shows a comparison between reclaimed material binder grades and virgin binder grades used in various states (Epps-Martin et al. 2019). It can be seen that the high and low temperature grades of the reclaimed materials exceed that of the virgin, due to oxidative aging.

Table 1. Comparison of Virgin Binder to Recycled Materials (Epps-Martin et al. 2019)

Material		Source	PG	Continuous PGH (°C)	Continuous PGL (°C)	ΔT_c (°C)
Virgin/Base Binders		TX	64-22	68.2	−24.6	−4.6
		NH	64-28	66.9	−28.0	+1.2
		NV	64-28P[a]	65.6	−30.7	−3.6
		IN	64-22	66.2	−25.3	−1.2
		IN	58-28	59.9	−28.2	−8.0
		MN	58-28	58.6	−28.0	+0.1
		WI	58-28	59.4	−28.6	−3.4
		WI	52-34	52.3	−34.2	+0.4
		DE	64-28	66.5	−29.0	+0.1
Recycled Materials	RAP	TX	—	106.6	−2.4	−9.8
		IN	88-10	90.4	−13.7	−6.2
		NV	82-16	84.4	−20.4	−3.4
		NH	88-16	90.2	−20.6	−2.1
		WI	82-10	83.5	−10.9	−7.3
		DE	82-10	86.2	−13.8	−4.4
	MWAS	TX	—	130.7	—	—
		IN	—	123.3	—	—
		DE	—	146.0	—	—
	TOAS	TX	—	178.0	—	—
		CA	—	166.0	—	—

Note: — = not available because RAS binders were very stiff and did not meet the m-value criteria (>0.3), even at high testing temperatures.
[a] Polymer-modified binder.

2.4 Additive Types

2.4.1 Recycling Agents

Recycling agents are a class of materials used to improve the cracking resistance and, in some cases, workability of RAP and RAS mixtures without adversely affecting rutting resistance (Epps Martin et al. 2020). Recycling agents are often separated into two classes of materials: softening agents and rejuvenators. Softening agents are soft asphalt binders or other additives that simply lower the viscosity of the blended binder. Rejuvenators are additives that are

intended to restore physical and chemical properties of the unaged binder (Daly 2017). Many types of recycling agents are used in practice, as outlined in Table 2 (NCAT 2014). The composition of rejuvenators is typically proprietary (Daly 2017).

Table 2. Types of Rejuvenators (NCAT 2014)

Category	Description
Paraffinic Oils	Refined used lubricating oils
Aromatic Extracts	Refined crude oil products with polar aromatic components
Naphthenic Oils	Engineered hydrocarbons
Vegetable Oils	Triglycerides and fatty acids
Tall Oils	Paper industry by-products, same chemical family as liquid antistrip agents and emulsifiers

Kaseer et al. (2019) conducted an extensive review of the effect of recycling agents on the performance of recycled binder blends and asphalt mixtures and found significant variation among different products, potentially due to differences in rejuvenation mechanisms. The mechanisms driving the "rejuvenation" caused by recycling agents are generally poorly quantified. Previous researchers have suggested the ideal methods for rejuvenation, such as Nahar et al. (2013), who suggested addition of volatile and light constituents lost during aging, and Roberts et al. (2009), who preferred oils comprised of aromatics and resins to restore the I_c. It has also been suggested that rejuvenators containing waxes should be avoided due to their tendency to crystallize and lead to cracking at low temperatures (Roberts et al. 2009). Epps Martin et al. (2019) postulated that some recycling agents may work by reducing the size of asphaltene agglomerations, possibly by breaking apart strong polar bonds or aromatic interactions. Other products may simply work by improving the dispersive power of the maltene phase to lower the viscosity and minimize additional asphaltene agglomeration. To assess compatibility, Epps-Martin et al. (2019) tested mixtures rejuvenated with tall oil using a modified SARA fractionation technique with additional separation of the asphaltenes, and found that while rheological tests showed improvement, the SARA fractionation and additional asphaltene information did not show clear benefits of the rejuvenator. It was determined that the SARA analysis could neither prove nor disprove whether the asphaltene agglomerates were reduced in size (Epps-Martin et al. 2019).

Currently, specifications pertaining to recycling agents are sparse and variable (Daly 2017). Epps-Martin et al. (2019) distributed a survey to state highway agencies to identify the laboratory tests used in practice to characterize asphalt binders modified by recycling agents. The

results of their survey are presented in Figure 4, which demonstrates a wide variation in practices, with 40 percent of agencies that use recycling agents performing no characterization of the recycling agent itself or of the recycling agent blended with asphalt. As of 2015, 83 percent of state highway agencies did not allow the use of recycling agents in surface mixtures (Epps Martin et al. 2020). It is inferred that the limited use of recycling agents is largely a result the lack of robust specifications.

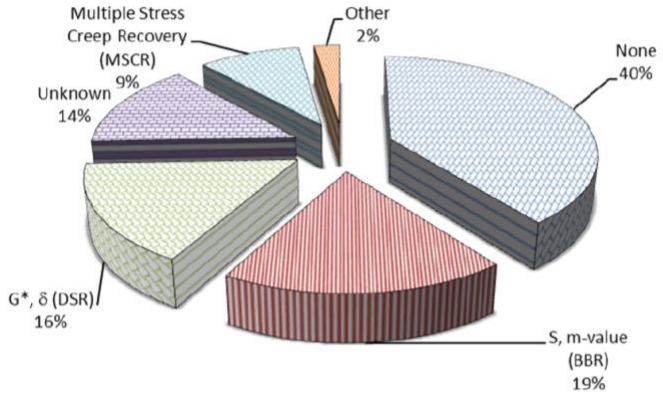

Figure 4. National survey results of laboratory tests used in practice to characterize the properties of asphalt binders modified by recycling agents (Epps Martin et al. 2020).

2.4.2 Extenders

Extenders are often needed to meet asphalt binder grade requirements due to recent changes in petroleum refining and the need for softer virgin binder grades to meet pay grade requirements. While additional extenders are available, this review focuses on two major classes of extenders that have been gaining interest in recent years: bio-based materials and REOB.

2.4.2.1 Bio-based Materials

The uncertainty of liquid asphalt supply and spike in price that occurred in 2008 prompted increased interest in non-petroleum based extenders. Bio-based materials constitute the majority of non-petroleum based extenders (Daly 2017). Efforts have been made to directly use biological materials and waste as asphalt modifiers, including waste cooking vegetable oil (Wen et al. 2012), lignin (McCready and Williams 2008), and soy fatty acids (Seidel and Haddock 2014). Additionally, efforts have been made to use bio-oil produced from thermo-chemical conversion of biomass as “bio-binders” using a variety of feedstocks, including agricultural byproducts (Ratouf and Williams 2010) and animal manure (Fini et al. 2011. While bio-based materials have been primarily proposed for use as extenders, it should be noted that bio-binder have also been

proposed for use as recycling agents (Oldham et al. 2015). The literature on the characterization of asphalt modified by bio-based materials has primarily focused on rheological characterization with little relatively little attention given to long-term oxidative aging and performance within asphalt mixtures (Daly 2017). Su et al. (2018) conducted an extensive review of bio-binders, including soybean oil, palm oil, vegetable oil, engine oil residue combined with an unmodified binder and subjected to short-term aging and found effective softening from all products. It was also found that the bio-binder can potentially lead to a reduction of compaction temperature (Sun et al. 2016). This could be caused by the increase of maltenes; saturates, resins, and aromatics which would dilute the hardening effect of asphaltenes (Sun et al. 2016). While the literature suggests promising performance benefits from the use of bio-based extenders, their composition can differ significantly from asphalt, which suggests that the metrics used within the current PG system may be insufficient to adequately capture performance concerns. For example, Fini et al. (2011) found that bio-binders derived from swine manure have very low molecular weight and relatively high oxygen content compared to asphalt binder. Williams and Ratouf (2010) found that the bio-binders produced from pyrolysis of agricultural products exhibit significant volatilization and oxidation compared to asphalt. Yang et al. (2017) also noted concerning levels of age-induced hardening in bio-oil modified binders.

2.4.2.2 Re-refined Engine Oil Bottoms (REOB)

REOB, also known as Vacuum Tower Asphalt Extender (VTAE), is defined as "the non-distillable residuum from a vacuum tower in a used oil re-refinery" (Asphalt Institute 2019). REOB has been used as an extender to soften asphalt since the 1980s, with typical dosage rates falling between 4 and 8 percent (Asphalt Institute 2019. The increasing use of softer virgin asphalt binders to meet grade requirements in RAP and RAS mixtures has prompted increased use of REOB in recent years (Asphalt Institute 2016). Research has demonstrated that REOB can exacerbate oxidation induced embrittlement, which led 10 states to ban its use as of 2016 (Asphalt Institute 2019). In response to the heightened use and concern regarding REOB, the Asphalt Institute prepared a state of the knowledge report on the use of REOB/VTAE in 2016 (Asphalt Institute 2019). Their review highlights that the oxidation induced embrittlement caused by REOB may not be adequately captured using conventional Rolling Thin Film Oven (RTFO) plus 20-hour PAV aging coupled with standard Dynamic Shear Rheometer (DSR) and Bending Beam Rheometer (BBR) test parameters. Rather, it was found that the detrimental effects of

REOB were only captured after prolonged PAV aging coupled with the characterization of properties that more directly relate to ductility. Also, Fatigue tests conducted on numerous comparative asphalt mixtures without and with VTAE demonstrated an overall reduction in fatigue life of mixtures with VTAE compared to those without. No significant change in rutting performance with VTAE modification was noted (Wielinksi et al. 2015).

The presence of REOB can be inferred within asphalt binder by the detection of metals. X-ray fluorescence (XRF) can be used to determine the REOB content of an asphalt binder (ASTM D6481-14). XRF examines the average intensities of elements and can compare the results to what should be expected, significant differences point to a sample having REOB (Karki and Zhou 2017). The XRF functions by exciting electrons with x-rays. When the x-ray is sent through a sample an electron moves from the outer layer of an atom and moves to the inner layer. This sends out a certain wavelength that can be perceived by the test as a specific atom ranging from fluorine to uranium (Karki and Zhou 2017). XRFs have two detectors, one is filled with P10 gas and can identify longer wavelengths, while another is a scintillation detector and identifies shorter wavelengths. The machine calculates the number of times each wavelength is counted, and this gives a chemical breakdown of the sample.

The simultaneous detection of calcium, zinc, copper, and molybdenum are used to detect REOB and infer its concentration (Asphalt Institute 2019). Detecting REOB using XRF was also part of a study by the Texas Department of Transportation (Barborak 2016). Texas DOT focused on matching sulfur versus vanadium of known intensities from samples without REOB and compared those values to binders that may or may not have contained REOB. For identifying REOB the XRF was looking for the atoms of Ca, Cu, MO, ZN, K, P, S, V, Fe, Ni, and Si. These atoms were identified by a study done for Texas DOT as well as by a report by FHWA (2018).

2.4.2.3 Vacuum Gas Oils (VGO)

VGOs are another waste product that occurs during the refining of crude oil. Often referred to as heavy vacuum gas oils, VGOs are an unfavorable product to work with due to having a high viscosity, high density, and high sulfur content. These issues can arise when trying to transport the material and make it overall, difficult to work with (Smith et. al 2008). As it is a waste product, interest in it as a recycling agent is relatively low, however understanding how to identify it in samples would be of interest to agencies attempting to screen it out in blends. The chemical composition of VGOs are carbon, hydrogen, and sulfur. One study performed by Ristic

et al. (2018) performed SARA fractionation on a VGO and found that the VGO had higher levels of aromatics and lower levels of asphaltenes than another bio-oil examined in the study.

2.4.3 Composition of Additives Reported in the Literature

A review of the SARA and Fourier Transform Infrared (FTIR) spectroscopy results of eight RAs and extenders was provided by Haghshenas et al. (2020). Table 3 summarizes the SARA composition of paraffinic oil (P), aromatic extract (A), tryglyceride and fatty acid-derived (TF), and tall oil (TO) additives reported by Hagshenas et al. (2020). Note that results are reported for two additives in some of the categories, hence the 1 and 2 designations. The results show that the P evaluated is primarily composed of saturates, the As evaluated are primarily aromatics, the TFs are primarily comprised of resins, and the TOs are a combination of saturates and aromatics. While Hagshenas et al. (2020 did not report SARA results for a VGO, one was identified by Ristic et al. (2018) and is incorporated in Table 3. These results indicate that VGO may contain a high concentration of aromatics but also contains resins and asphaltenes.

Table 3. SARA Results of Additives Reported by Hagshenas et al. (2020)

Additive	Asphaltenes (wt%)	Resins (wt%)	Aromatics (wt%)	Saturates (wt%)
P1	0.1	0.0	7.9	91.9
A1	0.2	6.4	84.0	9.5
A2	1.9	25.1	55.1	17.9
TF1	0.4	99.6	0.0	0.0
TF2	0.3	99.7	0.0	0.0
TO1	0.6	27.7	71.7	0.0
TO2	0.2	48.8	51.0	0.0
V-PFO*	15.1	20.7	63.5	0.7

*Ristic et al. 2018 had the SARA breakdown for a VGO material

FTIR results provide further insights into the compositions and classification of additive types. Hagshenas et al. (2020) reported similar peaks in the FTIR spectra of P and A additive types to asphalt binders. However, both Hagshenas et al. (2020) and Baja et al. (2020) report that TF and TO additive types introduce a sharp, identifiable peak in FTIR spectra between 1740 and 1744 cm^{-1}. These wavenumbers correspond with esters and aldehydes, which are carbonyl components that are polar. While carbonyls are generally products of asphalt oxidation and thus, may be perceived as detrimental, they resulted in resins rather than asphaltenes based on the SARA analysis and thus, may serve to restore the chemical compatibility (CII) of the blend. An additional peak at 1162 cm^{-1} was also observed in TF additive types by Hagshenas et al. (2020),

which are most likely associated with dialkyl/aryl sulfones, also highly polar components. Correspondingly, the TF and TO additives were found to have higher oxygen contents (9.8 to 11.5 percent) compared to the other additive types (less than 1 percent). Hagshenas et al. (2020) also reported that the asphalt binders generally display a peak in FTIR spectra at 1602 cm^{-1}, corresponding to conjugated carbon double bonds, but that this peak was absent in the As evaluated.

REOB generally contains heavy metals that are not naturally present in asphalt binders or other additive types, which can be quantified using x-ray fluorescence spectroscopy (XRF) (FHWA 2020). Several states have implemented XRF for quality control of the presence of REOB in virgin asphalt binders. The high saturates content of paraffinic additives and REOB can lead to the crystallization of waxes in the asphalt. Wax crystallization is detectable through MDSC and in some cases the formation of waxes are linked to poor relaxation characteristics as the waxes form during isothermal physical hardening (Kumbargeri et. al 2023). MDSC relies on identifying glass transition temperatures, which is the point where a material undergoes a molecular phase transition, e.g. solid-liquid melting of waxes or solid-solid transition from amorphous wax to crystalline waxes (Kumbargeri et. al 2023).

2.5 Binder Performance Characterization Concerns

Bahia et al. (2001) found that modified and unmodified binders often demonstrate similar properties according to AASHTO M 320 Superpave PG but drastically different cracking performance. Furthermore, recent efforts that have investigated recycling agents and extenders have largely focused on non-load related cracking (i.e., thermal and block cracking). Findings suggest that current Bending Beam Rheometer (BBR) stiffness (i.e., S(60)) and relaxation rate (i.e., m(60)) parameters are insufficient to capture the potential negative effects of recycling agents and extenders on cracking susceptibility (Anderson et al. 2011). There has been growing interest in the identification of an easy-to-measure rheological parameter that captures the ductility of the binder to adequately capture non-load related cracking performance (Asphalt Institute 2019).

In addition, fatigue resistance is a primary concern when using high recycled content mixtures. Thus, the characterization of the fatigue resistance of binders is a necessary first step to designing appropriate asphalt binder blends. However, it has been demonstrated that the current Superpave binder PG intermediate temperature parameter to address fatigue resistance (i.e.,

|G*|×sin δ) lacks relationship to asphalt mixture and pavement performance when modified binders are used (Bahia et al. 2001). The current Superpave intermediate temperature DSR test consists of sinusoidal loading at a small strain amplitude over very few loading cycles. Therefore, it lacks the ability to evaluate actual cracking resistance and has been deemed insufficient to preclude fatigue resistant binders from use in practice.

Current Superpave PG specifications (AASHTO M 320 and AASHTO M 332) simulate short- and long-term aging of asphalt binder using the RTFO and PAV, respectively. Recent studies show that the current 20-hour PAV procedure provides insufficient oxidation to mimic the effects of prolonged field aging (Glover et al. 2005, Wright et al. 2011). Standard PAV aging has also been found to be insufficient to capture the negative effects of additives. Significant attention has been given to binders that contain re-refined engine oil bottoms (REOB) they contribute to the premature cracking of pavements as a result of embrittlement (Asphalt Institute 2019). Furthermore, it has been cautioned that the aging susceptibility of bio-materials has not been well-studied (Daly 2017) and preliminary evaluation indicates potential concerns. Kaseer et al. (2019) reported that numerous studies have reported a loss of recycling agent effectiveness with long-term aging, the extent of which depends upon the type and dose of the recycling agent. The need for an improved procedure to mimic field aging coupled with a test method to capture binder cracking resistance are further highlighted by three recent national projects; NCHRP 9-60: *Addressing Impacts of Changes in Asphalt Binder Formulation and Manufacture on Pavement Performance through Changes in Asphalt Binder Specifications*, NCHRP 9-59: *Relating Asphalt Binder Fatigue Properties to Asphalt Mixture Fatigue Performance*, and NCHRP 9-61: *Short- and Long-Term Binder Aging Methods to Accurately Reflect Aging in Asphalt Mixtures*. The following sections describe alternative binder properties and aging procedures that have been proposed to better capture asphalt binder durability.

2.5.1 Cracking Resistance

The *delta T critical* (ΔT_c), which is equal to the difference between the low-temperature critical PG specification temperatures for $S(60)$ and $m(60)$, has been given considerable attention in recent years for capturing the effects of embrittlement on pavement cracking potential. The parameter was first introduced by Anderson et al. (2011) who observed a strong correlation between ΔT_c and pavement block cracking; correspondingly, the authors postulated that ΔT_c is a

good indicator of asphalt binder ductility at low temperature. They found that the value of ΔT_c decreases with oxidative aging and thus, trends with aging level may be helpful to identifying binders susceptible to oxidative embrittlement. Subsequently, researchers have found that the parameter can be used to identify problems associated with REOB, with values falling below -5ºC indicating concern (Asphalt Institute 2019). The parameter could be implemented into practice relatively easily because it can be calculated using the results of standard BBR testing used for PG determination. ΔT_c is a useful parameter to examine in terms of performance because it can be used to measures the loss of relaxation properties and thus be utilized as another parameter for predicting crack performance (Turner and Hall 2019).

A survey distributed to a task force of 14 members from different state agencies was used to gain perspective on agencies' opinions and use of (ΔT_c). The majority agreed it is an indicator of age related cracking. However, the task force was more split on its use as an effective specification parameter. Two of the 14 respondents did not find enough data to support using ΔT_c as a binder parameter while the majority conditionally supported it due to the fact that it is needed to evaluate the quality of asphalt binders (Asphalt Institute 2019). Of the 12 members that support using ΔT_c, seven members have a current specification, indicated in Table 4 (Asphalt Institute 2019).

Table 4. Agencies and their selected parameter

Agency	ΔT_c Requirement	PAV Aging Duration, hrs	Status
Florida DOT	≥ -5.0	20	Current
Utah DOT	≥ -2.0	20	Current
PANYNJ	≥ -5.0	40	Current
Vermont DOT	≥ -5.0	40	Current
Maryland DOT	≥ -5.0	40	Current
Kansas DOT	≥ -5.0	40	Current
Ontario MTO	≥ -5.0	20	Current
Texas DOT	≥ -6.0	20	Current
Oklahoma DOT	≥ -6.0	20	2020
Delaware DOT	≥ -5.0	40	2020

The base value of ΔT_c can be either positive or negative depending on the binder used. If a binder is positive then the low-temperature grade it is governed by its creep stiffness whereas if it is negative it is governed by the m-value. There are many properties that can affect ΔT_c. Aging causes the ΔT_c value to decrease and typically become negative. Therefore, reclaimed binders tend to have a more negative ΔT_c than that of virgin binder. There is a linear relationship between the amount of binder being replaced with RAP and RAS and the decrease in ΔT_c which can be seen below in Figure 5 (Asphalt Institute 2019).

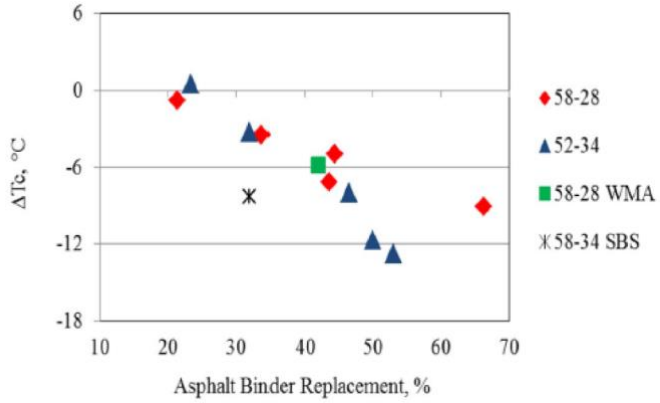

Figure 5. Relationship between RAP/RAS replacement and ΔT_c (Asphalt Institute 2019)

Researchers have demonstrated that several alternative rheological parameters related to brittleness can be derived from the DSR (Glover et al. 2005, Rowe 2011, Rowe et al. 2016, Christensen and Tran 2019). These parameters have been primarily proposed for capturing resistance to non-load associated cracking but also have promise for identifying asphalt binders susceptible to fatigue cracking. Glover (et al. 2005) first proposed a rheological parameter as an

indicator of ductility that could be determined using DSR testing rather than cumbersome force-ductility testing. Rowe (2011) simplified the Glover parameter as $|G^*|\times(\cos\delta)^2/\sin\delta$; this parameter is called the Glover-Rowe (GR) parameter. Anderson et al. (2011) demonstrated that the G-R parameter correlates with pavement durability (block cracking) when evaluated at 15°C and 0.0008 Hz (0.005 rad/s), with a higher GR value indicative of lower ductility. Based on the correlations observed between the GR parameter and pavement block cracking, Anderson et al. (2011) proposed that a value of 180 kPa corresponds to damage onset whereas a value exceeding 450 kPa corresponds to significant cracking. Directly measuring the GR parameter at 0.005 rad/s is not practical or feasible given the slow loading rate. Therefore, Glover et al. (2005) proposed evaluating the parameter at 44.7°C and 10 rad/s, which yielded approximately equivalent results as those based on 15°C and 0.005 rad/s based on time-temperature equivalencies. However, Anderson et al. (2011) demonstrated that a single time-temperature equivalency is not valid for all binders and therefore, that the GR parameters obtained from a master curve are more highly correlated with force-ductility results. Therefore, the authors proposed the use of temperature-frequency sweep testing coupled with a master curve model to obtain the GR parameter.

Master curves are used to describe the time and temperature dependence of the rheological behavior of asphalt binders. The Strategic Highway Research Program (SHRP) considered the use of master curves as the basis for providing rational specification parameters (Anderson et al. 1994). The effort yielded the Christensen-Anderson (CA) model (Christensen 1992), which persists as the most widely applied asphalt binder master curve model today. The CA model is a phenomenological model applied to describe the reduced frequency (ω_R) dependence of asphalt binder dynamic shear modulus ($|G^*|$) and phase angle (δ) and is given in Equation (**7**) and Equation (**8**).

$$|G^*|(\omega) = G_g\left[1+\left(\frac{\omega_c}{\omega_R}\right)^{(\log 2/R)}\right]^{-R/\log 2} \quad \textbf{(7)}$$

$$\delta(\omega) = \frac{90}{\left[1+\left(\frac{\omega_R}{\omega_c}\right)^{\log 2/R}\right]} \quad \textbf{(8)}$$

where G_g = glassy modulus, often assumed to equal 1 GPa, which is supported by experimental evidence from asphalt binders (Christensen 1992); ω_c = crossover frequency, equal to the

reduced frequency where the phase angle equals 45°; and R = rheological index, equal to the logarithmic distance between G_g and $|G^*|$ at ω_c.

The CA model parameters themselves have been proposed as potential measures to evaluate asphalt binder cracking resistance (Christensen 1992). The ω_c defines the point where the storage and loss moduli are equal and thus, constitutes a transition point from elastic- to viscous-dominated behavior. As asphalt binders undergo oxidative aging, the ω_c decreases and the R value increases. While single-point measurements were ultimately adopted for asphalt binder specification during SHRP, recent studies suggest master curve-based parameters may better capture the cracking resistance of asphalt binders than the current specification parameters. Studies suggest that the R value in the CA model is an indicator of asphalt binder cracking potential. Rowe and Sharrock (2011) demonstrated a positive correlation between asphalt binder R values and bending beam fatigue life results of asphalt mixtures. While master curve-based parameters have shown promise, a standard for conducting temperature-frequency sweep testing of asphalt binders and constructing corresponding master curves does not presently exist. There are two methods for constructing master curves, termed 'free shifting' and 'constrained shifting' (Rowe and Sharrock 2011). In the free shifting method, the isotherms are shifted horizontally along the log frequency or time axis to form a smooth, continuous master curve prior to and independent of determining the master curve model parameters. In the constrained shifting method, models are selected to describe both the master curve and time-temperature shift factors. The shift factor and master curve model parameters are then optimized simultaneously. Both methods are commonly applied to asphalt materials.

Gordon and Shaw (1994) proposed a robust free-shifting algorithm for creating master curves that has been successfully applied to asphalt binders (Rowe and Sharrock 2011). In the method, isotherms are shifted using a pairwise approach. Initially, a linear fit of each isotherm is used to estimate the shift factor between each isotherm in a given pair. Then, the shift factors are updated iteratively using weighted least square polynomial fits of the isotherms. Implementation of the method requires rather sophisticated software and thus, it would be advantageous if a more practically implementable approach were developed.

The NCHRP Project 09-59 proposed the replacement of the current intermediate temperature specification with the GR parameter (i.e., $|G^*|\times\cos^2\delta/\sin\delta$) measured at a frequency of 10 rad/s (and thereby negating the need for a master curve) and the addition of the R-value

(determined using standard Bending Beam Rheometer (BBR) testing) to address fatigue cracking (Christensen and Tran 2022). The equation for determining *R* based on BBR results is shown with Equation (**9**). The final report for 09-59 confirmed the theory concerning the utility of GR as a method for estimating a binder's fatigue specification. It was found that GR was a better indicator of fatigue strain capacity than $|G^*|\times\sin\delta$ due to its performance as an indicator of binder failure under specific test conditions at 10 rad/s, as well as establishing a maximum allowable value for GR for PAV aged samples at 5,000 kPa. The old standard of $|G^*|\times\sin\delta$ was found to not correlate with binder failure strain and in some cases allowed binders with poor strain capacity to pass. Replacing it with GR was found to be a more accurate representation of binder fatigue for both unmodified and modified binders. NCHRP Project 09-59 also examined replacing *R*-value with other, related parameters. Two potential alternatives proposed are ΔT_c and BBR stiffness (*S*) at the critical temperature where m = 0.3. The main reasoning for potentially moving away from *R*-value has to do with the ranges currently offered specifically on polymer modified binders. The authors recommended specifying a range of acceptable *R*-values, spanning 1.5 to 2.5. These are based on virgin binders and concerns that different maximums would have to be adopted depending on if it is polymer-modified. In the NCHRP 09-59 report it was found that polymer modified binders often had high *R* values, which indicated that they would have poor cracking performance based on the defined acceptance range. However, it was seen that polymer modified binders performed well and that *R* value was not able to be a good indicator of polymer-modified binder performance.

$$R = \log(2)\frac{\log\left(S/3000\right)}{\log(1-m)} \quad \textbf{(9)}$$

where *S* is the stiffness after 60 seconds at the critical temperature and *m* is the slope at the same point.

The NCHRP Project 09-60 evaluated the ability of rheological properties to reflect block cracking potential (Planche et al. 2018, Elwardany et al. 2020). Properties considered include those proposed by the NCHRP 09-59 project as well as. In addition, the NCHRP 09-60 project has established a DSR-based parameter to use as a surrogate for ΔT_c, called T_{ve} and defined as the difference between the glass transition temperature and crossover temperature. In addition, the Asphalt Binder Cracking Device (ABCD) was employed. The ABCD involves casting a sample of asphalt inside an instrumented ring before cooling the sample to induce thermal contraction

until the sample fractures; the critical fracture temperature is reported. It was found that consideration of failure properties, achieved by means of the ABCD was necessary to discriminate between the performance of polymer-modified binders. Linear viscoelastic properties, including ΔT_c and those proposed by the NCHRP 09-59 project failed to discriminate between the performance of polymer-modified binders but still may provide useful insight into RA and extender modified binders and their aging susceptibility and thus merit consideration herein.

Other studies have also suggested that asphalt binder failure properties are necessary to capture mixture cracking resistance. Consequently, several other fracture mechanics-based and continuum damage-based test methods have been proposed to quantify binder failure properties, as summarized in Table 5 under the categories of fracture mechanics-based and continuum damage-based tests. The Double Edge Notch Tension (DENT) and Single Edge Notch Bending (SENB) tests use notched direct tension and BBR geometries, respectively, and revised loading schemes to capture fracture mechanics-based properties. The LAS and time sweep tests consist of subjecting asphalt binder samples to repeated loading in the DSR using the standard 8-mm parallel plate geometry. Changes in loading resistance with respect to number of loading cycles are used to evaluate damage resistance and determine fatigue failure. The time sweep consists of loading whereas the LAS includes systematically increasing amplitudes to accelerate damage. The glass bead composite test also includes repeated loading in the DSR but uses a standard composite torsion bar of glass beads mixed with binder to recreates a state of stress as closely as possible to a real asphalt mixture. Similarly, the poker chip test attempts to reflect the state of a binder film in an asphalt mixture. In the poker chip test, a confined film to monotonic tension to measure tensile strength.

Table 5. Summary of Binder Cracking Indicators

Property/Test	Fatigue Cracking	Thermal Cracking	Block Cracking	References
Linear Viscoelastic Parameters				
G-R	X		X	Rowe 2011, Christensen and Tran (2019), NCHRP 09-61
R-Value	X		X	Christensen and Tran (2019), NCHRP 09-61
ΔT_c		X	X	Anderson et al. (2011)
T_{ve}			X	Planche et al. (2018)
Fracture Mechanics-Based Tests				
DENT	X	X		AASHTO TP 113
ABCD		X		AASHTO TP 92, Elwardany et al. (2020)
SENB		X		Velasquez et al. (2011)
Continuum Damage-Based Tests				
LAS	X			AASHTO TP 101
Time Sweep	X			Bahia et al. (2001)
Glass Bead Composite	X			Motamed et al. (2013)
Poker Chip	X			Sultana et al. (2014)

2.5.2 Long-term Aging

Recent research suggests that binder test results from 40-hours of PAV conditioning is a better means of gauging field performance after five or more years in service than standard 20-hour PAV aging (Asphalt Institute 2019). Research has demonstrated that embrittlement in modified binders can be captured by binder conditioning in the PAV for 40 hours but not with the standard 20 hours (Bennert 2015, Reinke et al. 2015). Concerns have been raised regarding the additional time burden of the extended PAV aging procedure. However, a reduction in the binder film thickness within the PAV and/or increasing the aging temperature can be used to alleviate this concern, which is the focus of NCHRP 09-61. The NCHRP 09-61 project sought to refine short- and long-term laboratory aging procedures for asphalt binders. The authors proposed no changes to the RTFO but is proposing several changes to the PAV (Bonaquist 2017, Bonaquist 2020). The refined long-term aging procedure will consist of a PAV procedure, retaining the standard air pressure of 2.1 MPa and 20 hour duration but decreasing the binder film thickness by using 12.5 g per pan rather than 50 g per pan and using elevated temperature compared to the current procedure. The aging temperatures was calibrated as a function of climatic conditions to reflect 10 years of field aging near the pavement surface using 26 binders; this level of field aging was selected based on the analysis of LTPP SPS 8 projects which showed an average time to

sustained transverse cracking of 12 years. The revised procedure induces a greater extent of aging compared to the current PAV procedure, which was developed to reflect five to seven years of in-service aging. The report found that if the same temperature was used that a 50 g sample aged at 40 hours at 2.1 MPa in a standard PAV pan would present the same level of aged when compared to a 12.5 g sample aged for 20 hours at 2.1 MPa in the same size pan (i.e., with lower film thickness). They also suggested the potential for conducting short-term aging using 12.5 g of binder conditioned in a PAV pan in an oven at 163°C as an alternative to the standard RTFO.

2.6 NCHRP 09-58 Findings

2.6.1 Dosage Selection

In addition to having adequate metrics to evaluate the performance of binders, a corresponding dosage selection procedure for recycling agents and extenders would be beneficial. Currently, the typical practice for dosage selection is to use the manufacturer's recommendations (Kaseer et al. 2019). This approach is questionable in cases where a single product is combined with different materials (e.g., virgin binder, RAP, RAS) of drastically different properties and concentrations. Therefore, there is a need for a method to select and/or verify additive dosages that can be used by agencies and contractors based upon the target virgin binder properties, which will vary as a function of the type of recycled material included within the mixture (i.e., RAP and/or RAS) and their proportion within the asphalt mixture (i.e., RBR%).

Significant effort has been dedicated to the development of a robust procedure for recycling agent dosage selection in NCHRP 09-58 (Epps-Martin et al. 2020). They have considered three means of dosage selection: (1) restore low-temperature PG, verify high-temperature PG, (2) achieve ΔT_c = -5.0 after 20 hours of PAV aging, and (3) restore high-temperature grade. Method 1 was found to yield the lowest recycling agent dosages. Method 2 resulted in the highest recycling agent dosages and corresponding high-temperature grades that could indicate rutting issues. In contrast, Method 3 allows as much recycling agent as possible without compromising rutting resistance below a certain threshold. Method 3 was found to restore the low-temperature PG at least to that of the target binder. Therefore, the NCHRP 09-58 research team is proposed the use of Method 3 in practice.

To implement Method 3 in practice, the NCHRP 09-58 project proposed a two step approach. First, the high-temperature performance grade of the virgin binder and reclaimed binder blend is calculated using Equation (**10**) based on the high temperature grades of the constituent binders and the blend ratios used. Then, the recycling agent dosage is calculated using Equation (**11**).

$$PGH_{Blend} = (RAP_{BR} \times PGH_{RAP}) + (RAS_{BR} \times PGH_{RAS}) + (B_{BR} \times PGH_{Base}) \quad \textbf{(10)}$$

where PGH_{Blend} is the Pavement Grade Blend; RAP_{RBR} is the Binder Ratio of RAP; PGH_{RAP} is the Pavement Grade of RAP; RAS_{RBR} is the Binder Ratio of RAS; PGH_{RAS} is the Pavement Grade of RAS; B_{RBR} is the Binder Ratio of Virgin Binder; PGH_{Base} is the Pavement Grade of Virgin Binder.

$$\text{RecyclingAgent}(\%) = \frac{(PGH_{Blend} - PGH_{Target})}{SlopeRate} \quad \textbf{(11)}$$

where PGH_{Blend} is the Pavement Grade of Virgin Binder Blend with RAP/RAS; PGH_{Target} is the Pavement Grade Target of binder blend; *SlopeRate* is the reduction rate of PG based on type of rejuvenator used, equal to 1.38 for aromatic extracts and 1.82 for tall oils, vegetable oils, reacted bio-based oils.

The *SlopeRate* values were derived from the linear relationship between recycling agent does and PGH when using virgin binders with grades between 64°C and 70°C and various reclaimed materials; the results used to obtain the *SlopeRate* values are shown in Figure 6 and Figure 7 for aromatic extracts and other recycling agent types, respectively.

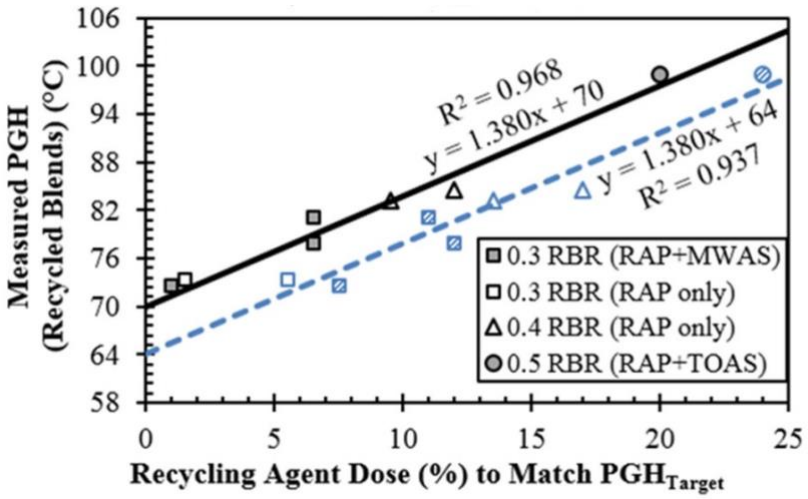

Figure 6. Rejuvenator dosage for aromatic extract (Epps-Martin et al. 2020)

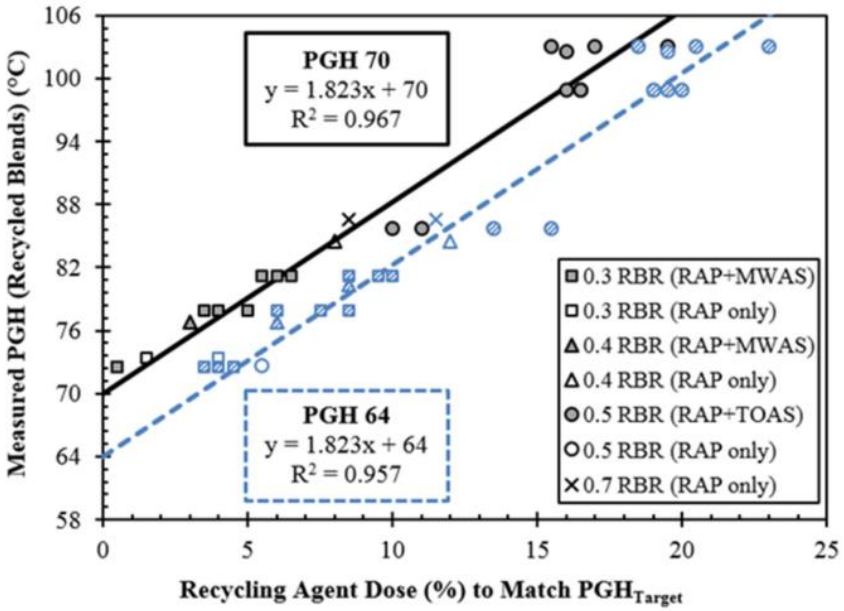

Figure 7. Recycling agent dosages combined for tail oils, vegetable oils, and reacted bio-based oils (Epps-Martin et al. 2020)

A critical component of a dosage selection procedure that NCHRP 9-58 does not consider is the appropriate assumption of the recycled binder contribution, which defines the target virgin binder properties. The results of the NCHRP Project 09-12 (McDaniel and Anderson 2001) indicate that the assumption of complete activation of recycled binder becomes invalid when the asphalt binder replacement ratio exceeds 40 percent. It was demonstrated that following the assumption of complete blending led to select virgin binders for very high recycled binder

contents yielded mixtures that were prone to rutting, which is consistent with expectations if the virgin and recycled binders do not fully blend. Thus, the target virgin binder properties used in a dosage selection procedure should be established based on the *activated* binder replacement ratio (i.e., the recycled binder that mobilizes and blends with the virgin binder).

2.6.2 Cracking and Aging Potential Evaluation

One aspect of NCHRP 09-58 was examining the impacts of different recycling agents have on cracking resistance and aging susceptibility. This was done by using the Glover-Rowe parameter in accordance with AASHTO T 315 and for low temperature cracking resistance using AASHTO T 313 and M 320. Using black-space diagrams (i.e., plots of |G*| versus phase angle), NCHRP Project 09-58 found that how dosage was determined had a large impact on the ability of a recycling agent to restore performance and reduce cracking. Using a dosage to restore low temperature grade resulted in binders with a long-term aged performance that was weaker than binders whose high-temperature grades had been restored. It was also found that using RAs at the dose selected to restore the high-temperature grade can delay cracking onset based on evaluation in the black space. However, it was found in both dosage selection scenarios that RA effectiveness diminishes with age, which merits further investigation.

The type of recycling agent was also shown to have an impact on performance. It was found that paraffinic oil RAs resulted in a more brittle asphalt binder than other types. Other types as recycling agents such as bio-oils and vegetable oils were effective at restoring rheological binder characteristics such as G-R.

The NCHRP 09-58 report examined the SARA compositional breakdown of RA modified systems at multiple age levels and concluded that while the SARA components allow for assessing the evolution of chemical compatibility with aging, the SARA composition does not provide a measure of the ability of RAs to restore binder rheology and thus, analysis of the effects of RAs and extenders on different measures of composition may provide further insight into the mechanisms by which these additives alter rheology and oxidative age induced hardening. Other studies have attempted to provide an explanation for the rheological behavior amongst different additives. One such study was Bajaj (et al. 2020). This study classified the materials as emulsifiers, softeners, and replenishers. Softeners function by increasing the saturates content and decreasing the CII of recycled binder blends. Emulsifiers function by increasing the content of resins in order to peptize the asphaltenes. Finally, replenishers function

by introducing additional aromatics to replace the aromatics lost due to oxidation without impacting the compatibility of a binder.

NCHRP 09-58 also examined the effect of RAs on aging by examining FTIR data. It was found that some RAs contain a significant amount of carbonyl absorbance before oxidation. Therefore, to properly account for the effects of aging, it was important to compare the difference in carbonyl peaks and areas at different age levels rather than simply looking at the maximum peak or area at the highest age level. It was also found that the addition of RAs changed the manner of the oxidation occurring in binders during PAV aging, where the blends had larger carbonyl content, yet the cracking resistance improved in some cases (Epps Martin et al. 2020).

2.7 Summary of Knowledge Gaps and Applications

There are wide range of RA and extenders in use. There is no widely accepted method for RA and extender dosage selection. NCHRP Project 09-58 proposed that dosage should be selected to restore the intended high-temperature climatic grade to maximize benefits without compromising rutting resistance. Their simplified procedure relies on the existence of class specific relationships between the blended system high-temperature grade and additive content. Further, the dosage selection procedure assumes complete recycled binder availability. There is general consensus that complete recycled binder availability is not achieved in practice, which may yield asphalt mixtures with poor rutting performance. However, the universality of the slopes proposed in NCHRP Project 09-58 to both extenders and RAs merits further investigation and the rutting resistance of asphalt mixtures prepared using additive dosages selected to restore the high-temperature grade of the blended binder system merits consideration given the likely scenario of partial recycled binder availability.

A wide range of rheological parameters have been proposed as better measures of durability than current AASHTO M 320 and M 332 specifications. Some of these require a master curve and there is not an accepted standard, prohibiting widespread use. Furthermore, the literature indicates some of these parameters may be closely related and therefore, redundant, which merits further investigation to identify a subset of parameters that provide unique insight.

NCHRP 09-58 used some of these parameters to evaluate RA effectiveness and found it diminished with prolonged laboratory aging, which merits further evaluation using both standard long-term aging (i.e., 20-hour PAV) and a harsher aging state that better reflects more prolonged

field aging (such as 40-hour PAV or thinner films in 20-hour PAV based on NCHRP Project 09-61). The NCHRP 09-58 project showed that SARA analysis was insufficient alone to understand the rheological effects of RAs. Therefore, additional measures, such as FTIR, XRF, and MDSC are necessary to better understand the compositional impact of additives and elucidate their function as softeners, replenishers, or emulsifiers. There have been relatively few studies that have combined rheological and compositional analysis of asphalt binders modified by RAs and extenders to understand the interrelationships between compositional effects and rheological impact.

2.8 References

1. AASHTO. AASHTO M 320 : Standard Specification for Performance-Graded Asphalt Binder. 2021.

2. AASHTO. AASHTO M 332 : Standard Specification for Performance-Graded Asphalt Binder Using Multiple Stress Creep Recovery. MSCR) Test. 2021.

3. AASHTO. AASHTO TP 101 : Standard Method of Test for Estimating Fatigue Resistance of Asphalt Binder Using the Linear Amplitude Sweep. 2012.

4. AASHTO. AASHTO TP 113 : Standard Method of Test for Determination of Asphalt Binder Resistance to Ductile Failure Using Double-Edge-Notched-Tension Test. 2022.

5. AASHTO, 2014. AASHTO TP 92 : Standard Method of Test for Determining the Cracking Temperature of Asphalt Binder Using the Asphalt Binder Cracking Device (ABCD)

6. Anderson, D. A., D. W. Christensen, H. U. Bahia, R. Dongre, M. G. Sharma, C. E. Antle, and J. Button. *SHRP Report A-369: Binder Characterization and Evaluation, Volume 3: Physical Characterization*. National Research Council, Washington, D.C., 1994.

7. Anderson, R. M., G. N. King, D. I. Hanson, and P. B. Blankenship. Evaluation of the Relationship between Asphalt Binder Properties and Non-load Related Cracking. *Journal of the Association of Asphalt Paving Technologists*, Vol. 80, pp. 615-663, 2011.

8. Asphalt Institute. State of the Knowledge: The Use of REOB/VTAE in Asphalt, *Asphalt Institute Information Series No. 240 (IS-240),* 2016.

9. Asphalt Institute. State of the Knowledge: The Use of REOB/VTAE in Asphalt, *Asphalt Institute Information Series No. 240 (IS-240)*. 2019.

10. Asphalt Institute. State-of-the-Knowledge: Use the Delta Tc Parameter to Characterize Asphalt Binder Behavior, *Asphalt Institute Information Series.* 2019.

11. ASTM. ASTM 6481-14 : Standard Test Method for Determination of Phosphorus, Sulfur, Calcium, and Zinc in Lubrication Oils. 2019.

12. Bahia, H. U., D. I. Zeng, H. Kharti, M. A. Zhai, & M. Anderson. Characterization of Modified Asphalt Binders in Superpave Mix Design, *NCHRP Report 459*, National Academies, Washington, D.C.. 2001.

13. Bajaj, A., Epps Martin, A., King, G., Glover, C., Kaseer, F., Arambula-Mercado, E. Evaluation and classification of recycling agents for asphalt binders. *Construction and Building Materials 260*. 2020.

14. Barborak, R., C. Coward, and R. Lee. Detection and Estimation of Re-Refined Engine Oil Bottoms in Asphalt Binders: Texas Department of Transportation's Approach with Wavelength Dispersive X-Ray Fluorescence Spectroscopy, *Transportation Research Record, No. 2574, pp. 48-56.* 2016.
15. Bennert, T. Asphalt Binder and Mixture Properties Produced with REOB Modified Asphalt Binders, *Presentation at the Asphalt Binder Expert Task Group Meeting,* Fall River, MA, 2015.
16. Sakib, N., Bhasin, A. Measuring polarity-based distributions (SARA) of bitumen using simplified chromatographic techniques. *International Journal of Pavement Engineering Vol. 20, No. 12, 1371-1384.* 2018.
17. Bonaquist, R. Short- and Long-Term Binder Aging Methods to Accurately Reflect Aging in Asphalt Mixtures, *NCHRP 09-61 Interim Report*, National Academies, Washington, D.C., 2017.
18. Bonaquist, R. Short- and Long-Term Binder Aging Methods to Accurately Reflect Aging in Asphalt Mixtures, *NCHRP 9-61 Update, Presented at the 99th Annual Meeting of the Transportation Research Board,* Washington, D.C., 2020.
19. Chakkoth, U., Krishna, K.R., Ramkumar, M., Rao, P.V.C., Ravindran, P., Krishnan, J. Characterization of Colloidal Stability of Blended Bitumen. *Transportation Research Lecture Notes Vol 45, pp. 883-894*. 2020.
20. Chandio, Z., M. Ramasamy, and H.B. Mukhtar. Temperature effects on solubility of asphaltenes in crude oils. *Chemical Engineering Research and Design, Vol. 94, pp. 573-583.* 2015.
21. Christensen, D. W., and N. Tran. Relationships Between the Fatigue Properties of Asphalt Binders and the Fatigue Performance of Asphalt Mixtures, *NCHRP Report 982,* Transportation Research Board, Washington, D.C., 2022.
22. Christensen, D. W. Mathematical Modeling of the Linear Viscoelastic Behavior of Asphalt Cements. Pennsylvania State University. 1992.
23. Christensen, D. W., and N. Tran. Relationships Between the Fatigue Properties of Asphalt Binders and the Fatigue Performance of Asphalt Mixtures. *NCHRP Report 982,* Transportation Research Board, Washington, D.C., 2022.

24. Daly, W.H. Relationship Between Chemical Makeup of Binders and Engineering Performance, *NCHRP Synthesis 511*, National Academies, Washington, D.C., 2017.
25. Ding, H., Hesp, S. Balancing the Use of Wax-Based Warm Mix Additives for Improved Asphalt Compaction with Long-Term Pavement Performance. *ACS Sustainable Chemistry and Engineering Vol 9, 7298-7305.* 2021.
26. Elkashef, Mohamed, et al. Effect of using Rejuvenators on the Chemical, Thermal, and Rheological Properties of Asphalt Binders. *Energy & Fuels, Vol. 34, No. 2, pp. 2152-2159.* 2020.
27. Elwardany, M., J.P. Planche, and G. King. A Tale of Two Deltas: Towards a Universal Blind Framework for Asphalt Durability. 2021.
28. Epps Martin, A., Kasser, F., Mercado, E., Bajaj, A., Cucalon, L., Yin, F., Chowdhury, A., Epps, J., Glover, C., Hajj, E., Morian, N., Daniel, J., Oshone, M., Rastegar, R., Ogbo, C., King, G. The Effects of Recycling Agents on Asphalt Mixtures with High RAS and RAP Binder Ratios, *NCHRP Report 927*, National Academies, Washington, D.C., 2020.
29. FHWA. Field Analysis of Asphalt Binders for Recycled Engine Oil Bottoms (REOB) Using Handheld XRF Spectrometers. *Tech Report FHWA-HRT-18-043*. 2020.
30. Fini, E. H., E. W. Kalberer, A. Shahbazi, M. Basti, Z. You, H. Ozer, and Q. Aurangzeb. Chemical Characterization of Biobinder from Swine Manure: Sustainable Modifier for Asphalt Binder, *Journal of Materials in Civil Engineering, Vol. 23, pp. 1506 -1513.* 2011.
31. Glover, C. Development of a New Method for Assessing Asphalt Binder Durability with Field Validation, *Report FHWA/TX-05/1872-2*, Texas Transportation Institute, College Station, TX, 2005.
32. Gordon, G. V., and M. T. Shaw. *Computer Programs for Rheologists*. Hanser/Garnder, 1994.
33. Haghshenas, H., Rea, R., Reinke, G., Haghshenas, D. Chemical Characterization of Recycling Agents. J*ournal of Materials in Civil Engineering, American Society of Civil Engineering. Vol 32.* 2020.
34. Heithaus, J. J., Measurement and Significance of Asphaltene Peptization. *Institute of Petroleum. Vol 48, pp. 45-53.* 1962.
35. Holleran, G., I. Holleran, D. J. Wilson. The Use of Automated Flocculation Titrimetry to Predict Performance of Bituminous Binders. *Sustainable Civil Infrastructures*. 2019.

36. Karki, P., and F. Zhou. Systematic Method for Quantifying Re-Refined Engine Oil Bottom Content in Binders: Using X-Ray Fluorescence Spectroscopy, *Transportation Research Record, No. 2632, pp. 52-59.* 2017.
37. Kaseer, F., A. Epps Martin, and E. Arambula-Mercado. Use of recycling agents in asphalt mixtures with high recycled materials contents in the United States: A literature review, *Construction and Building Materials, Vol. 211, pp. 974-987.* 2019.
38. Kaskow, J., Poppelen, S., Hesp, S. Methods for the Quantification of Recycled Engine Oil Bottoms in Performance-Grade Asphalt Cement. *Journal of Materials in Civil Engineering. Vol 30.* 2018.
39. Kleizine, R., M. Panasenkiene, and A. Vaitukus. Effect of Aging on Chemical Composition and Rheological Properties of Neat and Modified Bitumen, *Materials, Vol. 12*. 2019.
40. Kovinich, J., Hesp, S., Ding, H. Modulated differential scanning calorimetry study of wax-doped asphalt binders. *Thermochimica Acta 699*. 2021.
41. Kumbargeri, Y., Planche, J.P., Adams, J., Elwardany, M., King, G. Effect of Binder Chemistry and Related Properties on the Low-Temperature Performance Parameters of Asphalt Binders. *Transportation Research Record*. 2023.
42. Li, J., Feipeng, X., Amirkhanina, Serji, N. High temperature rheological characteristics of plasma-treated crumb rubber modified binders, *Construction and Building Materials, Vol. 236.* 2020.
43. McCready, N. S., & Williams, R. C. Utilization of Biofuel Coproducts as Performance Enhancers in Asphalt Binder. *Transportation Research Record, Vol 2051(1), pp. 8–14.* 2008.
44. McDaniel, R. and R.M. Anderson. Recommended Use of Reclaimed Asphalt Pavement in The Superpave Mix Design Method: Technician's Manual, *NCHRP Report 452*, National Academies, Washington, D.C., 2001.
45. Motamed, A., A. Bhasin, and A. Izadi. Evaluating Fatigue-Cracking Resistance of Asphalt Binders in a Standardized Composite Using Continuum Damage Theory, *Vol. 25, No. 9, pp. 1209-1219.* 2013.
46. Nahar, S.N., M. Mohajeri, A. Schmets, T. Scarpas, M.F. van de Ven, and G. Schitter. First Observation of Blending Zone Morphology at Interface of Reclaimed Asphalt Binder and Virgin Binder, *Transportation Research Record, Transportation Research Board, No. 2370, pp. 1-7.* 2013.

47. NCAT. NCAT Researchers Explore Multiple Uses of Rejuvenators, *Asphalt Technology News, Vol. 26, No. 1*. 2014.
48. Oldham, D., E. Fini, and E. Chailleux. Application of a bio-binder as a rejuvenator for wet processed asphalt shingles in pavement construction, *Construction and Building Materials, Vol. 86, pp. 75-84.* 2015.
49. Pauli, A. Asphalt compatibility testing using the automated Heithaus Titration Test. *Western Research Institute.* 1996.
50. Peterson, J.C. A Review of the Fundamentals of Asphalt Oxidation, *TRB Circular E-C140, Transportation Research Board*, Washington, D.C., 2009.
51. Planche, J. P., M. E. Elwardany, C. Rodezno, and D. Christensen. *NCHRP 09-60 Interim Report,* National Academies, Washington, D.C., 2018.
52. Ratouf, M. and R.C. Williams. Temperature Susceptibility of a Non-Petroleum Binder as a Paving Material, *Transportation Research Record, No. 2180, pp. 9-18.* 2010.
53. Reinke, G., A. Hanz, D. Herlitzka, S. Engber, and M. Ryan. Further Investigations into the Impact of REOB and Parrafinic Oils on the Performance of Bituminous Mixtures, *Presentation at the Asphalt Binder Expert Task Group Meeting*, Fall River, MA, 2015.
54. Ristic, N. D., M. R. Djokic, E. Delbeke, A. Gonzalez-Quiroga, C. V. Stevens, K. M. Van Geem, G. B. Marin. Compositional characterization of pyrolysis fuel oil from Naphtha and Vacuum Gas Oil. *Energy Fuels, Vol 32, pp. 1276-1286.* 2018.
55. Roberts, F. Hot mix asphalt materials, mixture design and construction (3rd Ed.). *National Asphalt Pavement Association Research and Education Foundation*, Lanham, MD, 2009.
56. Rowe, G. Prepared Discussion for Evaluation of the Relationship between Asphalt Binder Properties and Non-load Related Cracking. *Journal of the Association of Asphalt Paving Technologists, Vol. 80, pp. 615-663.* 2011.
57. Rowe, G. M., and M. J. Sharrock. Alternate Shift Factor Relationships for Describing Temperature Dependency of Viscoelastic Behavior of Asphalt Materials. *Transportation Research Record: Journal of the Transportation Research Board, Vol. 2207.* 2011.
58. Rowe, G. M., M. J. Sharrock, and S. Raposo. Cracking and Linear Viscoelastic Binder Properties. *8th RILEM International Conference on Mechanisms of Cracking and Debonding in Pavements, Vol. 13, pp. 3-8.* 2016.

59. Sandrasagra, J., Ma, J., Hesp, S. Understanding the field performance of asphalt binders in continental climates through modulated differential scanning calorimetry. *Construction and Building Materials Vol. 391*. 2023.
60. Seidel, J. C., J. E. Haddock. Rheological Characterization of Asphalt Binders Modified with Soybean Fatty Acids. *Construction & Building Materials, Vol. 53, pp. 324-332.* 2014.
61. Smith, D. F., P. Rahimi, A. Teclemariam, R. P. Rodgers, A. G. Marshal. Characterization of Athabasca bitumen Heavy Vacuum Gas Oil Distillation Cuts by Negative/Positive Electrospray Ionization and Automated Liquid Injection Field Desorption Ionization Fourier Transform Ion Cyclotron Resonance Mass Spectrometry. *Energy & Fuels, Vol. 22, pp. 3118-3125.* 2008.
62. Sreeram, A., Z. Leng, R. Hajj, A. Bhasin. Characterization of compatibility between aged and unaged binders in bituminous mixtures through an extended HSP model of solubility, *Elsevier Fuel, Vol. 254.* 2019.
63. Su, N. F. Xiao, J. Wang, L. Cong, and S. Amirkhanian. Production and applications of bio-asphalts – A Review. *Construction and Building Materials, Vol. 183, pp. 578-591*. 2018.
64. Sultana, S., and A. Bhasin. Effect of chemical composition on rheology and mechanical properties of asphalt binder, *Construction and Building Materials, Vol. 72, pp. 293-300.* 2014.
65. Sun, Z., J. Yi, Y. Huang, D. Feng, D., and C. Guo. Properties of asphalt binder modified by bio-oil derived from waste cooking oil, *Construction and Building Materials, Vol. 102, pp. 496-504.* 2016.
66. Turner, P., & Hall, C. How to use the Delta TC Parameter. *AsphaltPro Magazine.* 2019.
67. Velasquez, R., H. Tabatabaee, and H. U. Bahia. Low Temperature Cracking Characterization of Asphalt Binders by Means of the Single-Edge Notch Bending (SENB) Test, *Journal of the Association of Asphalt Paving Technologists, Vol. 80, pp. 583-613.* 2011.
68. Wen, H., S. Bhusal, and B. Wen. Laboratory Evaluation of Waste Cooking Oil-Based Bioasphalt as Sustainable Binder for Hot-Mix Asphalt, *Transportation Research Board E-Circular E-165, pp. 49-60.* 2012.
69. Wielinski, J., A. Kriech, A. Horton, T. Reece, and G. Huber. Laboratory Evaluation of Vacuum Tower Asphalt Extenders Impact on HMA Fatigue Resistance and Asphalt Binder

Aging, *Proceedings of the 94th Annual Meeting of the Transportation Research Board*, Washington, D.C., 2015.

70. Wright, L., A. Kanabar, E. Moult, S. Rubab, and S. Hesp. Oxidative Aging of Asphalt Cements from and Ontario Pavement Trial, *International Journal of Pavement Engineering, Vol. 4(5), pp. 259-267.* 2011.
71. Yang, X., J. J. Mills-Beale, and Z. You. Chemical characterization and oxidative aging of bio-asphalt and its compatibility with petroleum asphalt, *Journal of Cleaner Production, Vol. 142, pp. 1837-1847.* 2017.
72. Zhao, M., F. Shen, Q. Ding. Micro mechanism of the Dispersion Behavior of Polymer-Modified Rejuvenators in Aged Asphalt Material. *Applied Sciences, Vol 8.* 2018

Chapter 3 Evaluation of Recycling Agent and Extender Dosage Selection Procedures to Restore the High-temperature Climatic Grade

The work presented in this chapter has been published in the Transportation Research Record, Journal of the Transportation Research Board, © National Academy of Sciences: Transportation Research Board 2022. https://doi.org/10.1177/03611981221074361. It has been reprinted here according to SAGE's author archiving and re-use guidelines.

3.1 Introduction

Most asphalt mixtures produced today contain recycled asphalt from Reclaimed Asphalt Pavement (RAP) and/or Recycled Asphalt Shingles (RAS) due to the associated environmental and economic benefits (Williams et al. 2020). Recycled asphalt binders are oxidized and thus, harder and more susceptible to cracking than virgin binders (Williams et al. 2020). To compensate, asphalt mixtures containing high Recycled Binder Ratios (RBR) often include a softer virgin binder performance grade (PG) than dictated by the climate and/or an additive to yield the desired blended binder grade. Recycling agents are often used to achieve the desired blended binder grade and encompass a wide-range of both softening agents and rejuvenators, including paraffinic and aromatic extracts from crude oil, tall oils, vegetable oils, and reacted bio-based oils (Williams et al. 2020, NCAT 2014). Extenders are another similar class of product used to achieve softer binder grades. Crude oil extracts and bio-based oils are both commonly used as extenders (Daly 2017).

Dosage selection is an important step to the effective use of recycling agents and extenders. Low dosages may yield poor asphalt mixture cracking resistance whereas excessively high dosages may yield asphalt mixtures that are susceptible to rutting (Epps Martin et al. 2020). A standardized protocol for extender and recycling agent dosage selection does not presently exist. Therefore, most state agencies currently follow the additive manufacturer's recommendations for dosage selection (Kaseer et al. 2019).

NCHRP Project 09-58 (Epps Martin et al. 2020) proposed a recycling agent dosage selection procedure that aims to restore the blended binder's AASHTO M 320 high-temperature PG back to the target grade for the given climate. This approach was found to allow as much recycling agent into the blend as possible without compromising the potential rutting resistance and was found to restore the climatic low-temperature PG of the blend to the target or achieve a lower grade. The authors suggested that blends could be prepared with no additive and at two

additive dosage levels to determine the expected change in high-temperature PG per percent of additive added to the blend and correspondingly use Equation **(12)** to calculate the required grade for a given blend. In an effort to establish a simplified procedure, the authors further proposed that Equations **(12)** and **(13)** be used to calculate the additive dose with the average slope (*X*) values observed in the NCHRP Project 09-58 study for aromatic extract and other additive types, which consisted of the combination of tall oils, vegetable oils, and reacted bio-based oils.

$$\text{Additive (\%)} = \frac{PGH_{\text{Blend}} - PGH_{\text{Target}}}{X} \quad \textbf{(12)}$$

$$PGH_{\text{Blend}} = RAP_{BR} \times PGH_{RAP} + RAS_{BR} \times PGH_{RAS} + B_{BR} \times PGH_{Virgin} \quad \textbf{(13)}$$

where Additive (%) is additive content by total weight of asphalt binder; *X* is the slope (equal to 1.38 for aromatic extracts and 1.82 for all other products based on NCHRP 09-58 results); PGH_{Blend} is the continuous high-temperature PG of the blend of recycled and virgin binder (°C); PGH_{Target} is thetarget high-temperature PG for the blend (°C); RAP_{BR} is the RAP binder recycled binder ratio, equal to the weight of RAP binder in the mix divided by total binder weight in the mix; RAS_{BR} is the RAS binder recycled binder ratio, equal to the weight of RAS binder in the mix divided by total binder weight in the mix; B_{BR} is the $1 - RAP_{BR} - RAS_{BR}$; and $PGH_{Virgin}$is the virgin binder high-temperature continuous grade (°C).

While the NCHRP Project 09-58 sought to evaluate a diverse set of recycling agents and corresponding binder blends, the universality of the *X* values given in Equation **(12)** to all recycling agents and other types of softening additives remains unknown. NCHRP Project 09-58 did not focus on extenders and therefore, the slope values for extenders merits investigation. Furthermore, Equation **(13)** assumes that the recycled binder completely mobilizes and blends with the virgin binder and the recycling agent. However, there is general consensus that complete recycled binder availability is not achieved in practice (Epps et al. 2019, McDaniel & Anderson 2001, Al-Qadi et al. 2009). The erroneous assumption of complete recycled binder availability may yield additive dosages that are too high and consequently yield asphalt mixtures with poor rutting performance. Consequently, the objectives of this study are to; (1) evaluate the universality of the blended system high-temperature grade versus additive content slope values proposed in the NCHRP Project 09-58 and Copeland (2011) and (2) evaluate the rutting resistance of asphalt mixtures with additives dosages selected to restore the intended AASHTO M 320 high-temperature grade.

3.2 Methodology and Materials

Two North Carolina Department of Transportation (NCDOT) approved asphalt mixtures were evaluated in this study. Each mixture had a Nominal Maximum Aggregate Size (NMAS) of 9.5-mm. The first mixture contained 40 percent RAP by weight of aggregate with a corresponding RBR of 0.36. The second mixture contained 5 percent manufactured waste RAS by weight of aggregate with a corresponding RBR of 0.19. As per NCDOT standards, these mixtures specified a PG 58-28 virgin binder. The specified AASHTO M 320 PG for virgin binders in North Carolina is PG 64-22 in the absence of recycled materials or the requirement for polymer modification.

For this study, 10 binder blends containing different additives, recycled binder sources, and virgin binder were evaluated, as shown in Table 6. Asphalt binder was extracted and recovered from the RAP and RAS materials in accordance with ASTM D2172 Test Method A and ASTM D5404 for characterization and use in the preparation of the blends. The additives included two extenders and two recycling agents. To preserve the anonymity of the suppliers, the recycling agents are designated R1 and R2 and extenders are designated as E1 and E2. Both recycling agents are triglycerides and fatty acids derived from vegetable oils. Both extenders are petroleum-based extracts that contain re-refined engine oil bottom (REOB). The recycled binders were obtained from the RAP and RAS materials of the parent mixtures from this study. For the virgin binders, the same PG 58-28 binder used in the parent mixture designs was chosen as well as another common in North Carolina PG 64-22 binder. Preliminary blends of the PG 58-28 binder, extenders, and RAS indicated that dosage required to restore the blended binder high-temperature grade to 64°C would exceed the maximum limit for dosage proposed in the NCHRP Project 09-58 of 10 (Epps Martin et al. 2020); therefore, extenders were only evaluated in combination with the RAP binder. Select blends were prepared at a selected dosage to evaluate agreement between the measured and intended high-temperature grade.

Hamburg Wheel-track (HWT) testing was conducted on mixtures prepared using a subset of the blends at a selected dosage to restore the intended high-temperature AASHTO M 320 PG to evaluate rutting performance. In addition, the PG 58-28 binder was also blended with the recycled materials and no recycling agents to serve as a control case representing the current practice in North Carolina. An additional RAP mixture, mix ID 10 in Table 6, was prepared and tested that was expected to fail the rutting criteria to ensure this was captured by the HWT test;

this mix included a PG 58-28 virgin binder and R1, using the dosage established using the PG 64-22 virgin binder.

Within the results, the blends are identified based on the virgin binder (58 for the PG 58-28 binder versus 64 for the PG 64-22 binder), recycled binder (RAP versus RAS) and additive type as shown in Table 6.

Table 6. Blends Evaluated

Blend ID	Blend Designation	Recycled Binder	Virgin Binder	Additive	Dosage Selection	Blend Verification	Hamburg Testing
1	58.RAP	RAP	PG 58-28	None			✓
2	58.RAS	RAS	PG 58-28	None			✓
3	64.RAP.R1	RAP	PG 64-22	R1	✓	✓	✓
4	64.RAP.E1	RAP	PG 64-22	E1	✓		
5	58.RAP.E1	RAP	PG 58-28	E1	✓	✓	
6	58.RAP.E2	RAP	PG 58-28	E2	✓	✓	✓
7	64.RAS.R1	RAS	PG 64-22	R1	✓	✓	✓
8	58.RAS.R1	RAS	PG 58-28	R1	✓		
9	64.RAS.R2	RAS	PG 64-22	R2	✓	✓	✓
10	58.RAP.R1	RAP	PG 58-28	R1			✓

3.2.1 Virgin and Recycled Binder Characterization

The high-temperature continuous PGs of the two virgin binders, two recycled binders, and blends of each recycled binder and PG 58-28 at the respective mixture RBR were determined using Dynamic Shear Rheometer (DSR). All testing and analysis was conducted in accordance with AASHTO T 315 and the grading criteria specified in AASHTO M 320.

To prepare blends of virgin and RAP binder, the virgin binder was preheated to 140°C and the RAP was pre-heated to 165°C. The RAP and virgin binders were thoroughly blended using a power drill with a paddle attachment for one minute. This procedure generally adheres to the recommendations given in NCHRP 09-58 (Epps Martin et al. 2020) that suggested preheating the recycled binder to 160°C to 200°C until sufficiently fluid and then mixing with the virgin binder. However, NCHRP 09-58 recommended hand mixing of samples whereas the drill was used herein because the authors felt it produced more repeatable mixing. A temperature of 200°C was insufficient to liquefy the RAS binder. Therefore, the ambient temperature RAS binder was ground using a mortar and pestle and combined with virgin binder pre-heated to 140°C. The combination of RAS and virgin binder was then mixed using a power drill for one minute. Pre-heating the RAS following grinding was found to increase agglomeration when added to the virgin binder and therefore, avoided.

Rolling Thin Film Oven (RTFO) aging was used to prepare short-term aged binder according to AASHTO T 240 for the virgin binders, RAP binder, and blends of virgin and recycled binder. The RAS binder did not achieve sufficiently low viscosity at 163°C to allow for RTFO aging. For the blends of RAS and virgin binder, and also blends of RAS, virgin binder, and recycling agents, clumps of RAS were visually evident in the original binder as shown in Figure 8 (a). However, these clumps were not evident in RTFO-aged samples containing RAS as shown in Figure 8 (b); therefore, testing of all binder blends containing RAS relied on RTFO-aged binder testing only and original binder test results were omitted.

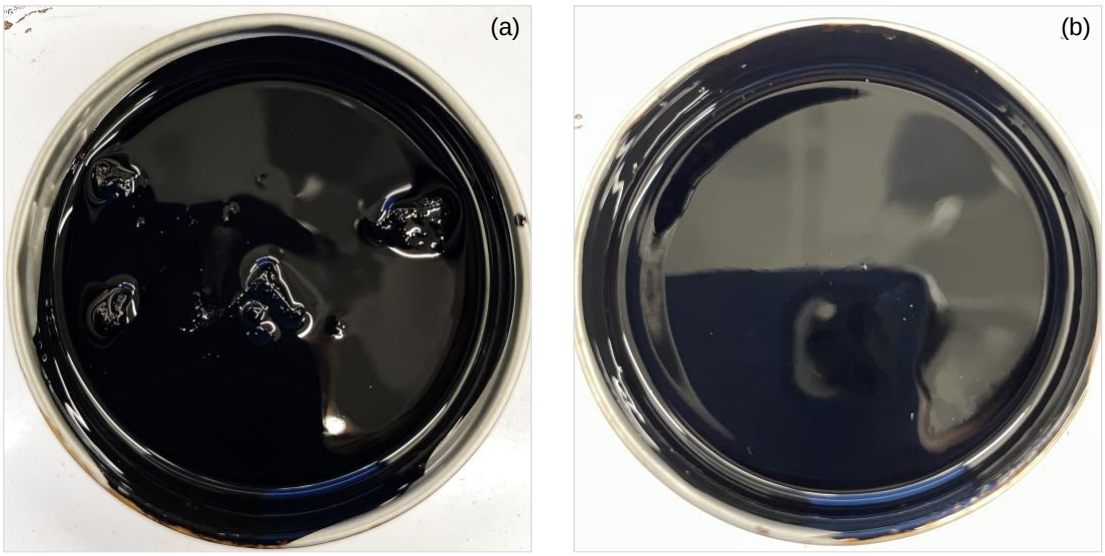

Figure 8. (a) RAS lumps visible after blending in original state (b) No RAS lumps visible after RTFO aging

DSR testing was conducted on original and RTFO aged samples according to AASHTO T 315. The results were analyzed to determine the standard high-temperature grade according to AASHTO M 320 and the continuous high-temperature grade according to ASTM D7463. DSR testing was conducted at a minimum of two temperatures, one passing the AASHTO M 320 high-temperature grading criteria and one failing. The RAS binder was only tested in the original age condition since RTFO testing was not possible; however, the RTFO-aged binder criteria given in AASHTO M 320 was used for high-temperature grade determination under the assumption that the binder would not undergo significant further oxidative age hardening if subjected to short-term aging.

3.2.2 Additive Dosage Selection

Blends 3 to 9 in Table 6 were each prepared at two trial additive dosage levels. For blends containing RAS, dosages of 10 percent and 6 percent by weight of total binder were used for all blends because the dosages estimated using Equations **(12)** and **(13)** exceeded the maximum dosage recommended in NCHRP 09-58 of 10 percent when using the PG 64-22 virgin binder and was very close to this limit when using the PG 58-28 virgin binder. For blends containing RAP, one of the two dosages was selected to coincide with the dosage level calculated using Equations (12) and (13) with X = 1.82. In this case, the high-temperature continuous grade of the blends of virgin and recycled binders were first calculated at the original ($PGH_{\text{Blend, original}}$) and RTFO ($PGH_{\text{Blend, RTFO}}$) levels using Equation **(13)** based on the measured high-temperature PG results of the recycled and virgin binders using the mixture RAP_{BR} of 0.36; the minimum of the two calculated grades was used in Equation **(12)** as the PGH_{Blend}. For a given blend, once PG_{Blend} was determined, it was used along with a PGH_{Target} of 64 and X value of 1.82 in Equation **(13)** to calculate the first dosage level. The second dosage level was set at 2 percent by total weight of binder.

Blends of virgin and recycled binder were prepared in the same way as described under Virgin and Recycled Binder Characterization. Following blending of the virgin and recycled binder, the blended system was placed back in an oven set to 165°C for one minute. Then, the binder was removed from the oven, the additive was added, and the system was mixed for an additional minute using the power drill. After mixing, a portion of each blend was poured into an RTFO bottle and subjected to short-term aging according to AASHTO T 240 and a portion was used directly for DSR testing. Original and RTFO-aged samples of blends containing RAP and RTFO-aged samples of blends containing RAS only were subjected to DSR testing in accordance with AASHTO T 315 and AASHTO M 320 for high-temperature grade determination. DSR testing was conducted at a minimum of two temperatures, one passing the AASHTO M 320 high-temperature grading criteria and one failing. Using the results, continuous high-temperature grades were calculated according to ASTM D7463. The results were used to evaluate four methods of selecting the additive dosages.

3.2.2.1 Method 1

Linear regression of the continuous high-temperature grade results was applied to determine the X_i values in Equations **(14)** and **(15)** using fixed intercepts corresponding to the $PGH_{\text{Blend, original}}$

and $PGH_{\text{Blend, RTFO}}$ values determined from Equation **(13)**. The corresponding additive dosages required to yield the target high-temperature grade of 64°C at the original and RTFO age levels (i.e., Selected $\text{Additive}_{\text{Original}}$ (%) and Selected $\text{Additive}_{\text{RTFO}}$ (%)) were calculated using Equations **(16)** and **(17**), respectively. The minimum of the calculated Selected Additive contents from the two age levels was reported as the selected dosage and the corresponding *X* values were tabulated. For the RAS blends, the same procedure was followed using results corresponding to the RTFO age level only.

$$PGH_{\text{Blend+Additve,original}} = PGH_{\text{Blend,original}} - X_{\text{original}} \times \text{Additive}(\%) \quad \textbf{(14)}$$

$$PGH_{\text{Blend+Additve,RTFO}} = PGH_{\text{Blend,RTFO}} - X_{\text{RTFO}} \times \text{Additive}(\%) \quad \textbf{(15)}$$

$$\text{Selected Additive}_{\text{original}}\ (\%) = \frac{PGH_{\text{Blend, original}} - 64}{X_{\text{original}}} \quad \textbf{(16)}$$

$$\text{Selected Additive}_{\text{RTFO}}\ (\%) = \frac{PGH_{\text{Blend, RTFO}} - 64}{X_{\text{RTFO}}} \quad \textbf{(17)}$$

where *PGH* is the high temperature grade; *X* is the slope rate of the additive; Selected Additive is the amount required to restore the high-temperature grade to 64°C.

3.2.2.2 Method 2

For the blends containing PG 58-28 virgin binder (i.e., Blends 5, 6, and 8 in Table 6), the required additive dosages were also calculated using an analogous approach as described above, but using the measured PGH_{Blend} values rather than those estimated using Equation **(13)**. This process allowed for assessing the impacts of any errors introduced from estimating the grade of virgin-recycled binder blends using Equation **(13)** on the selected additive dosage.

3.2.2.3 Method 3

The collective results of blends containing the same additive were used to evaluate the universality of the slope of the change in the continuous high-temperature PG at the RTFO age level (ΔPGH_{RTFO}) versus additive content (termed X_{Additive}). The results of blends with the same additive (i.e., Blends 3, 7, and 8 that all contain R1 were aggregated, and Blends 4 and 5 were aggregated that both contain E1) and linear regression was used to determine the X_{Additive} in Equation **(18**), using a fixed intercept of zero. Then, the selected additive contents according to Method 3 (i.e., Selected $\text{Additive}_{\text{RTFO}}$ (%)) were calculated using Equation **(19**). Method 3 was

only applied to the RTFO age level results because dosages selected using Methods 1 and 2 were found to be driven by the RTFO age level for these blends.

$$\Delta PGH_{RTFO} = PGH_{\text{Blend+Additve,RTFO}} - PGH_{\text{Blend,RTFO}} = X_{\text{Additive}} \times \text{Additive}(\%) \quad \textbf{(18)}$$

$$\text{Selected Additive}_{\text{RTFO}}\ (\%) = \frac{PGH_{\text{Blend, RTFO}} - 64}{X_{\text{Additive}}} \quad \textbf{(19)}$$

3.2.2.4 Method 4

Equations **(12)** and **(13)** were used to calculate the required dosage for each blend using the average *X* values reported in the NCHRP 09-58 project. The selected dosages corresponding to the *X* values suggested for both petroleum-based aromatic extracts (Method 4A) and other additive types (Method 4O) were tabulated for the blends containing extenders whereas dosages were only calculated using the *X* value suggested for all other additive types (Method 4O) for the blends containing recycling agents. The recycling agents evaluated are both vegetable oils. Vegetable oil recycling agents were included as part of the dosage selection procedure in NCHRP Project 09-58 and included in the non-aromatic extract category (Epps Martin et al. 2020). However, the slopes suggested for both classes of materials were evaluated for blends containing extenders because it is not clear if the extenders evaluated are more similar to aromatic extracts or the other product category used in NCHRP Project 09-58. The extenders evaluated herein are derived from petroleum extracts, similar to aromatic extracts. However, they contain REOB and most closely align with the paraffinic oil classification given in NCHRP Project 09-58, but paraffinic oils were not evaluated as part of the dosage selection procedure development in that project (Epps Martin et al. 2020).

3.2.3 Blend Verification at a Selected Dose

Blends 3, 5, 6, 7 and 9 in Table 6 were prepared at the additive dose selected using Method 1. The verification blends were prepared and tested using the same procedures used as part of dosage selection to determine their continuous high-temperature grades. The results were compared to the expected high-temperature PG from dosage selection analysis conducted according to Methods 1 through 4.

3.2.4 Hamburg Mixture Testing for Rutting Evaluation

HWT testing was completed in accordance with AASHTO T 324 for a subset of the study blends at the dosages selected according to Method 1, see Table 6. Laboratory-mixed samples were

prepared and subjected to short-term aging for two hours at 135°C as recommended in the NCHRP Project 09-52 (Newcomb et al. 2015); this procedure was found to yield approximately the same age level as the asphalt binder RTFO procedure in the NCHRP Project 09-61 (Bonaquist et al. 2021). The HWT test specimens were fabricated with 7 ± 0.5 percent air void content and a height of 62 mm (2.44 in.) and diameter of 150 mm (6 in.) using the gyratory compactor. Throughout the HWT test, specimens were submerged under the water at 50°C in order to induce moisture damage and control the testing temperature. After preconditioning the specimens for 45 minutes, they were subjected to the repeated rolling steel wheel with the constant load of 705 ± 4.5 N (158 ± 1.0 lb) and passing rate of 52 ± 2 passes/min. The rut depth was measured using the average of five readings from LVDTs along the specimen center. The test results were reported as the number of wheel passes to reach a 12.5-mm rut depth. Tests were terminated at 20,000 cycles if a rut depth of 12.5-mm had not been reached. NCHRP Project 09-58 proposed that mixtures in climates with grades of PG 64-22, such as North Carolina, should exceed 10,000 cycles to a failure rut depth of 12.5-mm to ensure adequate rutting resistance (Epps Martin et al. 2020).

3.3 Results

3.3.1 Virgin and Recycled Binder AASHTO M 320 High-Temperature Grades

Table 7 shows the continuous high-temperature grades for the virgin binders, recycled binders, and blends of virgin and recycled binders. The numbers in parentheses in Table 7 correspond to high-temperature grades estimated using Equation **(13)** from the virgin and recycled binder high-temperature grade results. The results show that the virgin binders met specified high-temperature grade. The RAS binder has an extremely high measured grade of 176.6°C. The RAS high-temperature grade is considered an estimate because the test temperatures used were outside of the calibration range of the rheometer so the accuracy of the temperature recording from the DSR is unknown. Nevertheless, the results were used as part of dosage selection according to Methods 1, 2, and 4.

For the binder blends, the results show that both the estimated and measured high-temperature grades exceed the intended grade of 64°C even when a PG 58-28 virgin binder is used. Comparing the results of direct measurements of the blends' high-temperature grades against those estimated using Equation **(13)** reveal differences ranging from 0.7°C (blend of PG

58-28 virgin binder and RAP at the RTFO age level) to 3.6°C (blend of PG 58-28 virgin binder and RAS binder). The implications of these discrepancies on additive dosage selection were assessed by comparing the results of Methods 1 and 2 for blends prepared with the PG 58-28 virgin binder.

Table 7. Virgin and Recycled Binder AASHTO M 320 Continuous High-temperature Grades

Recycled Binder	Virgin Binder	Original Binder Grade	RTFO Binder Grade
--	PG 58-28	60.7	61.2
--	PG 64-22	67.3	69.0
RAP	--	91.0	90.7
RAS	--		176.6
RAP	PG 58-28	73.4 (71.5)	72.5 (71.7)
RAS	PG 58-28	--	78.4 (82.0)
RAP	PG 64-22	(75.7)	(76.8)
RAS	PG 64-22	--	(88.4)

3.3.2 Dosage Selection

Table 8 shows the compiled slope of the blended systems according to Methods 1 through 4. A maximum dosage of 10 percent was recommended in NCHRP Project 09-58 (Epps Martin et al. 2020); therefore, 10 percent is shown in parentheses in cases where the calculated dose exceeded this maximum limit. A detailed discussion of the results of each method along with comparisons across the methods is provided in the following sections.

Table 8. Slopes and Selected Additive Dosages

Blend	Slope, *X*			Selected Additive (%)				
	Method 1	Method 2	Method 3	Method 1	Method 2	Method 3	Method 4	
							A	O
64.RAP.R1	2.33	--	2.42	5.5	--	5.3	--	6.4
64.RAP.E1	1.27	--	1.17	10.1 (10.0)	--	11.0 (10)	11.2 (10.0)	8.5
58.RAP.E1	1.08	1.23	1.17	7.0	6.9	6.6	5.4	4.1
58.RAP.E2	2.06	2.53	--	3.6	3.7	--	5.4	4.1
64.RAS.R1	2.20	--	2.42	11.0 (10.0)	--	10.1 (10.0)	--	13.4 (10)
58.RAS.R1	2.69	2.27	2.42	6.6	6.3	7.4	--	9.8
64.RAS.R2	3.23	--	--	7.4	--	--	--	13.4 (10.0)

3.3.2.1 Method 1

Figure 9 shows the dosage selection results according to Method 1 for Blends 3 to 9. The resultant Equation **(14**) or **(15)** used to select the dosage required to restore the continuous high-temperature grade to 64°C is shown for each blend in Figure 9. The legend in this figure indicates whether the original, Equation **(14**), or RTFO, Equation **(4)**, results dictated the selected dose (i.e., yielded a lower required dose). The selected dose data points correspond to those calculated using the equations shown to yield a high-temperature grade of 64°C. The intercept values shown correspond to the $PGH_{\text{Blend, original}}$ and $PGH_{\text{Blend, RTFO}}$ estimates using Equation (13). Figure 9 (a) through (d) shows that for three out of the four RAP blends evaluated, the RTFO age level results dictated the selected dose. Overall, Figure 9 shows that the relationship between the blend high-temperature grade and additive content adhere to the linear relationship prescribed by Equations **(14**) and **(15)** quite well based on the high R^2 values shown. The first exception is the RTFO aging level for 58.RAP.E2, Figure 9 (d). This blend is only RAP blend where the original age level dictated the selected dose. The second exception is 64.RAS.R2, shown in Figure 9 (g). Blend 64.RAS.R2 was the only blend that contained additive R2. The results in Figure 9 (b), (c), and (e) show that extrapolation was required to predict the dosage that would yield a high-temperature grade of 64°C. Note that higher dosages for these blends were not tried for additive E1, shown in Figure 9 (b) and (c), because this would have led to REOB contents that exceed the NCDOT's maximum limit. A higher dose was also not attempted for blend 64.RAS.R1, shown in Figure 9 (e), because this would have yielded a dose higher than the maximum of 10 percent recommended in NCHRP Project 09-58. Figure 9 shows that the slopes of the blend high-temperature PG versus additive content differ considerably among blends, spanning a range of 1.08 to 3.23. Within a given additive type (i.e., Figure 9 (a),

(e), and (f); Figure 9 (b) and (c)), the slopes for blends containing different virgin and recycled binders are generally more similar than across blends containing different additive types.

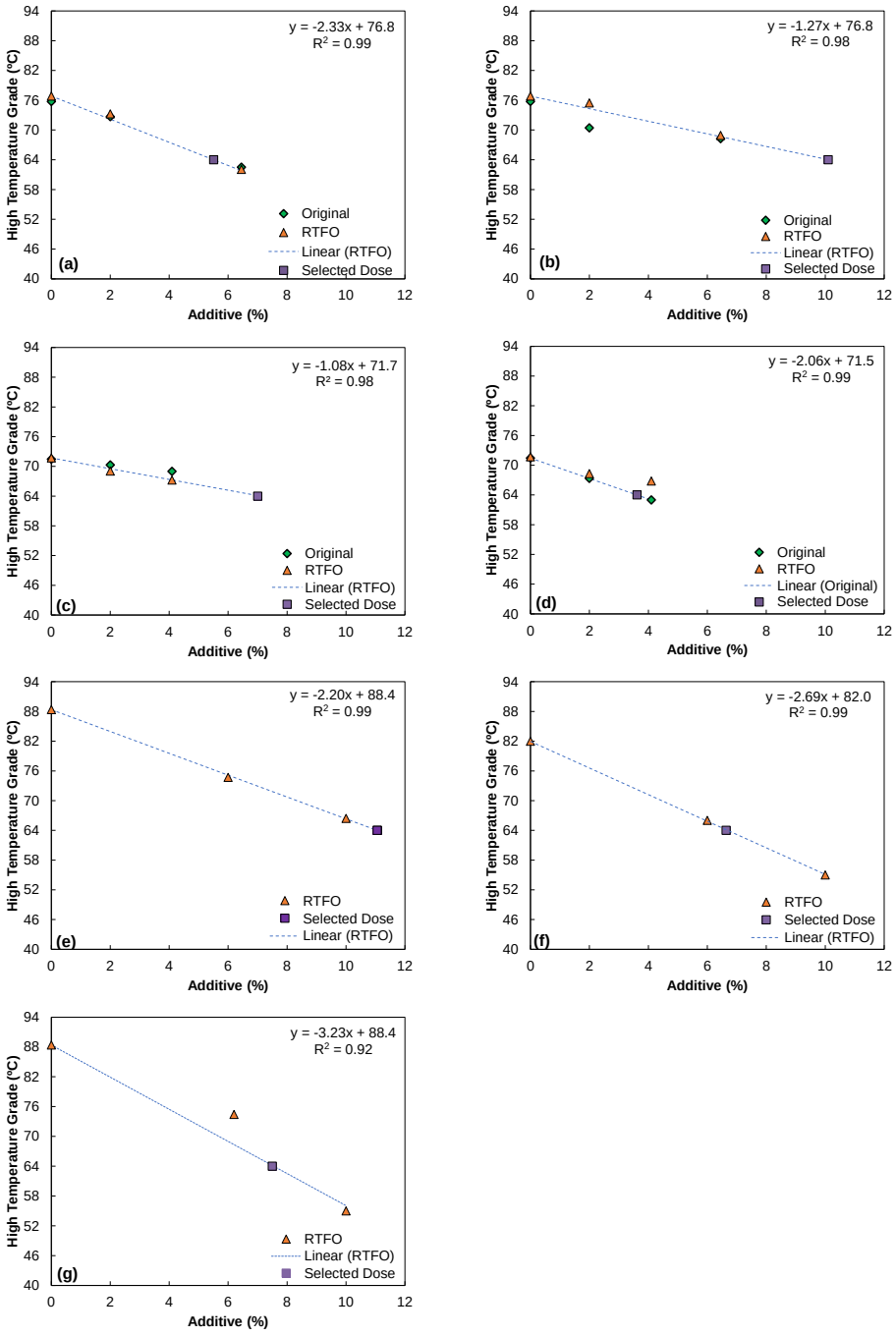

Figure 9. Dosage selection results for blends according to Method 1: (a) 64.RAP.R1, (b) 64.RAP.E1, (c) 58.RAP.E1, (d) 58.RAP.E2, (e) 64.RAS.R1, (f) 58.RAS.R1, (g) 64.RAS.R2.

3.3.2.2 Method 2

Figure 10 shows the comparison between the dosage selection results according to Method 1 and Method 2 for Blends 5, 6, and 8. Method 2 is the same as Method 1 with the exception that the intercept of the line fit to the relationship between the high-temperature grade and additive content is the measured grade of the blend of the recycled and virgin binder rather than that estimated using Equation **(13)**. Figure 10 includes the results at only the age level that dictated the selected dosage for the given blend (i.e., yielded the minimum selected dosage). The selected dose data points correspond to those calculated using the equations shown to yield a high-temperature grade of 64°C. The results show that the two methods yield somewhat different slopes of high-temperature grade versus additive content due to the difference in intercept values. However, the calculated dosages to restore the high-temperature grade to 64°C from the two methods are very close in all cases with a maximum difference of 0.3 percent.

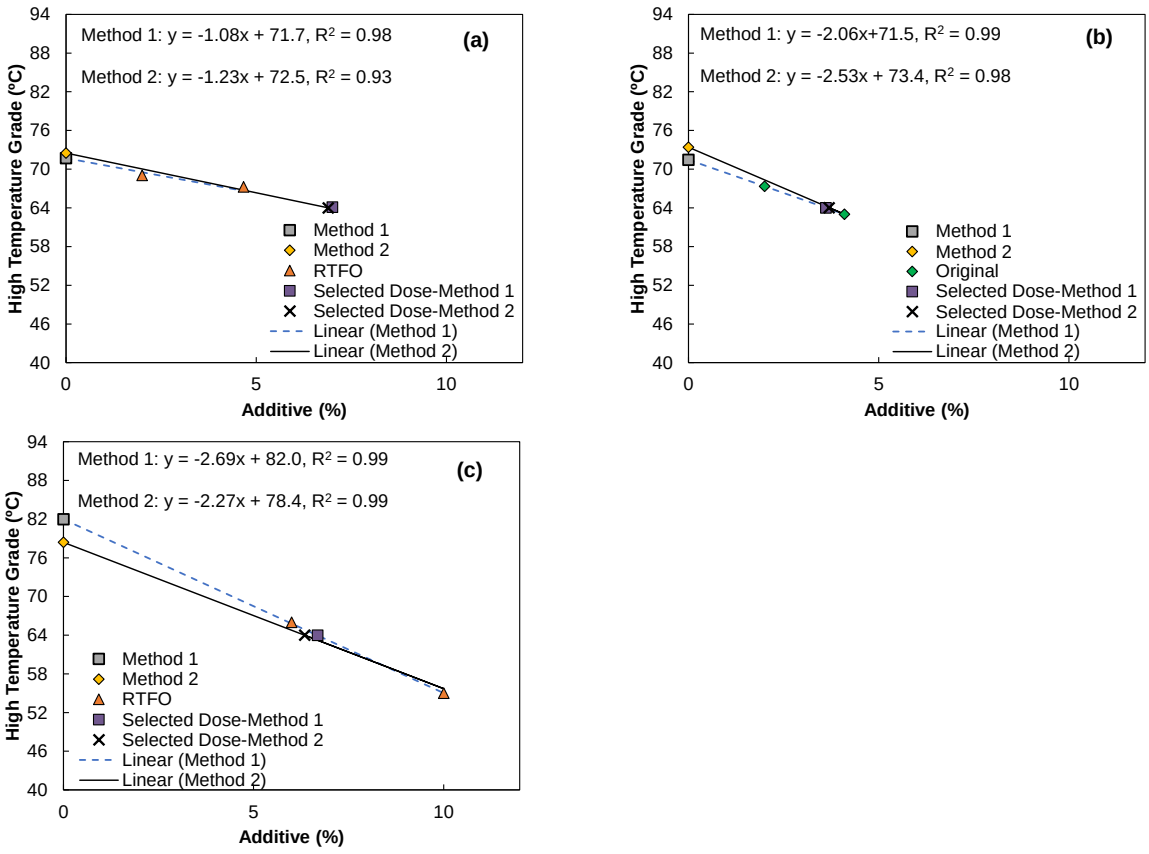

Figure 10. Comparison of dosage selection according to Methods 1 and 2 for (a) 58.RAP.E1, (b) 58.RAP.E2, and 58.RAS.R1

3.3.2.3 Method 3

Figure 11 shows the relationship between the change in high-temperature grade versus additive content at the RTFO age level for (a) the collective results of blends containing R1 (Blends 3, 7, and 8) and (b) the collective results of blends containing E1 according to Method 3 (Blends 4 and 5). The change in high-temperature grades were calculated using the estimate of the high-temperature grade of the blend of recycled and virgin binder using Equation **(13)**. Linear regression was used to determine the slope (X_{additive}) values for R1 and E1 given in Equation **(19)** using the results shown in Figure 11 (a) and (b), respectively. The corresponding X_{additive} values and R^2 values are conveyed by the equations shown in Figure 11. The values calculated when using the measured high-temperature grades to calculate the difference in high-temperature grade due to the additive are also shown for blends 58.RAS.R1 and 58.RAP.E1 as faded data series to visually show the effect of the error introduced by Equation **(13)** on the calculated high-temperature grade differences. The results suggest good agreement between the Equation **(18)**

results and the measured data, suggesting promise for the use of Method 3 in practice. Method 3 is advantageous in that it would not require testing of blends prepared at trial dosages for each new blend of virgin and recycled binder. Rather, a representative set of virgin binder, recycled binder, and additive blends could be tested and used to calibrate Equation **(18)**, which then could be applied for dosage selection for new virgin-recycled binder blends using the same additive. Some of the scatter in Figure 11 (a) could be due to the uncertainty in the RAS binder high-temperature grade used in Equation **(13)** as it is evident that the 58.RAS.R1 data better aligns with the PG 64.RAP.R1 data when the measured rather than estimated PGH_{Blend} value is used.

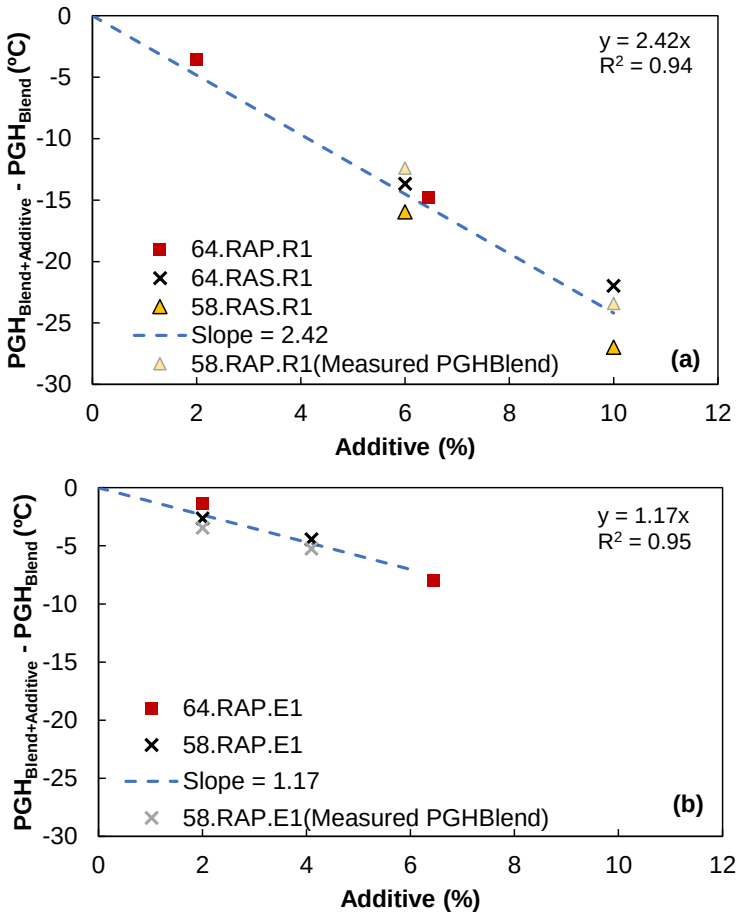

Figure 11. Relationships between high-temperature grade change and additive content for (a) all blends containing R1 and (b) all blends containing E1

3.3.3 Comparison of the Different Methods

Figure 12 shows the comparison of slopes of high-temperature grade versus additive content obtained from Methods 1 through 3 as well as the values used in Method 4 based on the average values measured for aromatic extracts (A) and other (O) additive types in the NCHRP Project 09-58. The error bars in Figure 12 convey the standard error of the slope values. Figure 13 shows the dosages intended to restore the binder grade to 64°C calculated using the different methods. Figure 12 shows that Methods 1 through 3 generally yield similar slope values and dosages. The maximum difference in selected dosages between Methods 1 and 2 was 0.3 percent and the maximum difference between Methods 1 and 3 was 0.9 percent. The maximum differences between Methods 1 and 3 coincide with calculated dosages that exceed 10 percent, which is the maximum limit recommended in the NCHRP Project 09-58 (Epps Martin et al. 2020) and therefore, both would effectively both lead to a selected dose of 10 percent. The slopes of all blends containing recycling agents determined using Methods 1 through 3 exceeded those from Method 4O. Consequently, Method 4O yielded a higher dose than Methods 1 through 3 for all blends containing R1 and R2, suggesting the approach may yield a high-temperature grade that falls below the intended grade. The slope used in Method 4A is close to the results of blends containing E1 and the slope in Method 4O is relatively close to the results of blends containing E2 results; therefore, the extenders evaluated do not align clearly with either aromatic or other additive type classification proposed in the NCHRP Project 09-58 simplified dosage selection procedure.

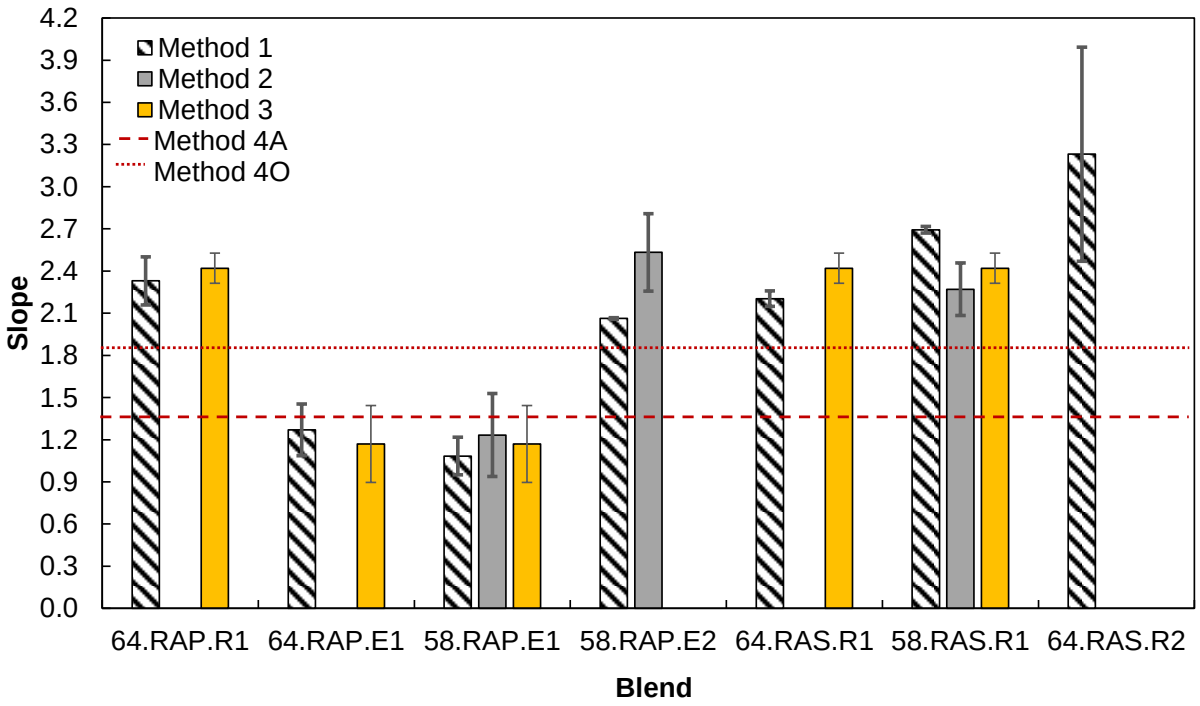

Figure 12. Slope of the continuous high-temperature grade change versus additive content based on the different methods evaluated

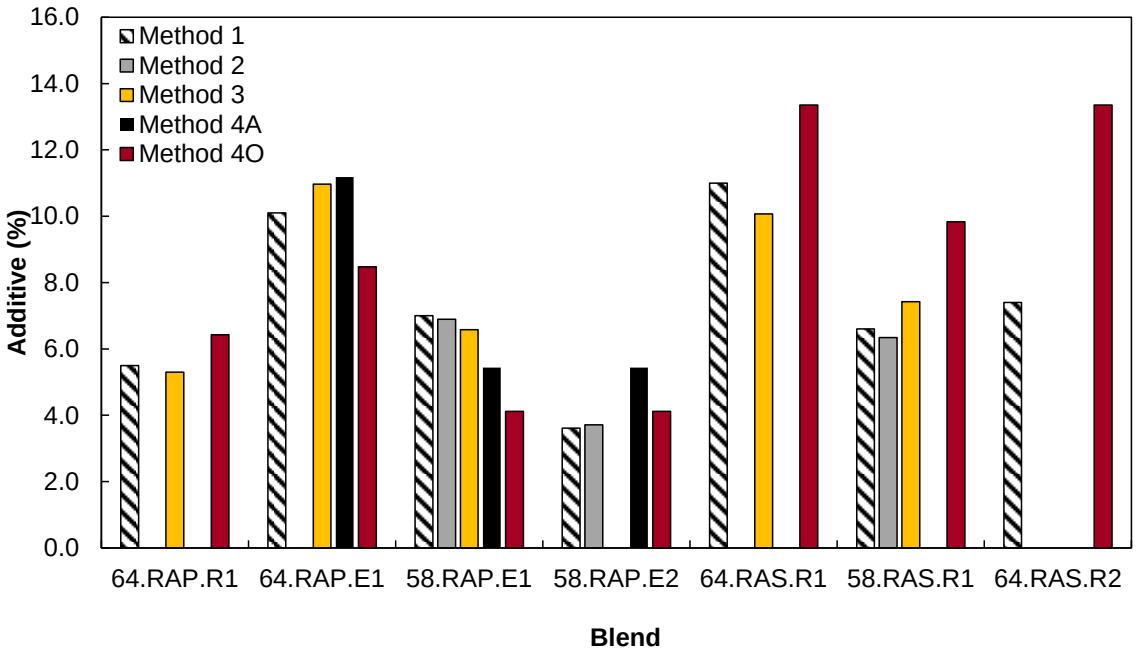

Figure 13. Selected doses according to the different methods evaluated

3.3.4 Verification Testing Results

Table 9 shows the verification testing results of the additional blends prepared at the dosages selected according to Method 1 along with the blends of recycled binder and the PG 58-28 binder in the absence of any additive. In addition, Table 9 shows the AASHTO M 320 continuous high-temperature grades predicted at the selected dosage based on the dosage selection results of Methods 1 through 4. Figure 14 shows the AASHTO M 320 continuous high-temperature grade results graphically. The verification blends all passed high-temperature grading criteria at 64°C according to AASHTO M 320. The results also show that blend 64.RAS.R2 passed grading criteria at 70°C despite the intended grade being 64°C.

The results demonstrate some notable discrepancies between the measured and predicted high-temperature grades. The expected grades according to Method 1 are very close to 64°C since this coincides with the basis for the dosage selection for the verification blends, with the exception of 64.RAS.R1 where the calculated dose exceeded the maximum limit of 10 percent. The expected grades according to Methods 2 through 4 differed from Method 1 somewhat due to differences in the intercept and/or slope values used to predict the relationship between high-temperature grade and additive content. Differences in the continuous high-temperature grades

measured using the verification samples compared to those expected from Method 1 range from 0.2°C to 5.8°C. The maximum difference in the continuous grade measured from the two replicate samples of a given verification blend was 0.2°C, indicating that the discrepancy between the measured grades of verification samples and the predicted values is due to variability among the batches of blends prepared with a given set of materials and/or deviation from the assumed linear relationship between the additive content and blend high-temperature grade.

With the exception of blend 64.RAS.R2, the average errors between expected grades and those measured using the verification samples were less than 2.0°C for Methods 1 through 3. Methods 1 through 3 yielded similar accuracy in terms of agreement with the verification testing results. Therefore, Method 3 is most appealing because it would negate the need for virgin binder-recycled binder blend-specific dosage selection testing after a reliable measure of the grade reduction versus additive content slope is obtained for a given product. Method 4 continuous high-temperature grade results are the most distinct from those measured in verification testing, further suggesting that additive-specific dosage selection calibration is necessary.

Table 9. Comparison between High-Temperature Grades Predicted by Methods 1 through 4 at the Dosages Selected According to Method 1 and Those Measured in Verification Testing

Blend	Additive (%)	AASHTO M 320 Continuous High-Temperature Grade (ºC)					
		Method 1	Method 2	Method 3	Method 4		Verification Result
					A	O	
58.RAP	--	--	--	--	--	--	72.5
58.RAS	--	--	--	--	--	--	78.4
64.RAP.R1	5.5	64.0	--	63.5	--	65.7	64.2
58.RAP.E1	7.0	64.2	63.9	63.6	61.8	58.8	67.3
58.RAP.E2	3.6	64.0	67.5	--	66.5	64.9	67.7
64.RAS.R1	10.0	66.3	--	64.2	--	70.2	65.0
64.RAS.R2	7.4	64.5	--		--	74.9	70.3

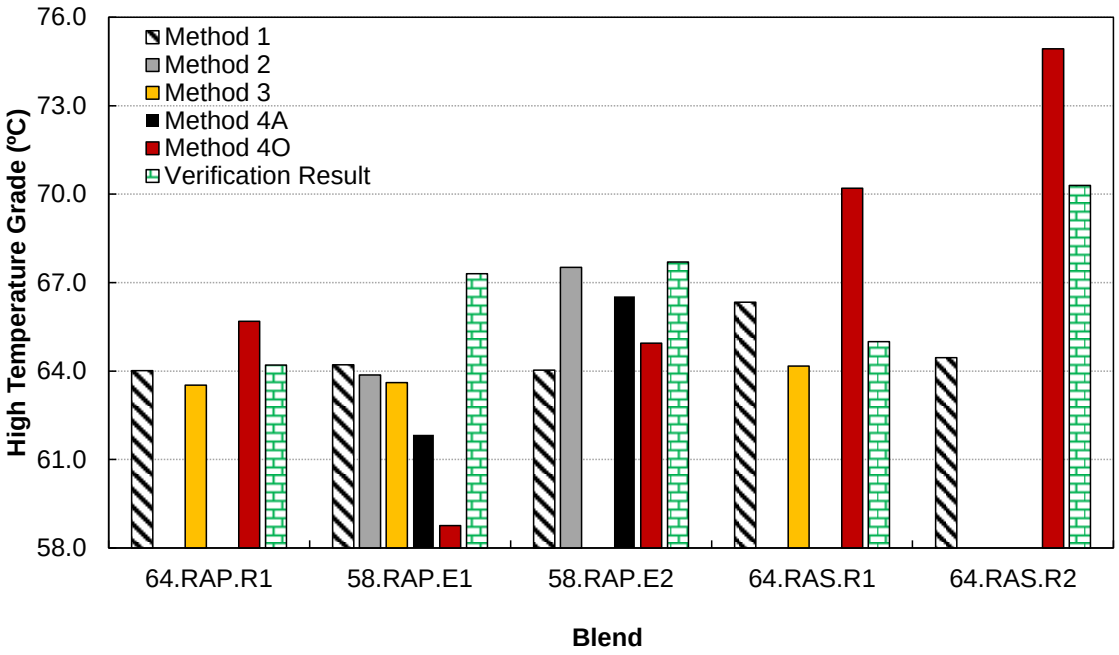

Figure 14. Continuous AASHTO M 320 high-temperature performance grades predicted based on the different dosage selection methods evaluated and measured via verification testing at the dosages selected according to Method 1

The verification testing results highlight inherent uncertainty in additive dosage selection procedure that should be accounted for as part of additive dosage selection. To visually depict the uncertainty in the dosage selection results herein, a 90 percent confidence interval was constructed for the Method 3, i.e., Equation **(18)**, results of additive R1. The results are shown in Figure 15. The results suggest uncertainty in the high-temperature grade reduction of around 3°C to 4°C at additive contents near six percent, and higher uncertainty at lower and higher dosages. Efforts to reduce uncertainty should be considered as part of the establishment of a robust dosage selection procedure. Potential ways to reduce the span of the confidence interval include incorporating the results of additional blends of the same materials at additional dosages and incorporating additional virgin and recycled binder blends. In addition, it is speculated that using the measured rather than estimated high-temperature grade of the blend of recycled and virgin binder, particularly in the case of RAS binders, may reduce uncertainty. A reduction in variability may also be achieved by establishing more robust sample preparation and blending procedures. Even with these measures, uncertainty will still exist. Therefore, it is suggested that uncertainty quantification be incorporated into the additive dosage selection process either by

dosage selection according to the lower bound of a confidence interval or by targeting a higher continuous high-temperature than the minimum accepted based on measured uncertainty.

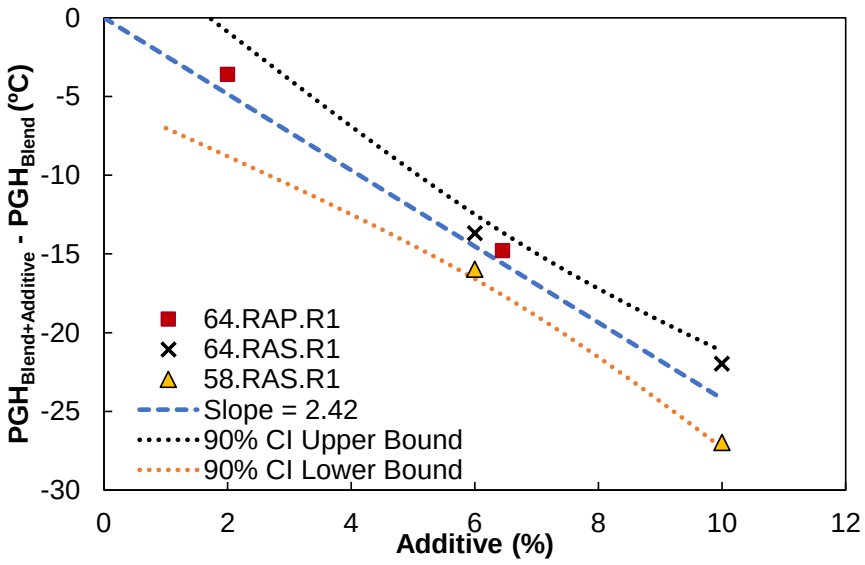

Figure 15. Confidence interval (CI) for Method 3 results of blends prepared using R1

3.3.5 Hamburg Wheel-Track Test Results

Figure 16 shows the HWT test results of the mixtures prepared at the dosages selected according to Method 1 for select blends along with the results of control mixtures prepared without any additives, which coincide with current mixture practices in North Carolina. Figure 16 also includes the results of a mixture prepared that was expected to fail the HWT rutting criteria (58.RAP.R1); this mix was prepared using the same R1 content as 64.RAP.R1 and thus, expected to have a high-temperature grade below 64°C. The error bars shown in Figure 16 reflect the standard error of the test results. NCHRP Project 09-58 suggested a minimum of 10,000 cycles to failure before a rut depth of 12.5 mm is reached in the HWT for warm climates, such as North Carolina to ensure adequate rutting resistance (Epps Martin et al. 2020). With the exception of the mix intentionally designed with inferior rutting resistance, all mixtures pass this minimum limit, suggesting that dosage selection to restore the high-temperature grade may yield adequate rutting resistance even if only partial recycled binder availability exists in the mixture. However, this finding should be confirmed with testing of additional mixtures. Interestingly, the mixture containing 58.RAP.E2 mixture exhibits superior rutting resistance to the 58.RAP mixture based on the HWT results despite including a softening additive. The other mixtures

containing an additive show a reduction in rutting resistance compared to the corresponding control mixture without any additive.

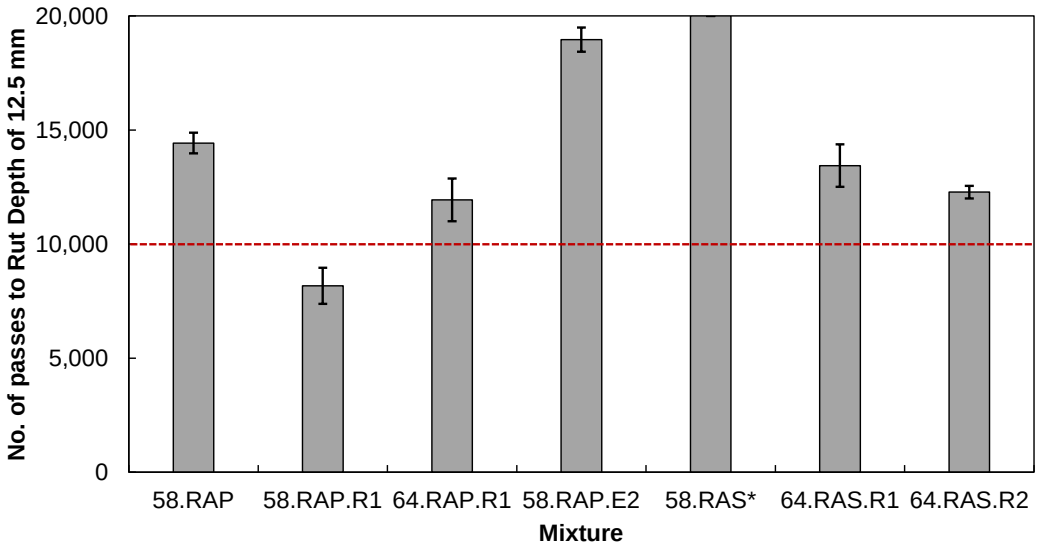

*Failure not reached after 20,000 cycles

Figure 16. Hamburg Wheel-track test results

3.4 Conclusions and Recommendations

The following conclusions and recommendations are drawn from the results of this study:

1. Different recycling agent and extender products can yield different rates of change in the asphalt binder continuous AASHTO M 320 high-temperature grade with additive content.
2. The rate of change in asphalt binder continuous AASHTO M 320 high-temperature grade with additive content for a given additive was similar for different recycled binder and virgin binder combinations, suggesting that an additive-specific dosage selection procedure could be established using testing of a limited set of recycled and virgin binder blends and then applied to estimate the required additive dose for alternative recycled-virgin binder blends if the high-temperature grade of the virgin-recycled binder blend in the absence of any additive is known.
3. Testing of blends containing RAS at the original age level should be avoided as residual agglomerations of RAS may remain. It was found that RTFO aging can be used to achieve a homogenous binder blend with RAS.

4. Testing of virgin-recycled binder blends rather than relying on linear blending theory to estimate the high-temperature grade is recommended, especially in the case of RAS binders because conducting high-temperature grading of RAS binders imparts considerable uncertainty.
5. The AASHTO M 320 high-temperature grading results of verification blends prepared at selected dosages yielded considerable discrepancies with those predicted from dosage selection testing in some cases; these results suggest uncertainty in the dosage selection results should be incorporated into the dosage selection procedure.
6. All Hamburg Wheel-Track tests conducted on asphalt mixtures prepared at dosages intended to achieve a continuous AASHTO M 320 grade of 64°C, which coincides with the minimum specified grade for the mixtures evaluated in the absence of recycled materials, passed the minimum criteria proposed in NCHRP Project 09-58 for the climatic conditions in which the mixtures were designed for.

3.5 Acknowledgements

The author would like to acknowledge Lei Xue, Saqib Gulzar, and Jaime Preciado for their assistance in sample preparation and analysis. Testing and analysis was supported by the North Carolina Department of Transportation under NCDOT RP 2020-16

3.6 References

1. Williams, B.A., J. R. Willis, and J. Shacat. Asphalt Pavement Industry Survey on Recycled Materials and Warm-Mix Asphalt Usage 2019, *NAPA Information Series 138*, 2020.
2. Copeland, A. Reclaimed Asphalt Pavement in Asphalt Mixtures: State of the Practice, *Report No. FHWA-HRT-11-021*, Federal Highway Administration, Washington, D.C., 2011.
3. NCAT. NCAT Researchers Explore Multiple Uses of Rejuvenators, *Asphalt Technology News, Vol. 26, No. 1.* 2014.
4. Daly, W.H. Relationship Between Chemical Makeup of Binders and Engineering Performance, *NCHRP Synthesis 511*, National Academies, Washington, D.C., 2017.
5. Kaseer, F., A. Epps Martin, and E. Arambula-Mercado. Use of recycling agents in asphalt mixtures with high recycled materials contents in the United States: A literature review, *Construction and Building Materials, Vol. 211, pp. 974-987.* 2019.
6. Epps Martin, A., et al. The Effects of Recycling Agents on Asphalt Mixtures with High RAS and RAP Binder Ratios, *NCHRP Report 927*, National Academies, Washington, D.C., 2019.
7. McDaniel, R. and R.M. Anderson. Recommended Use of Reclaimed Asphalt Pavement in The Superpave Mix Design Method: Technician's Manual, *NCHRP Report 452*, National Academies, Washington, D.C., 2001.
8. Al-Qadi, I., S. Carpenter, G. Roberts, H. Ozer, Q. Aurangzeb, M. Elseifi, and J. Trepanier. Determination of Usable Residual Asphalt Binder in RAP. *FHWA Report FHWA-ICT-09-031*, Illinois Center for Transportation Series No. 09-031, 2009.
9. Newcomb, D., A. Epps Martin, F. Yin, E. Arambula, E. Park, A. Chowdury, R. Brown, C. Rodezno, N. Tran, E. Coleri, D. Jones, J. Harvey, and J. Signore. Short-term Laboratory Conditioning of Asphalt Mixtures. *NCHRP Report 815*, National Academies, Washington, D.C., 2015.
10. Bonaquist, R., J. Adams, and D. Anderson. Asphalt Binder Aging Methods to Accurately Reflect Asphalt Mixture Aging. *NCHRP Report 967*, National Academies, Washington, D.C., 2021.

Chapter 4 Practical Methods to Construct Asphalt Binder Master Curves and Calculate Christensen-Anderson Model Parameters

The work presented in this chapter has been published in the Transportation Research Record, Journal of the Transportation Research Board, © National Academy of Sciences: Transportation Research Board 2023. https://doi.org/10.1177/03611981231169274. It has been reprinted here according to SAGE's author archiving and re-use guidelines.

4.1 Introduction

Master curves are used to describe the time and temperature dependence of the rheological behavior of asphalt binders. Master curves are constructed by conducting rheological measurements over a range of frequencies (or times) and temperatures. The set of measurements (e.g., modulus, phase angle) at a given temperature is called an isotherm. For thermorheologically simple materials, such as asphalt binder, isotherms can be shifted along the log frequency (or log time) axis by temperature-dependent shift factors to form a smooth and continuous 'master curve'. Models are fit to represent the master curve and shift factors to understand the overall rheological behavior of asphalt binders and readily obtain properties at any desired temperature and frequency (or time) combination.

The Strategic Highway Research Program (SHRP) considered the use of master curves as the basis for providing rational specification parameters (Anderson et al. 1994). The effort yielded the Christensen-Anderson (CA) model (Christensen 1992), which persists as the most widely applied asphalt binder master curve model today. The CA model is a phenomenological model applied to describe the reduced frequency (ω_R) dependence of asphalt binder dynamic shear modulus ($|G^*|$) and phase angle (δ) and is given in Equations **(20)** and **(21)**.

$$|G^*|(\omega) = G_g \left[1 + \left(\frac{\omega_c}{\omega_R} \right)^{(\log 2/R)} \right]^{-R/\log 2} \quad \textbf{(20)}$$

$$\delta(\omega) = \frac{90}{\left[1 + \left(\frac{\omega_R}{\omega_c} \right)^{\log 2/R} \right]} \quad \textbf{(21)}$$

where G_g = glassy modulus, often assumed to equal 1 GPa, which is supported by experimental evidence from asphalt binders (Christensen 1992) and is also commonly accepted for other organic materials (Ferry 1980); ω_c = crossover frequency, equal to the reduced frequency where

the phase angle equals 45º; and R = rheological index, equal to the logarithmic distance between G_g and $|G^*|$ at ω_c.

The $|G^*|$ model was derived from the cumulative form of a skewed logistic function (Christensen 1992). The δ was derived from earlier work by Dickinson and Witt (Dickinson & Witt 1974) that indicates δ is directly proportional to the first derivative of log $|G^*|$ with respect to log ω_R (Christensen 1992).

The CA model parameters themselves have been proposed as potential measures to evaluate asphalt binders (Christensen 1992). The ω_c defines the point where the storage and loss moduli are equal and thus, constitutes a transition point from elastic- to viscous-dominated behavior. As asphalt binders undergo oxidative aging, the ω_c decreases and the R value increases. While single-point measurements were ultimately adopted for asphalt binder specification during SHRP, recent studies suggest master curve-based parameters may better capture the cracking resistance of asphalt binders than the current specification parameters. Studies suggest that the R value in the CA model is an indicator of asphalt binder cracking potential. Rowe and Sharrock (2016) demonstrated a positive correlation between asphalt binder R values and bending beam fatigue life results of asphalt mixtures. Furthermore, Christensen and Tran (2022) recently proposed that the R value of an asphalt binder is an indicator of its fatigue strain capacity. Cucalon et al. (2019) introduced another master curve-based parameter closely related to ω_c, termed the cross over temperature, equal to the temperature where δ = 45°. The authors proposed the crossover temperature as both a parameter for tracking asphalt binder aging and a measure of rheological balance in terms of rutting and age-induced embrittlement when combined with a binder's high-temperature grade.

Master curves are also applied to calculate parameters indicative of asphalt binder ductility. Glover (et al. 2005) first proposed a rheological parameter as an indicator of ductility that could be determined using DSR testing rather than the more cumbersome force-ductility testing. For unmodified asphalt binders, the Glover parameter is highly correlated with force-ductility tests conducted at 15°C and a loading rate of 1 cm/min when evaluated at 15°C and 0.005 rad/s, with a higher G-R value indicative of lower ductility. Rowe (2011) subsequently simplified the Glover parameter to yield the so-called Glover-Rowe (G-R) parameter, equal to $|G^*|\cdot(\cos\delta)^2/\sin\delta$. Anderson et al. (2011) demonstrated that the G-R parameter correlates with pavement block cracking when evaluated at 15°C and 0.005 rad/s. Directly measuring the G-R

parameter at 0.005 rad/s is not practical or feasible given the slow loading rate. Therefore, Glover (et al. 2005) proposed evaluating the parameter at 44.7°C and 10 rad/s, which yielded approximately equivalent results as those based on 15°C and 0.005 rad/s based on time-temperature equivalencies. However, Anderson et al. (2011) demonstrated that a single time-temperature equivalency is not valid for all binders and therefore, that the G-R parameters obtained from a master curve are more highly correlated with force-ductility results. Therefore, the authors proposed the use of temperature-frequency sweep testing coupled with a master curve model to obtain the G-R parameter. Asphalt binder master curves also offer a potential basis for predicting asphalt mixture behavior on the basis of asphalt mixture constituents (Olard & Benedetto 2003, Zeng et al. 2001).

An impediment to the more widespread implementation of master curves and associated parameters is the lack of standardized procedures constructing and modeling asphalt binder master curves. Likewise, there are very limited accounts in the literature of the implications of the chosen method for constructing asphalt binder master curves and determining CA model parameter values on the resultant model accuracy and values of associated calculated parameters. Standardization is necessary to ensure the repeatability and reproducibility of master curve results if adopted in future specifications. Correspondingly, the objective of this study is to establish robust algorithms for constructing multiple methods of modeling asphalt binder master curves, comparing the different methods directly, and fitting the CA model to oscillatory Dynamic Shear Rheometer (DSR) test data that are easily implementable in Microsoft Excel®.

4.2 Materials and Test Procedures

Table 10 summarizes the asphalt binders and temperature-frequency sweep test procedures used in this study. The test results used in this study includes two groups of binders, denoted A and B. The Group A binders encompass two typical virgin binders as well as blends of virgin binder with recycled binder, and in some cases additives. The additives included in the Group A binders include both a recycling agent (RA) and extender (E). The recycled binder sources included reclaimed asphalt pavement (RAP) and recycled asphalt shingles (RAS) binders from North Carolina. The performance grades (PG) reported in Table 10 correspond to binder system tested. For example, binder 4 is a blend of virgin binder, RAP binder, and an RA and the PG of this blend is 64-28. Tests results of the Group A binders were acquired by the authors. The Group B binders are all polymer-modified and the corresponding temperature-frequency sweep tests were

acquired in a previous research effort (Gundla & Underwood 2020). Temperature-frequency sweep testing was conducted on each binder after undergoing Rolling Thin Film Oven (RTFO) and Pressure Aging Vessel (PAV) aging in accordance with AASHTO T 240 and R 28, respectively. This age level is denoted P20. Additional age levels were also used for select binders, encompassing original (O), RTFO (R), and RTFO plus 40 hours of aging in the PAV (P40) conditions. Collectively, the experimental plan yielded a broad range of asphalt binder types and characteristics. Test results are identified by the binder code followed by the age level. For example, 8|P20 results correspond to the PG 70V-16 binder from Group B tested at the standard RTFO + 20-hour PAV age level.

Temperature-frequency sweep testing was conducted using the 8-mm parallel plate geometry in a DSR. Testing adhered to AASHTO T 315. A minimum of two replicate tests were conducted for each binder and age level combination. Replicates were run until repeatability was evaluated and verified to meet AASHTO T 315 precision limits. The average test results for a given binder and age level combination were used to construct the master curves.

Table 10 Summary of the Asphalt Binders and Test Procedures

Group	Code	PG	Additive	Recycled Binder	Test Temp (ºC)	Frequency Range (Hz)	Strain Amplitude	Age Levels
A	1	58-28	--	--	5, 20, 35, 50	0.1 to 10	1.0% at 50 ºC,35 ºC 0.1% at 20 ºC,5 ºC	O, R, P20
	2	64-22	--	--				O, R, P20, P40
	3	70-22	--	RAP				P20, P40
	4	64-28	RA	RAP				O, R, P20, P40
	5	64-28	Extender	RAP				R, P20
	6	64-34	RA	RAS				P40
B	7	64V-22	Polymer	--	10, 20, 30, 40, 54	0.1 to 30	0.5%	P20
	8	70V-16	Polymer	--				P20
	9	76-22	Polymer	--				P20

-- Not included

4.3 Test Analysis

4.3.1 Data Screening

As the test frequency increases at a given test temperature, the $|G^*|$ is expected to increase and the δ is expected to decrease. However, it is common for δ data acquired at high frequencies to exhibit so-called 'feathering' that deviates from these trends. Feathering can be visually observed and used to identify and remove spurious data when the relationship between $|G^*|$ and phase angle (so-called the 'black space' is examined) (Marasteanu & Anderson 2001). In this study, an initial filter was applied to identify and remove spurious data from the temperature-frequency sweep test results prior to constructing asphalt binder master curves. Data points at each isotherm are removed if the measurement exhibited a higher δ than the previous data point acquired at a lower frequency. Figure 17 shows a black space diagram where feathers are visually evident for 4|O (i.e., binder 4 at the original age level) before trimming that are trimmed by the filter to form a smoother black space curve. A second data filter following the recommendations of Marasteanu and Anderson (2001) was also tried after applying the initial filter. Marasteanu and Anderson (2001) proposed that measurements that deviate substantially from the expected proportionality of $|G^*|$ and δ constitute erroneous measurements. To apply the filter, the slope of log $|G^*|$ with respect to log of the frequency (ω) was calculated for each data point using the point of interest and the two nearest points. This slope was divided by the quantity of $\delta/90$. If the calculated value was less than 0.95 or greater than 1.05, it was removed. However, in all cases, all data passed the second filter criteria after removal of spurious data according to the first filter, making it an extraneous addition. Many of the temperature-frequency sweep tests did not contain spurious data. Spurious data was most common in the polymer-modified asphalt binders and the unmodified binders tested at the highest test temperature.

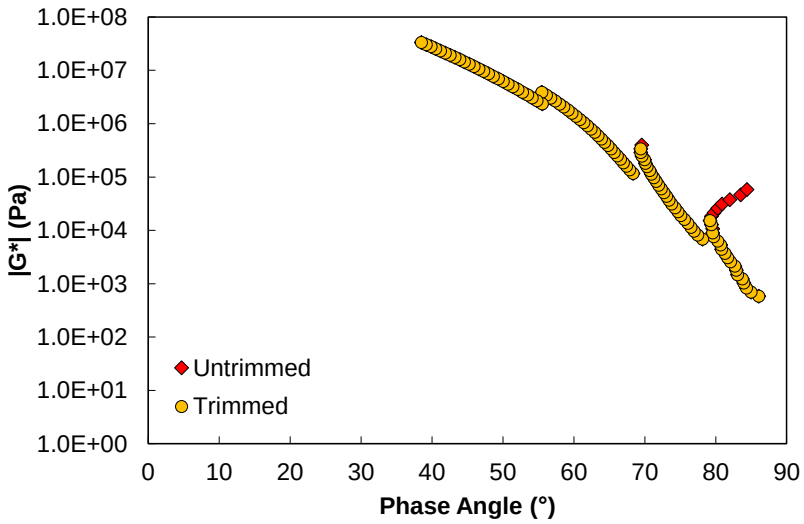

Figure 17 Example of the effects of data screening for binder 4|O

4.3.2 Master Curve Construction

There are two methods for constructing master curves, termed 'free shifting' and 'constrained shifting' (Rowe & Sharrock 2011). In the free shifting method, the isotherms are shifted horizontally along the log frequency or time axis to form a smooth, continuous master curve prior to and independent of determining the master curve model parameters. In the constrained shifting method, models are selected to describe both the master curve and time-temperature shift factors. The shift factor and master curve model parameters are then optimized simultaneously. Both methods are commonly applied to asphalt materials and Marasteanu demonstrated that both can yield satisfactory master curves (Marasteanu 1999). The free shifting approach is adopted herein because optimizing numerous model coefficients simultaneously, as required in the constrained optimization approach, can lead to results that are dependent on the initial values assigned to the parameters and constraints of the optimization.

Gordon and Shaw (1994) proposed a robust free-shifting algorithm for creating master curves that has been successfully applied to asphalt binders (Rowe & Sharrock 2011). In the method, isotherms are shifted using a pairwise approach. Initially, a linear fit of each isotherm is used to estimate the shift factor between each isotherm in a given pair. Then, the shift factors are updated iteratively using weighted least square polynomial fits of the isotherms. Implementation of the method requires rather sophisticated software and cannot be readily implemented in Excel. Marasteanu employed an alternative free shifting method to calculate shift factors based on

storage and loss moduli that also required software to implement (Marasteanu 1999). Therefore, a simpler approach is devised herein, termed pairwise interpolation.

The pairwise interpolation approaches first determines a shift factor (a_T) for each successive pair of isotherms that reflects the shift factor for the higher temperature isotherm with temperature equal to T_H using a reference temperature equal to the lower temperature isotherm with temperature equal to T_L. For example, if the data includes test temperatures of 5°C, 20°C, 35°C, and 50°C, this would involve determining the shift from 5°C to 20°C, from 20°C to 35°C, and from 35°C to 50°C. Then, these shift factors are used to calculate the final shift factors relative to the desired reference temperature. Note that application of the pairwise interpolation approach requires overlap in the range of property values among successive isotherms. In contrast, the Gordon and Shaw (1994) method does not require overlap in the range of values among successive isotherms.

The following steps describe how to determine the shift factor factors using the pairwise interpolation method. The steps are written including storage modulus ($G'=|G^*|\times\cos\delta$). However, the steps were applied to both G' and loss modulus ($G''=|G^*|\times\sin\delta$) for each binder and then averaged to determine the final shift factors; this approach is adopted to incorporate and balance $|G^*|$ and phase angle considerations. Note that Marasteanu (1999) also considered both storage and loss moduli when free shifting data to construct asphalt binder master curves.

1. Identify the minimum measurement frequency at T_H for which the corresponding G' value falls above the minimum property value measured at T_L. Denote this frequency ω_m and the G' value at this frequency $G'(T_H, \omega_m)$.
2. Calculate the equivalent frequency at T_L that will yield $G'(T_H, \omega_m)$ using linear interpolation of log G' versus log frequency for two nearest data points, termed the equivalent frequency (ω_e). To do so, identify the measurement at T_L with the closest G' value lower than $G'(T_H, \omega_m)$ and the measurement with the closest G' value higher than $G'(T_H, \omega_m)$, denoted points 1 and 2, respectively. Then, calculate the equivalent frequency at the T_L (ω_e) using Equation **(22**).

$$\log\omega_e = \log\omega_1 + (\log G'(T_H,\omega_m) - \log G'(T_L,\omega_1)) \times \frac{\log\omega_2 - \log\omega_1}{\log G'(T_L,\omega_2) - \log G'(T_L,\omega_1)} \qquad \textbf{(22)}$$

3. Calculate the logarithm of the shift factor (log a_T) based on the equivalent frequency using Equation **(23)**.

$$\log a_T = \log\left(\frac{\omega_e}{\omega_m}\right) \quad \textbf{(23)}$$

4. Repeat Steps 2 and 3 for each measurement frequency at T_H that is greater than ω_m (replacing ω_m in Equations **(22)** and **(23)** with the ω of interest).
5. Average the calculated log a_T values and report as the log a_T (T_H, $T_{ref} = T_L$) value for the isotherm pair; this log a_T defines the time-temperature shift factor at T_H for a reference temperature (T_{ref}) equal to T_L.
6. Select one of the test temperatures as the reference temperature for constructing the master curve. The log a_T at this temperature equals zero. Use the log a_T values from Step 1 to calculate the shift factors at the other test temperatures based on the values from Step 1 and the corresponding direction and distance from the reference temperature. For example, if the temperature-frequency sweep included test temperatures of 5°C, 20°C, 35°C, and 50°C, the log a_T (50, T_{ref} = 20) = log a_T (35, T_{ref} = 20) + log a_T (50, T_{ref} = 35) and the log a_T (5, T_{ref} = 20) = -log a_T (20, T_{ref} = 5).

The pairwise interpolation method was applied to construct master curves herein and the resultant log a_T values were compared to those determined using the RHEA software v2.1.2, which implements the Gordon and Shaw (1994) method. To enable the most direct comparison with the pairwise interpolation method, the log a_T values reported from RHEA were determined using the average of those calculated from G' and G''. A reference temperature of 20°C was used in all cases. The log a_T results from the pairwise interpolation method were used for subsequent calculation of the master curve model coefficients according to all methods described below. A direct comparison of the shift factors determined from RHEA using the Gordon-Shaw approach and shift factors determined using the pairwise interpolation approach were also used to construct master curve models according to the linear regression described below.

4.3.3 Shift Factor Model

Equation **(24)** was used to model the time-temperature shift factors. Equation **(24)** is included in AASHTO R 62 as a suitable model for describing the temperature-dependence of shift factors for asphalt mixtures and also works well for asphalt binders. The model coefficients a and b were

determined using the LINEST function in Excel, which uses an objective least squares method to calculate linear or polynomial model coefficients. A shift factor model R^2 of 1.00 was achieved in all cases; note that alternative shift factors models may be more appropriate if considering low temperatures where the binder approaches glassy behavior (Rowe & Sharrock 2011).

$$\log a_T(T) = a(T - T_{ref})^2 + b(T - T_{ref}) \quad \textbf{(24)}$$

4.3.4 Master Curve Model

The CA model given in Equations **(20)** and **(21)** includes three model parameters: G_g, ω_c and R. The G_g in Equations **(20)** was assumed to equal 1 GPa in this study because testing was conducted at a minimum temperature of 5°C, which did not permit measurement of the binder response in a glassy state. Testing at lower temperatures was avoided for two reasons: (1) most DSRs used for asphalt binder testing are not equipped to cool the asphalt below 0°C and (2) while temperature-control systems can be upgraded for most rheometers to permit testing at lower temperatures, upper torque limits and instrument compliance effects can pose challenges when testing at lower temperatures. However, it is noted that past studies that have performed testing at temperature approaching the glass transition temperature have reported G_g values can differ among asphalt binders (Sui et al. 2010).

Measures were taken when determining the ω_c and R values in Equations **(20)** and **(21)** to ensure that they retain the underlying principle of the CA model; that is that the ω_c and R values reflect the reduced frequency and logarithmic distance of the $|G^*|$ from the glassy modulus (assumed to be 1 GPa in this study) at the point where $\delta = 45°$. If both parameters are simultaneously and freely optimized using a least squares approach, the ω_c and therefore, R value may not reflect the point where $\delta = 45°$. Also, the simultaneous optimization of parameters can yield results that are sensitive to the initial values assigned to the parameters and the constraints of the optimization. A single method was applied to determine ω_c value in all cases whereas several different methods were evaluated for subsequently calculating the R value, termed the linear regression (LR), Average, and least squares optimization (LSO) herein. Anderson et al. (1994) proposed simple methods to estimate the ω_c and R values in the CA model given in Equations **(20)** and **(21)**. To estimate ω_c, the authors proposed fitting a line to log ω_c versus log tan δ for tan δ values falling between 0.5 and 2 wherein the relationship is generally linear as evident by Figure 18. The intercept of this line is ω_c (i.e., reduced frequency where δ = 45° and

therefore, log tan δ = 0). This method was used to determine all ω_c values herein with the additional constraint of only considering values for which $|G^*|$ exceeds 10^5 Pa based on the results of Christensen (1992) which suggests that the CA model can fail to accurately reflect binder behavior when the $|G^*|$ falls below this limit.

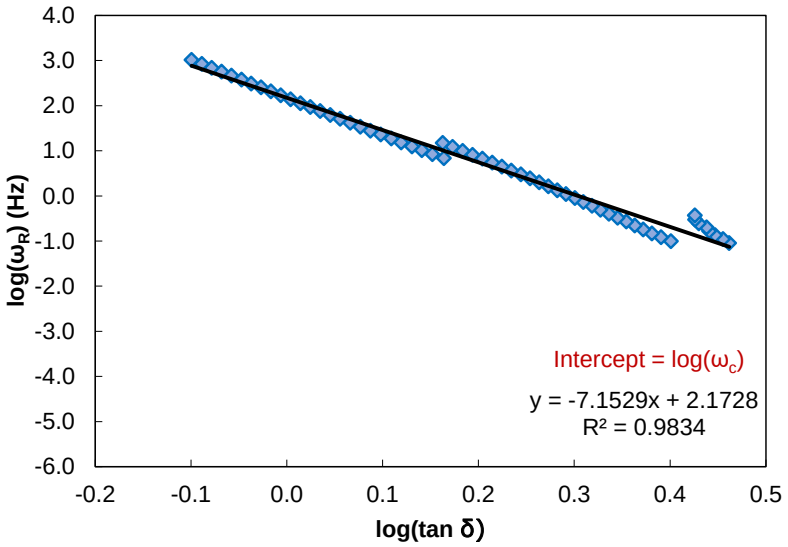

Figure 18. Example of relationship used to determine ω_c for binder 4|O

Linear Regression: Anderson et al. (1994) proposed that the *R* value can be estimated from fitting a line to log (log $|G^*|$) versus tan δ, which is also generally linear for tan δ values falling between 0.5 and 2. In this case, the intercept of the line is equal to log *R*. The method suggested by Anderson et al. (1994), termed the 'LR' method herein, was used to estimate *R* values for all binders evaluated; similar to the calculation of ω_c, only data with tan δ values falling between 0.5 and 2 and $|G^*|$ greater than 10^5 Pa were considered when implementing the LR method to calculate *R*. Figure 19 shows an example of the graph used to calculate *R* according to the LR method.

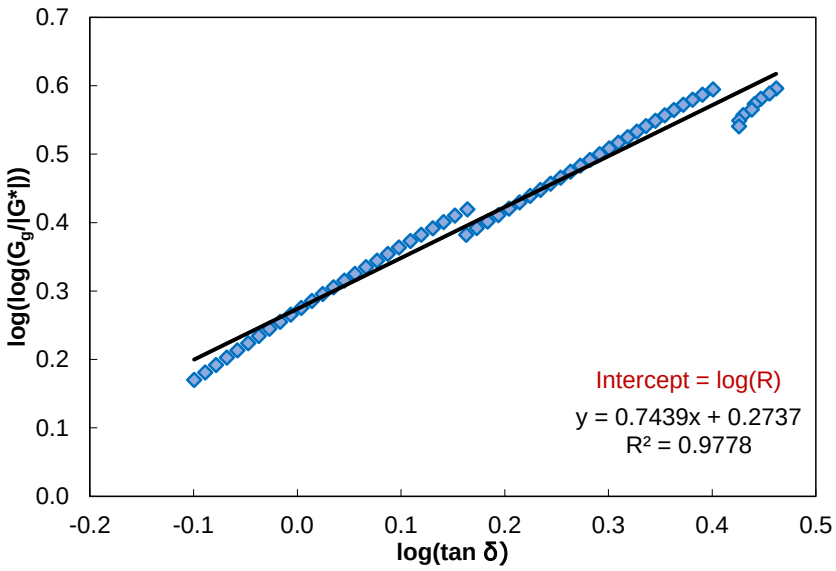

Figure 19. Example relationship used to determine *R* in the LR method

Average: As part of the NCHRP 09-59 Project, Christensen and Tran (2022) recently proposed that the *R* value can be calculated from Equation **(25)** using measurements of $|G^*|$ and δ obtained at a single temperature and frequency so long as the resultant $|G^*|$ exceeds 10^6 Pa and G_g is assumed to equal 1 GPa. Equation **(25)** is a direct derivation from the CA model. While Christensen and Tran (2022) suggested a single measurement point can determine *R*, the *R* values herein were determined by averaging the *R* values calculated using Equation **(25)** at all temperature and frequency combinations for which $|G^*|$ exceeded 10^6 Pa.

$$R = \log(2)\frac{\log(|G^*|/G_g)}{\log(1-\delta/90)} \quad \textbf{(25)}$$

Figure 20 shows three examples that are illustrative of the three trends observed when calculating *R* according to Equation **(25)**. In original and RTFO aged binders evaluated, the calculated *R* value did not vary with the measured $|G^*|$ (e.g., binder 1|O). In polymer-modified asphalts, the calculated *R* value fluctuated randomly over a small range (e.g., binder 9|P20). Unmodified binders at the P20 and P40 conditions generally exhibited a decreasing trend with respect to $|G^*|$ (e.g., binder 6|P40). These latter cases suggest that the data does not perfectly conform to the CA model. However, the model may still provide acceptable accuracy.

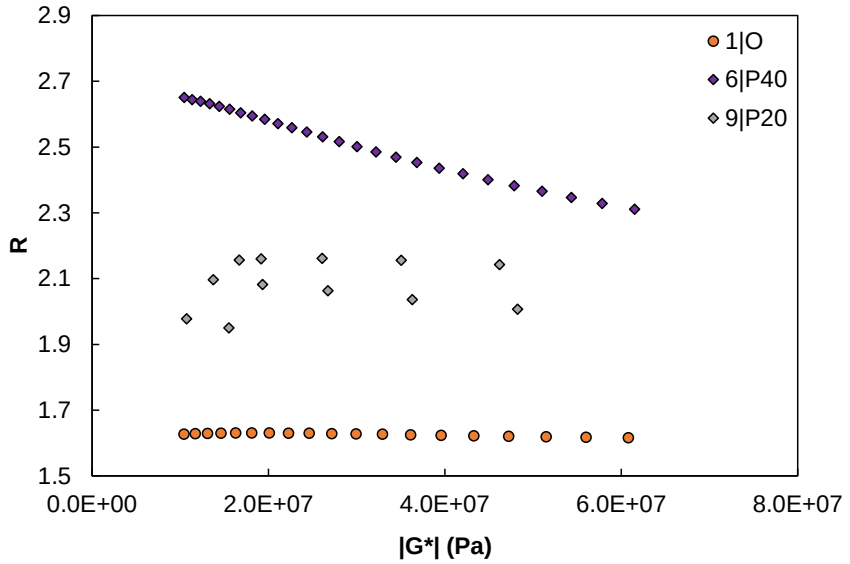

Figure 20 Examples of trends of R values calculated according to Equation (6) with respect to $|G^*|$

LSO: Two least squares optimizations (LSO) were also applied to determine *R* values after previously determining the ω_c as described above. The optimization of only one parameter alleviates concerns associated with the simultaneous optimization of model parameters that were previously discussed. Least squares optimizations were carried out using Microsoft Excel Solver to minimize the two objective functions defined in Equations **(26)** and **(27**), termed the LSO log and LSO approaches, respectively. In both cases, the squared errors for both *G*' and *G*" are summed in an effort to balance the resultant $|G^*|$ and δ model accuracy. In Equation (26), the sum of squared errors is calculated on the basis of log *G*' and log *G*" values because the basis for the CA model is the phenomenological observation of the shape of the $|G^*|$ master curve in logarithmic space. The errors are computed based on the arithmetic values in Equation **(27**). An initial value of 2.00 was assigned to *R* when performing the numerical optimizations.

$$Error = \sum_{i=1}^{n} [\log(G'_{measured,i}) - \log(G'_{predicted,i})]^2 + [\log(G''_{measured,i}) - \log(G''_{predicted,i})]^2 \quad \textbf{(26)}$$

$$Error = \sum_{i=1}^{n} [G'_{measured,i} - G'_{predicted,i}]^2 + [G''_{measured,i} - G''_{predicted,i}]^2 \quad \textbf{(27)}$$

where $G'_{measured}$ is the measured *G*' value; $G'_{predicted}$ is the *G*' value predicted by the master curve model; $G''_{measured}$ is the measured *G*" value; $G''_{predicted}$ is the *G*" value predicted by the master curve model; and *n* is the number of data points.

4.3.5 Evaluation of the Master Curve Model Results

Several criteria were used to evaluate the ability of the CA model to represent asphalt binder rheological behavior over the measurement range and to compare the different approaches for calculating the *R* value. The coefficient of determination (R^2) values of the models were calculated for both $|G^*|$ and δ models. The normalized root mean squared error (*RMSE*(%)) of the $|G^*|$ model was also calculated as defined in Equation (28), which reflects the ratio of the model RMSE to the standard deviation of the logarithm of the average $|G^*|$ results.

$$RMSE(\%) = \frac{\sqrt{\frac{1}{n}\sum_{i=1}^{n}\left(\log|G^*|_{predicted,i} - \log|G^*|_{measured,i}\right)^2}}{\sqrt{\frac{1}{n}\sum_{i=1}^{n}\left(\log|\bar{G}^*| - \log|G^*|_{measured,i}\right)^2}} \times 100\% \quad \textbf{(28)}$$

where $|G^*|_{measured}$ = measured $|G^*|$ value, $|G^*|_{predicted}$ = $|G^*|$value predicted by the master curve model, and $|\bar{G}^*|$ = average $|G^*|$ value.

AASHTO R 84, which is a standard practice for developing asphalt mixture dynamic modulus master curves, specifies that the master curve *RMSE*(%) should be less than 5 percent, which is adopted herein to evaluate asphalt binder $|G^*|$ master curve model results. The R^2 and mean absolute percent error (MAPE) were chosen to evaluate δ master curve model accuracy. Note that AASHTO R 84 does not include specifications for constructing or evaluating asphalt mixture δ master curves and the MAPE was thought to constitute an intuitive measure of the model accuracy. The fit statistics were calculated in two ways: (1) including all data that was not omitted in the data screening process and (2) also omitting data corresponding to $|G^*|$ values falling below 10^5 Pa based on precedent in the literature that suggests the CA model only accurately reflects binder behavior for higher $|G^*|$ values (1992). In addition, the G-R parameter values were calculated at 15°C and 0.005 rad/s using the CA and shift factor models to evaluate the effects of the differences in the *R* values calculated according to the various methods on a practical application of master curves.

Two methods of constructing model master curves were examined as each method has a different approach for determining the shift factors. The Gordon-Shaw method is utilized in the RHEA® software and provides different shift factors than the pairwise interpolation method in Excel which relies on overlap between successive isotherms. To contrast the effect of the Gordon-Shaw method on master curve construction, the shift factors determined for a specific

binder were taken from RHEA and input into the Excel to construct the master curves using the linear regression method. The two models were then contrasted using *RMSE*(%) for |*G**| and MAPE for phase angle. Differences in the parameters of crossover frequency and Glover-Rowe were noted. Likewise, predicted |*G**| and phase angle comparisons were contrasted with lines of equality to determine differences caused by the difference in shift factors.

4.4 Results

4.4.1 Evaluation of the Pairwise Interpolation Approach for Constructing Master Curves

Figure 21 shows the comparison between the log a_T values determined according to the Gordon and Shaw method (1994) and pairwise interpolation method developed herein. The results indicate that the two methods yield very similar log a_T values with an average difference of approximately two percent. The best agreement between the two methods is observed at the higher temperature isotherms. A small bias from the line of equality (LOE) is observed for the log a_T values at 5°C and 10°C, where the pairwise interpolation method resulted in slightly smaller log a_T values than the Gordon and Shaw (1994) method. The maximum difference in log a_T values observed among the two methods was 4.2 percent, coinciding with the results of binder 8|P20 at 10°C. It is noted that the percent difference between log a_T values calculated from the Gordon and Shaw (1994) and pairwise interpolation method were found to increase slightly as the age level increased for a given asphalt binder but this increase was generally less than one percent.

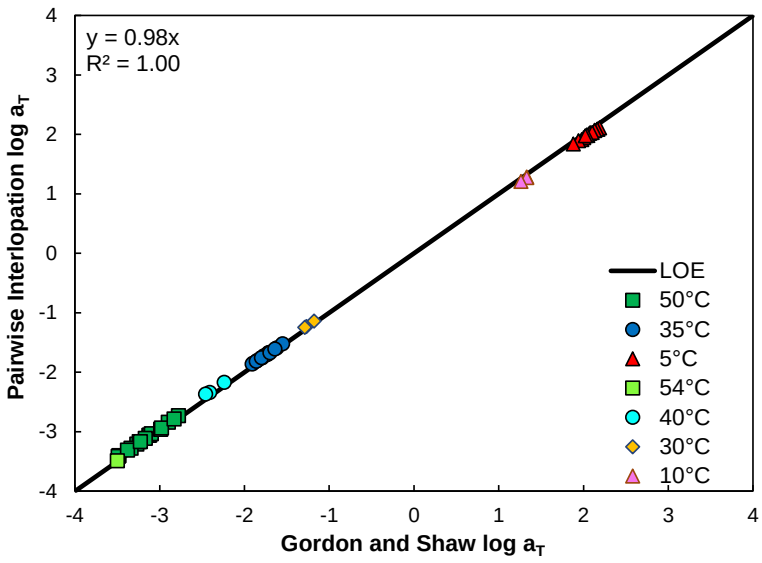

Figure 21. Comparison of log a_T values determined using the Gordon and Shaw and pairwise interpolation methods

4.4.2 Evaluation of the CA Model Results

Table 11 summarizes CA model ω_c and R parameter values determined after applying the log a_T values calculated using the pairwise interpolation method to construct $|G^*|$ and δ master curves. The R values are also shown graphically in Figure 22. In all cases, the results for a given binder tested at multiple age levels follow the expected trend of a decrease in ω_c and increase in R value (1992). The R values calculated by the different approaches are generally similar for a given binder. The two LSO approaches yield the most similar R values results among the four methods evaluated with the Average method generally exhibiting the most distinct result. The binder age level appears to have a small effect on the sensitivity of the R value to the method of calculation with the more heavily aged materials generally displaying slightly higher variation than lesser aged materials. The maximum discrepancy in R values determined from the four methods coincides with binder 8|P20, a polymer-modified binder, where the percent difference between the maximum and minimum calculates R values is 12 percent. The higher sensitivity of the R values to the method of calculation in more highly aged and polymer-modified binders was expected because these were the cases where the R values calculated using Equation **(6)** were found to vary with respect to $|G^*|$ as discussed within the methodology. Nevertheless, the differences in the R values calculated using the different methods are generally quite small. The average percentage difference between the highest and lowest R value calculated for a given

binder and age level combination across the different methods is four percent. When the Average method is neglected, this average percent difference reduces to 2.4 percent and the maximum observed difference reduces to 4.2 percent.

Table 11. Summary of the CA Model Parameters

Binder	Age	ω_c	LR R	Average R	LSO R	LSO log *R*
1	O	176.87	1.63	1.63	1.63	1.68
1	R	56.79	1.75	1.79	1.77	1.79
1	PAV-20	6.25	2.08	2.17	2.13	2.14
2	O	45.29	1.62	1.68	1.65	1.69
2	R	11.15	1.76	1.82	1.82	1.78
2	PAV-20	1.26	2.01	2.13	2.08	2.08
2	PAV-40	0.23	2.30	2.49	2.37	2.36
3	PAV-20	0.83	2.09	2.12	2.15	2.15
3	PAV-40	0.09	2.31	2.31	2.36	2.37
4	O	148.88	1.88	1.86	1.87	1.90
4	R	28.09	1.98	1.99	2.00	2.00
4	PAV-20	3.13	2.25	2.33	2.29	2.30
4	PAV-40	0.71	2.35	2.43	2.40	2.40
5	R	7.75	2.02	2.06	2.06	2.06
5	PAV-20	1.11	2.24	2.29	2.29	2.29
6	PAV-40	0.45	2.52	2.50	2.55	2.56
7	PAV-20	2.00	2.28	2.22	2.30	2.29
8	PAV-20	0.11	2.69	2.38	2.65	2.69
9	PAV-20	0.48	2.06	2.08	2.08	2.10

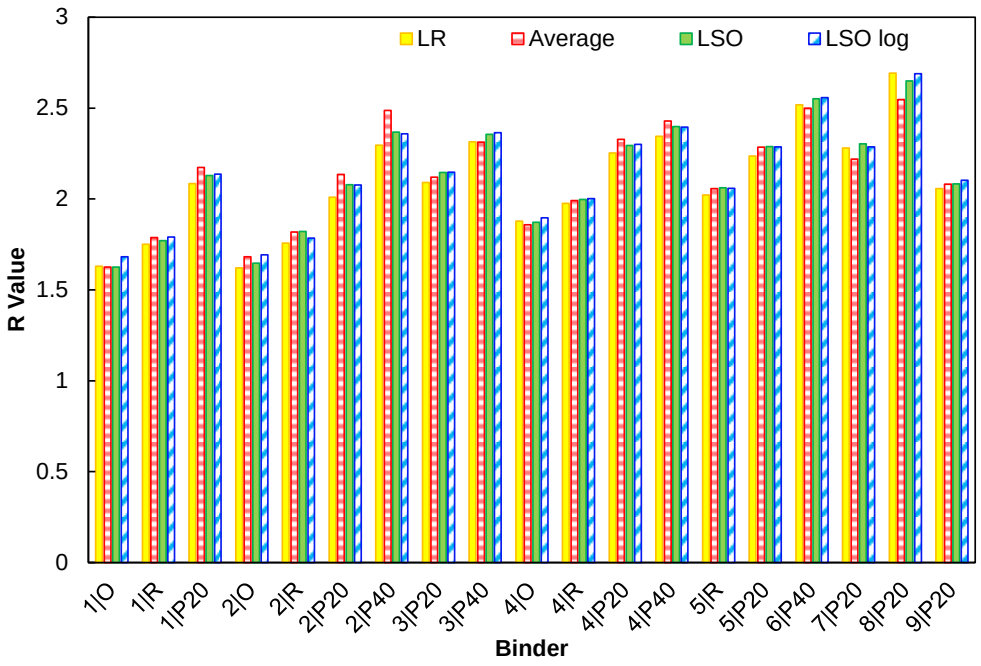

Figure 22. *R* values

Example master curves are shown for binder 4|P40 and 8|P20 in Figure 23 and Figure 24, respectively. These examples show that, in general, the CA model visually agrees with the measured data. Figure 23 is illustrative of most cases observed wherein small discrepancies between the measured data and model predicts are apparent in the $|G^*|$ and δ master curves at low reduced frequencies in Figure 23, which matches expectations based on the literature (1992). In Figure 23, it is difficult to visually distinguish among the different methods used to calculate the CA model *R* value which was the case for most binders evaluated. The difference among the different methods is somewhat more apparent in Figure 24, which constitutes the case that exhibited the largest variation in *R* values calculated from the different methods. In Figure 24, the CA model predictions from the Average method are most distinct. This was a case where the R value calculated according to Equation **(25)** fluctuated with respect to $|G^*|$ Figure 23 and Figure 24 also reveal that the application of time-temperature superposition results in a smoother $|G^*|$ master curve than δ, which matches expectations based on previous studies (Rowe & Sharrock 2011).

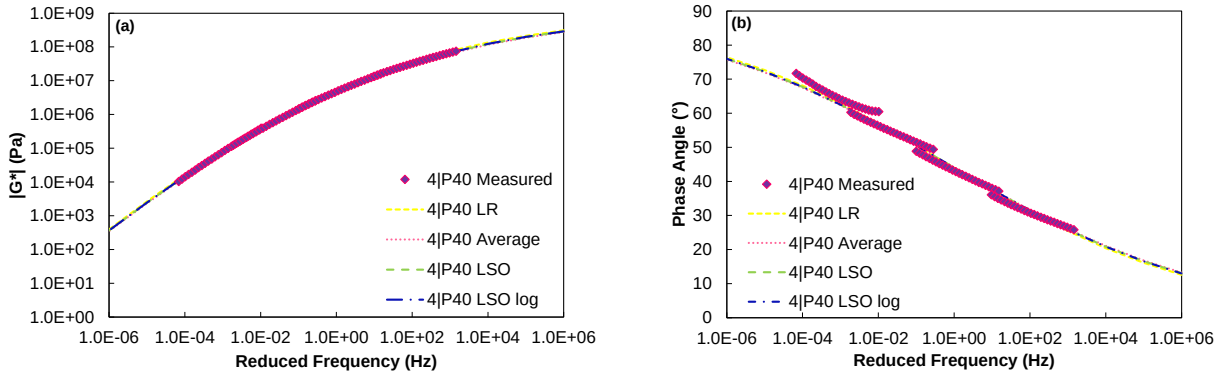

Figure 23. Master curves for binder 4|PAV-40: (a) |*G| and (b) δ**

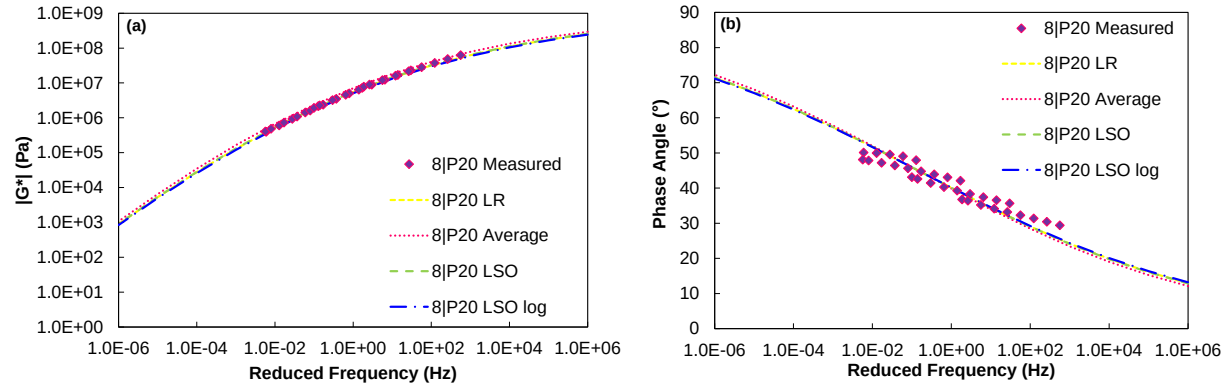

Figure 24. Master curves for binder 8|PAV-20: (a) |*G| and (b) δ**

To further evaluate the CA model results, the CA model predictions of |*G**| and δ are plotted against the measured values in Figure 25. Group A and B binders are plotted separately to better allow for visually distinguishing trends among polymer-modified (i.e., Group B) and unmodified binders (i.e., Group A). To reduce clutter in these graphs, only select test frequencies are plotted in Figure 25. For Group A binders, results corresponding test frequencies of 0.15 Hz, 1.35 Hz, and 10 Hz are plotted from each test temperature whereas for the Group B binders, the selected test frequencies are 0.1 Hz, 1.4 Hz, 6.5 Hz. Note that different frequencies were used in the two groups of binders and thus, similar but not identical frequencies are plotted for Groups A and B.

Figure 25 (a) and (b) shows that the |*G**| results generally fall very close to LOE. Somewhat higher deviation from the LOE is apparent in the few points where |*G**| falls below approximately 10^4 Pa. The literature suggests that CA model accuracy is best when |*G**| exceeds 10^5 Pa (1992). For both groups of binders, it is apparent that the Average method for calculating

the *R* value generally yields poorer |*G**| model accuracy compared to the other methods. In the case of the Group A binders, the Average method tends to underestimate |*G**| whereas for the Group B binders, it tends to overestimate |*G**|. Figure 25 (c) shows that the δ model results for the binders without polymer modification (Group A) are very close to the LOE, indicating high accuracy, when the δ is below 70° whereas for polymer-modified asphalt binders, deviation from the LOE begins to occur when the δ exceeds 60°. Visually, it is difficult to distinguish among the CA model predictions of δ obtained from the different *R* calculation methods. Generally, the data where the δ model accuracy tends to diminish coincide with |*G**| values falling below 10^5 Pa and thus, the data generally assign to align with the literature (1992). One alternative to the CA model to potentially improve model accuracy at low |*G**| values is the Christensen-Anderson-Marasteanu (CAM) model (Marasteanu 1999), which incorporates and additional model parameter to allow for better capturing how fast or slow log |*G**| versus log ω_R data converge to the glassy and equilibrium asymptotes.

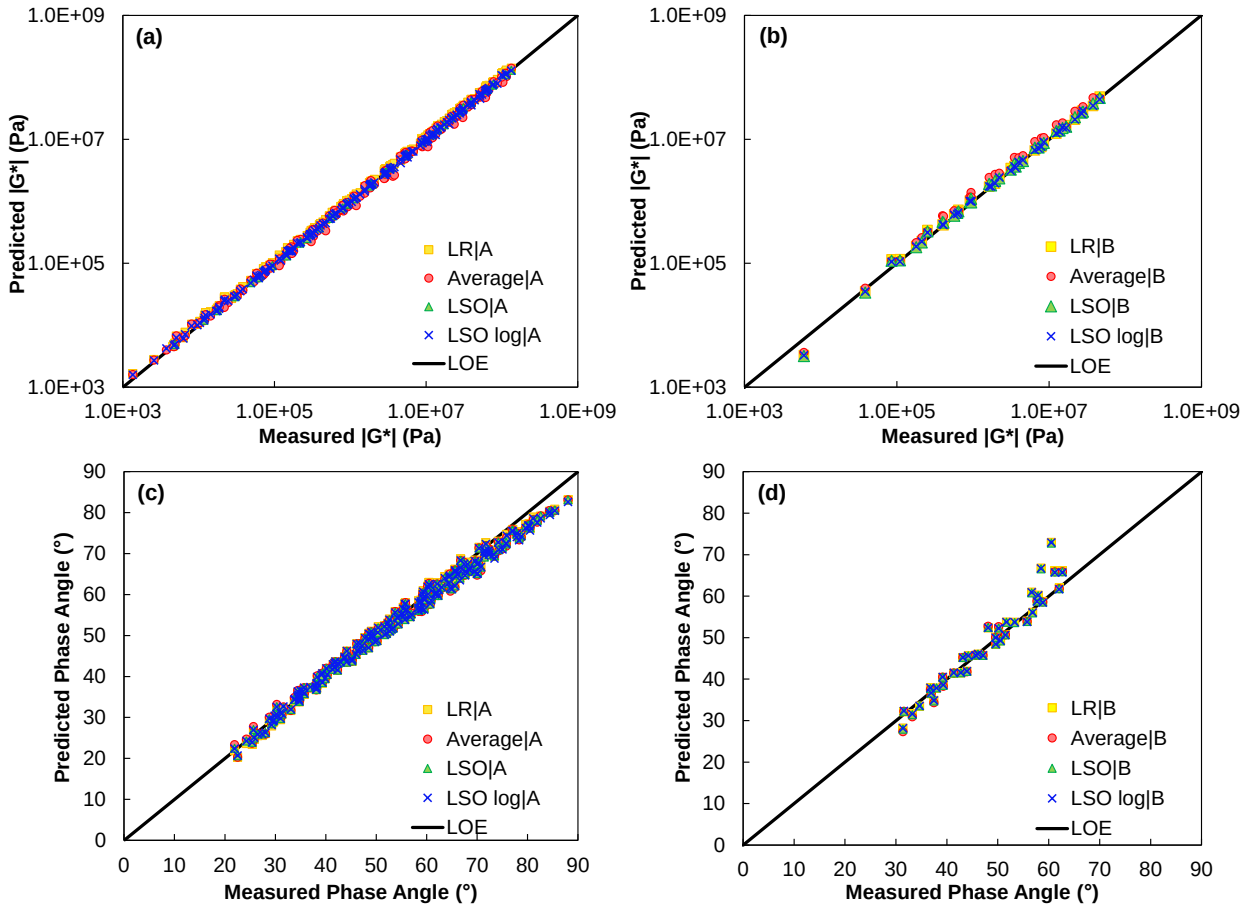

Figure 25. Comparison of the measured and predicted (a) |*G| values for the Group A binders, (b) |G*| values for the Group B binders, (c) *δ* for the Group A binders, and (d) *δ* for the Group B binders.**

The CA model fit statistics for |*G**| and *δ* are presented in Table 12 through Table 15. Table 12 and Table 13 show the |*G**| fit statistics, including all data and neglecting data where |G*| falls below 10^5 Pa, respectively. Table 14 and Table 15 show the *δ* fit statistics, including all data and neglecting data where |G*| falls below 10^5 Pa, respectively. Note that all model fit statistics are calculated using only data that was retained after screening. The |*G**| model fit statistics reflect visual observations in Figure 25 for the Average method, suggesting it is inferior to the other approaches. In general, the LSO method to calculate *R* yields the highest R^2 and lowest RMSE(%) values for the CA model for |*G**|. However, it is noted that the RMSE(%) values corresponding to the LR method are comparable to those from the LSO method in many cases and the maximum RMSE(%) is only slightly higher for LR method when all data is considered (5.81 vs. 5.75) and only data where |*G**| exceeds 10^5 Pa (3.91 vs. 2.85). The LR

method is considered practically advantageous in that it does not require numerical optimization and therefore, could more easily be specified than the LSO and LSO log methods. Both the LSO and LR methods provide acceptable RMSE(%) values based on the AASHTO R 84 criterion (for asphalt mixture dynamic modulus master curves) when data where |G*| falls below 105 Pa is omitted. These methods both yield R2 values of 0.97 or higher when all data is included and yield values of 1.00 when data where |G*| falls below 105 Pa is excluded for both unmodified and polymer-modified binders. Comparison of the fit statistics in Table 12 and Table 13 does demonstrate an improvement in model accuracy when |G*| data falling below 105 Pa is omitted. For example, the average RMSE(%) decreases from 3.22 to 2.49 for the LR method and from 1.87 to 1.02 for the LSO method.

The four methods for calculating *R* values yield comparable model fit statistics for δ with average MAPE values of approximately three percent when all data is included and approximately two percent when data corresponding to $|G^*|$ values falling below 10^5 Pa is omitted. The R^2 values are generally lower for δ than $|G^*|$ and the poorest fit statistics for both $|G^*|$ and δ generally coincide with the polymer-modified binders (i.e., binders 7, 8, and 9).

Table 12. |G^*| Model Fit Statistics Including All Data

Binder	Age	LR		Average		LSO		LSO log	
		R^2	RMSE	R^2	RMSE	R^2	RMSE	R^2	RMSE
1	O	1.00	3.83%	1.00	3.93%	1.00	3.93%	0.98	3.26%
1	R	1.00	2.03%	1.00	1.38%	1.00	1.52%	1.00	1.40%
1	PAV-20	0.99	2.70%	0.99	2.66%	1.00	1.03%	1.00	1.12%
2	O	1.00	3.98%	0.99	2.79%	1.00	3.23%	0.99	2.83%
2	R	0.98	1.76%	1.00	2.25%	1.00	2.41%	0.99	1.24%
2	PAV-20	0.98	3.81%	0.98	3.98%	1.00	1.07%	1.00	1.03%
2	PAV-40	0.97	4.20%	0.91	9.35%	1.00	1.93%	1.00	1.63%
3	PAV-20	0.98	2.70%	1.00	2.66%	1.00	1.03%	1.00	1.12%
3	PAV-40	0.99	3.93%	0.99	3.96%	1.00	1.03%	1.00	0.73%
4	O	1.00	0.98%	1.00	1.64%	1.00	1.15%	1.00	0.96%
4	R	1.00	1.42%	1.00	0.81%	1.00	0.69%	1.00	0.69%
4	PAV-20	0.99	2.80%	0.99	2.10%	1.00	0.73%	1.00	0.77%
4	PAV-40	0.99	3.34%	0.99	2.53%	1.00	0.70%	1.00	0.64%
5	R	0.99	2.09%	1.00	0.77%	1.00	0.82%	1.00	0.77%
5	PAV-20	0.99	3.27%	1.00	0.65%	1.00	0.70%	1.00	0.67%
6	PAV-40	0.99	3.09%	0.99	4.36%	1.00	0.78%	1.00	0.65%
7	PAV-20	1.00	5.78%	0.96	7.94%	1.00	5.75%	1.00	5.72%
8	PAV-20	0.98	3.72%	0.94	12.03%	1.00	2.85%	0.98	7.45%
9	PAV-20	1.00	5.81%	1.00	4.26%	1.00	4.24%	1.00	3.71%
		Max	5.81%	Max	12.03%	Max	5.75%	Max	7.45%
		Avg.	3.22%	Avg.	3.69%	Avg.	1.87%	Avg.	1.91%

Table 13. |G^*| Model Fit Statistics Excluding |G^*| values Below 10^5 Pa

Binder	Age	LR		Average.		LSO		LSO log	
		R^2	RMSE	R^2	RMSE	R^2	RMSE	R^2	RMSE
1	O	1.00	1.19%	1.00	1.28%	1.00	1.29%	1.00	1.52%
1	R	1.00	1.01%	1.00	0.62%	1.00	0.41%	1.00	0.72%
1	PAV-20	1.00	1.99%	1.00	2.42%	1.00	0.39%	1.00	0.70%
2	O	1.00	1.95%	1.00	1.44%	1.00	1.19%	1.00	1.76%
2	R	1.00	1.74%	1.00	2.07%	1.00	2.21%	1.00	1.18%
2	PAV-20	1.00	3.29%	1.00	3.92%	1.00	0.83%	1.00	0.76%
2	PAV-40	1.00	3.42%	1.00	9.16%	1.00	1.71%	1.00	1.21%
3	PAV-20	1.00	3.61%	1.00	1.89%	1.00	0.64%	1.00	0.62%
3	PAV-40	1.00	3.84%	1.00	3.87%	1.00	1.03%	1.00	0.71%
4	O	1.00	0.56%	1.00	1.15%	1.00	0.70%	1.00	0.77%
4	R	1.00	1.22%	1.00	0.62%	1.00	0.49%	1.00	0.51%
4	PAV-20	1.00	2.36%	1.00	2.02%	1.00	0.37%	1.00	0.54%
4	PAV-40	1.00	2.99%	1.00	2.45%	1.00	0.62%	1.00	0.53%
5	R	1.00	2.03%	1.00	0.39%	1.00	0.34%	1.00	0.37%

5	PAV-20	1.00	3.02%	1.00	0.59%	1.00	0.64%	1.00	0.61%
6	PAV-40	1.00	2.95%	1.00	4.15%	1.00	0.78%	1.00	0.63%
7	PAV-20	1.00	2.43%	1.00	6.66%	1.00	1.00%	1.00	1.98%
8	PAV-20	1.00	3.70%	1.00	11.26%	1.00	2.85%	1.00	7.27%
9	PAV-20	1.00	3.91%	1.00	1.89%	1.00	1.87%	1.00	1.49%
		Max	3.91%	Max	11.26%	Max	2.85%	Max	7.27%
		Avg.	2.49%	Avg.	3.04%	Avg.	1.02%	Avg.	1.26%

Table 14. Phase Angle Model Fit Statistics Including All Data

Binder	Age	LR		Average		LSO		LSO log	
		R^2	MAPE	R^2	MAPE	R^2	MAPE	R^2	MAPE
1	O	0.95	3.41%	0.95	3.36%	0.95	3.36%	0.93	4.01%
1	R	0.98	2.25%	0.97	2.51%	0.98	2.38%	0.97	2.54%
1	PAV-20	0.98	2.54%	0.97	3.01%	0.97	2.77%	0.97	2.81%
2	O	0.97	3.33%	0.96	4.10%	0.97	3.67%	0.95	4.23%
2	R	0.99	1.83%	0.99	1.88%	0.99	1.89%	0.99	1.83%
2	PAV-20	0.99	2.32%	0.98	3.31%	0.99	2.72%	0.99	2.70%
2	PAV-40	0.98	2.93%	0.96	5.09%	0.98	3.78%	0.98	3.66%
3	PAV-20	0.98	2.54%	0.97	3.01%	0.97	2.77%	0.97	2.81%
3	PAV-40	0.99	2.71%	0.99	2.71%	0.99	2.42%	0.99	2.37%
4	O	0.97	2.22%	0.97	2.09%	0.97	2.18%	0.97	2.34%
4	R	0.99	1.75%	0.99	1.75%	0.99	1.75%	0.99	1.75%
4	PAV-20	0.99	2.02%	0.98	2.18%	0.99	2.09%	0.99	2.10%
4	PAV-40	0.99	2.24%	0.99	2.40%	0.99	2.32%	0.99	2.31%
5	R	0.99	2.20%	0.99	2.18%	0.99	2.18%	0.99	2.18%
5	PAV-20	0.99	2.46%	0.99	2.45%	0.99	2.45%	0.99	2.45%
6	PAV-40	0.99	2.26%	0.99	2.31%	0.99	2.19%	0.99	2.18%
7	PAV-20	0.86	5.31%	0.85	5.73%	0.87	5.16%	0.86	5.27%
8	PAV-20	0.90	5.24%	0.89	5.80%	0.90	5.28%	0.90	5.09%
9	PAV-20	0.97	2.42%	0.98	2.39%	0.98	2.39%	0.98	2.37%
		Max	5.31%	Max	5.80%	Max	5.28%	Max	5.27%
		Avg.	2.87%	Avg.	3.21%	Avg.	2.95%	Avg.	3.01%

Table 15. δ Model Fit Statistics Excluding Data Corresponding to $|G^*|$ values Below 10^5 Pa

Binder	Age	LR		Average		LSO		LSO log	
		R^2	MAPE	R^2	MAPE	R^2	MAPE	R^2	MAPE
1	O	0.98	1.44%	0.99	1.42%	0.99	1.42%	0.98	1.75%
1	R	1.00	1.05%	0.99	1.13%	1.00	1.09%	0.99	1.14%
1	PAV-20	1.00	1.36%	0.99	1.50%	1.00	1.41%	0.99	1.43%
2	O	0.99	2.03%	0.98	2.50%	0.98	2.24%	0.98	2.58%
2	R	1.00	1.45%	1.00	1.34%	1.00	1.34%	1.00	1.38%
2	PAV-20	0.99	1.84%	0.99	2.58%	0.99	2.09%	0.99	2.08%
2	PAV-40	0.99	2.36%	0.98	4.28%	0.99	3.11%	0.99	3.01%
3	PAV-20	0.99	2.22%	0.99	2.09%	0.99	2.00%	0.99	1.99%
3	PAV-40	0.99	2.65%	0.99	2.65%	0.99	2.39%	0.99	2.34%
4	O	0.99	1.03%	0.99	1.00%	0.99	1.02%	0.99	1.06%
4	R	1.00	1.25%	1.00	1.21%	1.00	1.19%	1.00	1.18%
4	PAV-20	0.99	1.40%	0.99	1.40%	0.99	1.38%	0.99	1.38%
4	PAV-40	0.99	1.87%	0.99	1.89%	0.99	1.86%	0.99	1.86%
5	R	0.99	1.66%	0.99	1.53%	0.99	1.52%	0.99	1.53%
5	PAV-20	0.99	2.12%	0.99	2.02%	0.99	2.01%	0.99	2.01%
6	PAV-40	0.99	2.19%	0.99	2.24%	0.99	2.09%	0.99	2.07%
7	PAV-20	0.98	2.73%	0.97	3.01%	0.98	2.63%	0.98	2.70%
8	PAV-20	0.91	4.96%	0.89	5.50%	0.91	5.00%	0.91	4.82%
9	PAV-20	0.98	2.33%	0.98	2.29%	0.98	2.29%	0.98	2.26%
		Max	4.96%	Max	5.50%	Max	5.00%	Max	4.82%
		Avg.	2.00%	Avg.	2.19%	Avg.	2.00%	Avg.	2.03%

To further compare the different methods for calculating *R* values on a practical application of master curves, G-R parameter values were calculated at 15°C and 0.005 rad/s (0.0008 Hz) using the time-temperature shift model and CA model results. As discussed, the G-R parameter evaluated at this condition has been proposed as an indicator of ductility (Anderson et al. 2011). The temperature-frequency combination of 15°C and 0.005 rad/s coincides with reduced frequencies near the lower end of the measured data, coinciding within the measurement range of the highest temperature isotherm in most cases. Recall that generally the CA model fits are poorest at low reduced frequencies, corresponding to low $|G^*|$ values and high δ values and thus, constitute a condition where the highest discrepancies among model fits may be expected. In 9 out of the 19 binders evaluated, the predicted $|G^*|$ fell below 10^5 Pa and/or δ value was above 70° at the reduced frequency corresponding to 15°C and 0.005 rad/s. In the case of one binder, 8|PAV-20, the reduced frequency corresponding to 15°C and 0.005 rad/s was outside the

accepted measurement range after the screening of spurious data. In all other cases, the corresponding reduced frequency was within the measurement range.

Figure 26 presents the G-R value results where trends for a given binder generally match those for the *R* values shown in Figure 22. In general, the results obtained when using the Average method to calculate *R* are most distinct from the other methods. Binders 2|PAV-20, 2|PAV-40, and 8|PAV-20 showed notable sensitivity in *R* values to the method of calculation, which persists in the G-R results. While differences exist, the rankings of the binders evaluated on the basis of G-R does not change with the method used to calculate the *R* value. The average percent difference in G-R values for a given binder calculated using the LSO and LR methods is 5.17% when calculated on an arithmetic basis and 1.59% went calculated on a logarithmic basis.

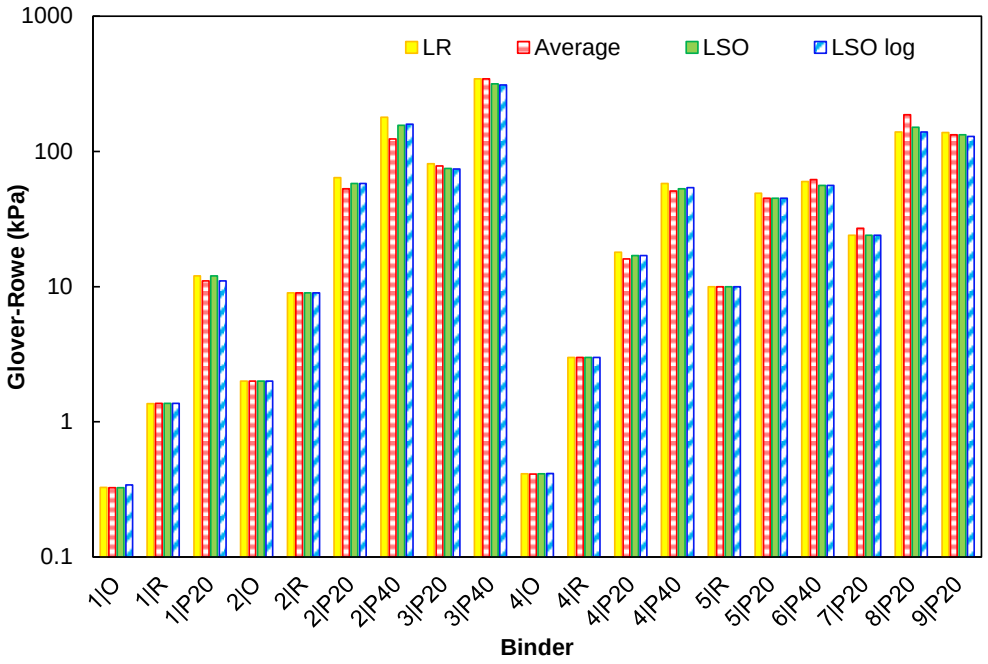

Figure 26. Glover-Rowe values calculated at 15°C and 0.005 rad/s using the shift factor and CA models

4.4.3 Comparison of the CA Model Results from the Shift Factors Determined using Pairwise Interpolation versus Gordon and Shaw

The effectiveness of the using pairwise interpolation (PI) master curve construction method was further evaluated by contrasting the previously presented master curve results obtained using the LR method with master curves constructed using the shift factors determined from RHEA

coupled with the LR method. Recall that the RHEA software uses the Gordon-Shaw (GS) method to determine the time-temperature shift factors.

The *R* values calculated using the LR method are the same irrespective of the shifting method since the calculation of *R* does not involve reduced frequency. In contrast, the calculation of the ω_c is contingent upon the time-temperature shift factors. Figure 27 shows the comparison between the ω_c values calculated using the time-temperature shift factors from the PI method and GS method. The results demonstrate small differences in the ω_c values from the two methods for a given binder. This is supported by the differences in $|G^*|$ for the model constructed using PI and GS were minor. On average the difference between the modulus determined by PI and GS was 0.61% and the maximum difference was 2.90%. When contrasting the differences between the PI and the GS method, with differences are not consistently lower or higher from a given method compared to the other.

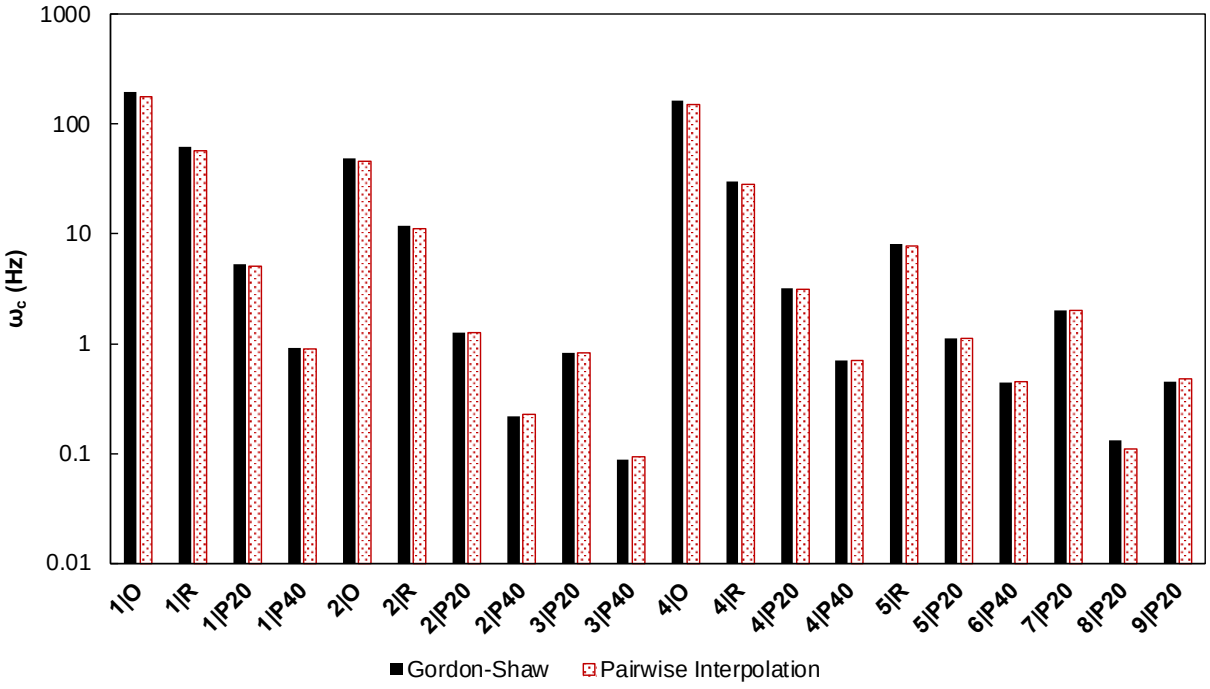

Figure 27. Comparison of ω_c values calculated using PI and GS shift factors

Figure 28 shows the CA model predictions of $|G^*|$ and phase angle using the ω_c values calculated from the shift factors obtained from the PI and GS methods. These figures showcase that shifting using PI and the GS methods result in similar model prediction accuracy. The RMSE and MAPE values in Figure 28 (a) and (b), respectively, were calculated from the collective Group A and Group B temperature-frequency sweep test results. The $|G^*|$ model

RMSE values are slightly lower for the GS compared to PI method whereas the phase angle MAPE values for the PI method are slightly lower than those from the GS method. It can be seen in Figure 28 (b) that at the higher phase angles recorded for each material, a higher deviation from the LOE can be observed for both shifting methods. In the case of binders from Group A, the model accuracy starts to drop around phase angles larger than 70° and for Group B binders it is around 60°, irrespective of the shifting method.

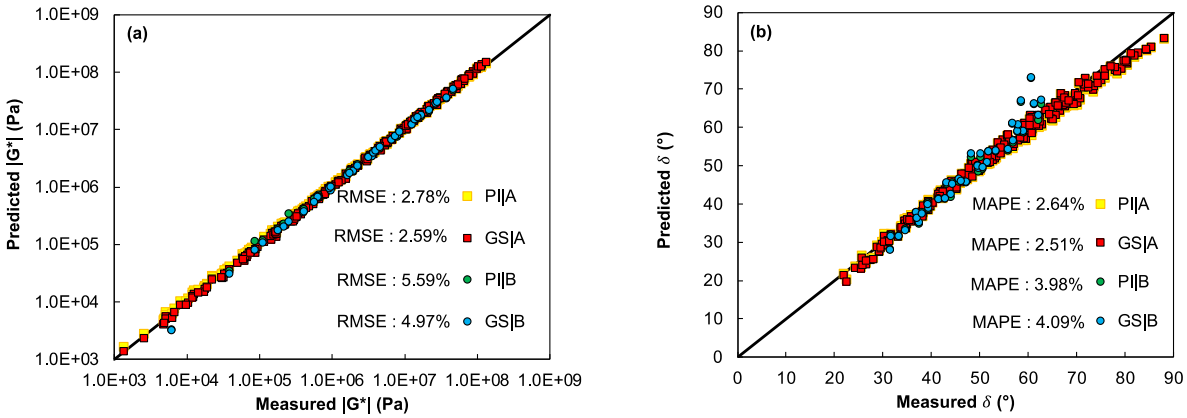

Figure 28. Comparison of CA model predictions using pairwise PI and GS methods for: (a) |*G| and (b) *Phase Angle***

To further evaluate the differences between the CA model predictions obtained from the two shifting methods, the model predictions are directly compared in Figure 29. The difference between the model predictions of the PI and GS methods for determining the shift factor is quite small, which would indicate that either method is appropriate for constructing master curves. Showcased in Figure 29 (a), the predicted |*G**| results between the PI and GS method are close, with binder Group A and binder Group B both having best fit lines with slopes of 0.96 and an R^2 of 1.00, indicating an average difference of approximately 4%. Figure 29 (b) showcases similar findings for phase angle where the best fit lines for Group A and B binders have slopes of 0.98 and 0.99, respectively. It can be seen the findings discussed in Figure 25 remain true for either method of master curve construction.

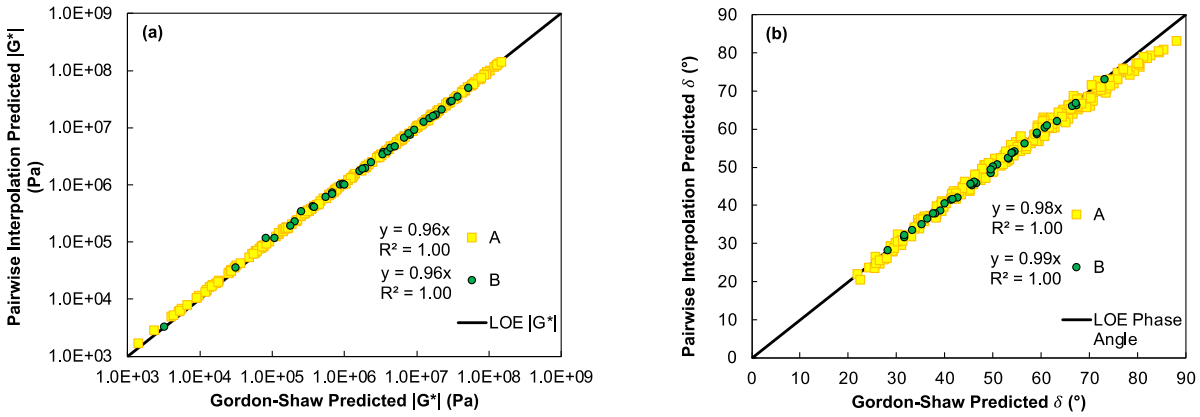

Figure 29. Comparison between PI and GS shift factors on CA model predictions

The overall fitting statistics using the collective Group A and B results are summarized in Table 16. The R^2 values indicate good overall model performance regardless of which shifting method is used (0.98 or higher). The findings show that the RMSE for each method are relatively low (less than 5%), with the model being more accurate for Group A (unmodified) materials and slightly less accurate for Group B (polymer-modified) materials. Likewise, the difference in RMSE for the different methods amongst the same group is generally small.

Table 16. Summary of Model Differences

Method of Shifting|Group	$\|G^*\|$ RMSE	δ MAPE	$\|G^*\|$ R^2	δ R^2
PI|A	2.78%	2.64%	1.00	1.00
GS|A	2.59%	8.54%	1.00	1.00
PI|B	5.59%	3.98%	1.00	0.97
GS|B	4.97%	4.09%	1.00	0.98

To further compare the CA model predictions using the shift factors determined using the PI and GS methods, the G-R parameter values were calculated at 15°C and 0.005 rad/s (0.0008 Hz) using the time-temperature shift model and CA model results. Figure 30 shows the comparison between the G-R values obtained using the two different methods to construct master curves. The average and maximum percent differences in G-R values determined by GS and PI are 4.4% and 9.0% for group A and 5.5% and 8.0% for Group B, respectively, indicating the methods yield similar G-R values regardless of material used.

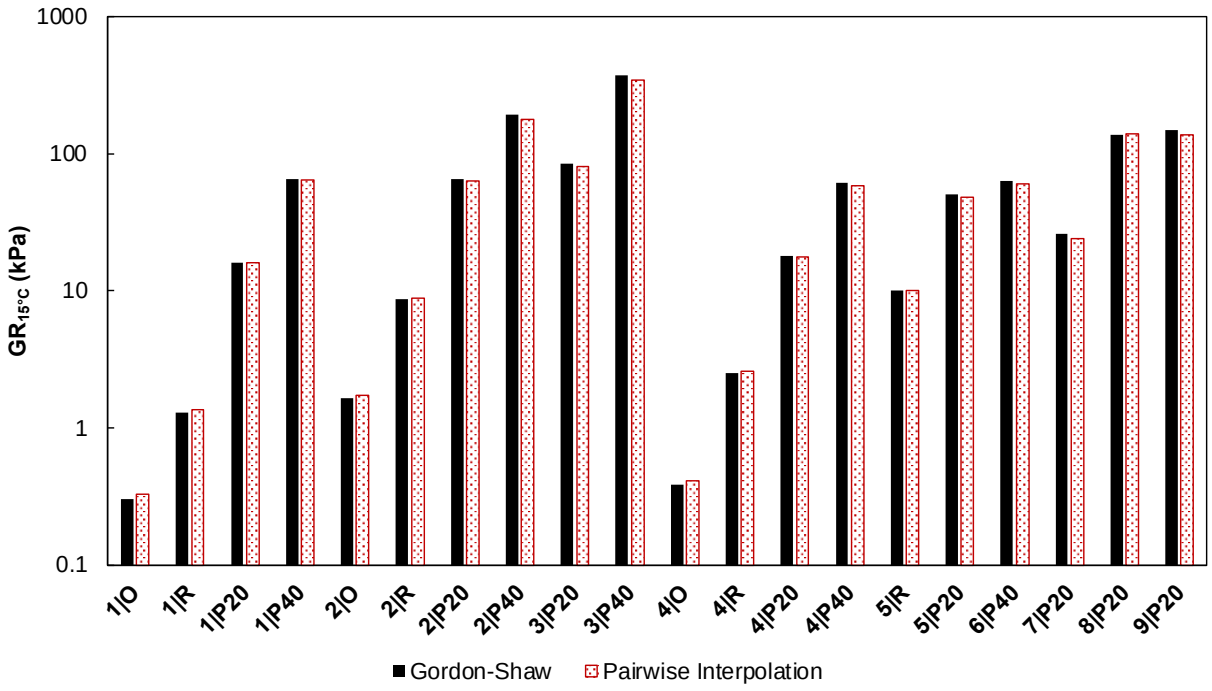

Figure 30. Comparison of Glover-Rowe predictions at 15°C and 0.005 rad/s using the PI and GS shift factors

Overall, the findings showcase that either method would be appropriate for constructing master curves as there is not a significant statistical benefit for utilizing the shift factors determined using the PI or GS method.

4.5 Conclusions and Recommendations

The following conclusions and recommendations are drawn from the results of this study:

- The pairwise interpolation for constructing asphalt binder master curves developed herein yields good agreement with the Gordon and Shaw (1994) method. The pairwise interpolation method can be more easily implemented than the Gordon and Shaw method but does require that there is overlap in the range of storage and loss moduli in successive isotherms. Furthermore, CA model results obtained using the Gordon and Shaw and pairwise interpolation methods were very similar when using the LR method to obtain *R*, which indicates either method for determining shift factors can be used.
- Rheological measurements where δ increases as the measurement frequency increases should be removed from temperature-frequency sweep data prior to constructing master curves.

- The relationship between reduced frequency and tan δ in logarithmic space over tan δ values spanning from 0.2 to 0.5 is generally linear and can be used to determine the crossover frequency as proposed by Anderson et al. (1994).
- Calculating the CA model *R* value on the basis of measurements at a single temperature-frequency combination as proposed by Christensen and Tran (2022) or the average over a range of temperature-frequency combinations should be avoided because the calculated *R* value can vary with the temperature-frequency combination in long-term aged and polymer-modified asphalts, which leads to poorer $|G^*|$ model predictions than alternative methods.
- Solving for the CA model *R* value using least squares optimization using a previously determined ω_c values on the basis of log storage and log loss moduli values generally yields slightly poorer model accuracy than when computing the squared errors without logarithmic transforms. Least squares optimization to minimize the sum of squared errors for storage and loss moduli was found to yield the highest model accuracy among the methods evaluated.
- The relationship between log (log $|G^*|$) and tan δ is generally linear for tan δ values falling between 0.5 and 2 and can be used to estimate the CA Model *R* value. This approach provided acceptable and comparable model accuracy to least squares optimization in most of the cases evaluated and thus, constitutes a viable alternative to numerical optimization.
- Based on the asphalt binders evaluated in this study, the CA model can accurately reflect asphalt binder rheological behavior when the $|G^*|$ exceeds 10^5 Pa and δ is less than 70° for unmodified asphalts or less than 60° for polymer-modified asphalts.
- This study focused on identifying practically implementable methods to construct asphalt binder master curves and determine CA model parameters. Research is also needed to develop standardized procedures for temperature-frequency sweep testing.

4.6 Validation

To validate the PI method for constructing asphalt binder master curves coupled with the LR method to calculate CA model parameters, the methods were applied to the binders and blends evaluated in Chapter 5 of this dissertation at multiple age levels. The resultant RMSE values for $|G^*|$ model predictions and MAPE for phase angle model predictions are shown in Appendix B. These results support the findings that pairwise interpolation provided good agreement between the model and measured data series. The mean RMSE across all blends assessed was 3.62%,

while the maximum was 4.60%. Both measures were below the acceptable threshold of 5.0% set in mixture dynamic modulus master curve standards. There was a similar performance for MAPE for measured and model phase angle, with an average MAPE of 2.14% and a maximum MAPE of 3.92%.

4.7 Acknowledgements

Testing and analysis of the Group A binders was supported by the North Carolina Department of Transportation under NCDOT RP 2020-16. Several of the Group A tests were performed by Saqib Gulzar and Jaime Preciado. The Group B binder test results were acquired and graciously shared by Dr. Akshay Gundla and Dr. Shane Underwood. Geoff Rowe and Sergio Raposo of Abatach, Inc. kindly shared RHEA software v2.1.2.

4.8 References

1. Anderson, D. A., D. W. Christensen, H. U. Bahia, R. Dongre, M. G. Sharma, C. E. Antle, and J. Button. *SHRP Report A-369: Binder Characterization and Evaluation, Volume 3: Physical Characterization*. National Research Council, Washington, D.C., 1994.
2. Christensen, D. W. Mathematical Modeling of the Linear Viscoelastic Behavior of Asphalt Cements. Ph.D. Dissertation, Pennsylvania State University, College Station, PA, 1992.
3. Dickinson, E. J., and H. P. Witt. The Dynamic Shear Modulus of Paving Asphalts as a Function of Frequency. *Transactions of the Society of Rheology, Vol. 18, No. 4, pp. 591-606.* 1974.
4. Ferry, J. D. *Viscoelastic Properties of Polymers*. Wiley, New York, NY, 1980.
5. Rowe, G. M., and M. J. Sharrock. Cracking of Asphalt Pavements and the Development of Specifications with Rheological Measurements. *Proceedings of the 6th Eurasphalt and Eurobitume Congress*, 2016.
6. Christensen, D. W., and N. Tran. NCHRP Report 982: Relationships Between the Fatigue Properties of Asphalt Binders and the Fatigue Performance of Asphalt Mixtures. Transportation Research Board, Washington, D.C., 2022.
7. Cucalon, L. G., F. Kaseer, E. Arambula-Mercado, A. E. Martin, N. Morian, S. Pournoman, and E. Hajj. The Crossover Temperature: Significance and Application Towards Engineering Balanced Recycled Binder Blends. *Road Materials and Pavement Design. Vol. 20, No. 6.* 2019.
8. Glover, C. J., R. R. Davison, C. H. Domke, Y. Ruan, P. Juristyarini, D. B. Knorr, and S. H. Jung. *Development of a New Method for Assessing Asphalt Binder Durability with Field Validation*. *FHWA/TX Report 05/1872-2*, Texas Department of Transportation, Austin, TX, 2005.
9. Rowe, G. Evaluation of the Relationship between Asphalt Binder Properties and Non-load Related Cracking. *Journal of the Association of Asphalt Paving Technologists, Prepared Discussion, Vol. 80, pp. 649-663.* 2011.
10. Anderson, R. M., G. N. King, D. I. Hanson, and P. B. Blankenship. Evaluation of the Relationship between Asphalt Binder Properties and Non-load Related Cracking. *Journal of the Association of Asphalt Paving Technologists, Vol. 80, pp. 615-663.* 2011.

11. Olard, F., and H. Di Benedetto. General “2S2P1D” Model and Relation between the Linear Viscoelastic Behaviors of Bituminous Binders and Mixtures. *Road Materials and Pavement Design. Vol. 4, No. 2.* 2003.
12. Zeng, M., H. U. Bahia, H. Zhai, M. R. Anderson, and P. Turner. Rheological Modeling of Modified Asphalt Binders and Mixtures. *Journal of the Association of Asphalt Paving Technologists, Vol. 70, pp. 403-441.* 2001.
13. Marasteanu, M. O., Anderson, D. A., "Techniques for Determining Errors in Asphalt Binders Rheological Data," *Transportation Research Record, No. 1766, pp. 32-39.* 2001.
14. Gundla, A., and B. S. Underwood. Molecular Weight Distribution of Asphalt Binders from Laser Desorption Mass Spectroscopy (LDMS) Technique and its Relationship to Linear Viscoelastic Relaxation Spectra. *Fuel, Vol. 262.* 2020.
15. Sui, C., M. J. Farrar, W. H. Tuminello, and T. F. Turner. “New Techniques for Measuring Low-Temperature Properties of Asphalt Binders with Small Amounts of Material,” *Transportation Research Record: Journal of the Transportation Research Board, No. 2179, pp. 23-38.* 2010.
16. Rowe, G. M., and M. J. Sharrock. Alternate Shift Factor Relationships for Describing Temperature Dependency of Viscoelastic Behavior of Asphalt Materials. *Transportation Research Record: Journal of the Transportation Research Board, Vol. 2207.* 2011.
17. Marasteanu, M. O. Inter-conversions of the Linear Viscoelastic Functions Used for the Rheological Characterization of Asphalt Binders, *Ph.D. Dissertation*, The Pennsylvania State University, College Station, PA, 1999.
18. Gordon, G. V., and M. T. Shaw. *Computer Programs for Rheologists*. Hanser/Garnder, 1994.

Chapter 5 Evaluation of Alternative Approaches to Restore the Rheology of Recycled Asphalt Binders

5.1 Introduction

The incorporation of reclaimed asphalt pavement (RAP) into new asphalt mixtures offers economic and environmental benefits, in addition to the performance gains when properly accounted for. The asphalt binder contained within RAP is generally oxidized from in-service aging. Oxidation results in increased stiffness and poorer relaxation characteristics that generally yield poor cracking resistance compared to virgin asphalt binder.

Several strategies exist to counteract the adverse effects of RAP binders. One strategy specified by many state agencies is the use of a softer virgin binder than warranted by the climatic conditions (McDaniel et al. 2000). Another strategy is to incorporate additives, including recycling agents (RAs) and extenders. The effectiveness of RAs has been a topic of great interest in recent years (Haghshenas et al. 2020, Nogueira et al. 2019, Epps Martin et al. 2020, Christensen & Tran 2022). RAs intend to restore the rheological characteristics of recycled binders. RAs are derived from a variety of products and classified into five categories according to the National Center for Asphalt Technology (NCAT) description (2014); paraffinic oils, aromatics extracts, naphthenic oils, triglycerides and fatty acids, and tall oils. Extenders are a similar class of products used to achieve softer binder grades. Crude oil extracts and bio-oils are commonly used to formulate extenders (Daly 2017).

An important aspect of effective RA and extender use is the dosage selection. Various dosage selection procedures exist. For example, NCHRP Project 09-58 suggested selecting the dose of an RA to achieve the intended AASHTO M 320 high-temperature grade in the blend of virgin binder, recycled binder, and additive (Epps Martin et al. 2020). This approach was found to allow as much RA into the blend as possible without compromising the potential rutting resistance. However, this approach could increase the costs of material depending on the overall cost of the additive and too much additive runs the risk of overly softening the binder. Other studies have selected the additive dose to restore the intended low-temperature grade (Preciado et al. 2023). Restoring performance to a low-temperature grade would result in a smaller quantity of additive being used and could potentially lower costs of blends but runs the risk of reducing cracking resistance. Preciado et al. (2023) demonstrated that both dosage selection procedures are successful in achieving rheological properties in recycled binder blends that are similar to

those of virgin binders at the temperature regime that the dosage selection was based on but are distinct at other temperatures. Other studies have relied on fixed dosages, irrespective of the constituent binder and additive properties (Zhang et al. 2023, Bajaj et al. 2020, Haghshenas et al. 2021).

Numerous studies evaluated the effects of RAs, extenders, and soft binders on the rheology of recycled binder blends (Haghshenas et al. 2020, Nogueira et al. 2019, Epps Martin et al. 2020, Christensen & Tran 2022, Zhang et al. 2023, Bajaj et al. 2020, Haghshenas et al. 2021). However, fewer studies compared the use of additives, selected using different dosage selection procedures, to the more conventional use of softer virgin binders at restoring rheology. Additionally, studies that benchmark the performance of recycled binder blends against virgin binders specified in the absence of recycled materials using statistical measures are limited. Furthermore, a wide range of rheological parameters and laboratory aging conditions are reported in past studies to evaluate the durability of recycled binder blends, which makes it challenging to reconcile the findings of different studies that report different rheological measures. While several past studies investigated relationships among alternative rheological parameters (e.g., Rahbar-Rastegar et al. 2017, Zhang et al. 2021) these studies do not encompass recycled binder blends containing RAs or extenders.

This study evaluates the ability of softer virgin binders, RAs, and extenders to restore the rheology of RAP binders to that of virgin binders specified in the absence of recycled materials, termed ‘control’ binders. Additionally, two dosage procedures are examined: restoration of the intended high-temperature climatic grade and restoration of the intended low-temperature grade. A broad range of intermediate- and low-temperature point parameters as well as rheological shape parameters that measure the balance of relaxation and stiffness characteristics of asphalt binder are examined at two long-term age levels. The results of recycled binder blends are compared to the control binders statistically. Furthermore, the acquired data is used to investigate correlations among different rheological parameters and among different long-term age levels for a specific parameter.

5.2 Objectives

The objectives of this chapter are to: (1) evaluate the ability of soft virgin asphalt binders, RAs, and extenders to restore the rheology of RAP binder systems, (2) identify correlations between

alternative rheological indicators of durability and between the results of a given parameter at different long-term age levels for the study materials.

5.3 Materials and Methods

5.3.1 Materials

This study involved testing four types of materials: (1) PG 64-22 virgin asphalt binders (termed control binders); (2) combinations of PG 58-28 virgin binder and recovered RAP binder at recycled binder replacement ratios (RBRs) that matched a specific asphalt mixture (termed reference blends); (3) combinations of virgin binder (either PG 58-28 virgin binder or PG 64-22 virgin binder), recovered RAP binder, and either an extender (termed the extender blends), and (4) combinations of PG 64-22 virgin binder, recovered RAP binder, and an RA (termed the RA blends). The collective RA and extender blends are referred to as the modified blends and the more generic term *blends* is used to refer collectively to reference blends and modified blends. The modified blends were prepared using the same RBRs as the respective reference blends.

Mixture designs from one North Carolina Department of Transportation (NCDOT) type RS9.5B approved surface mixture and three differently sourced Virginia DOT (VDOT) Type A approved surface mixtures were evaluated in this study. The NCDOT mixture with the RAP denoted as R1 had an RBR of 0.35. The three VDOT mixtures with RAP sources are denoted as R2, R3, and R4 and had RBRs of 0.35, 0.29 and 0.31, respectively. Three control binders were evaluated including one PG 64-22 binder from a NC supplier and two PG 64S-22 binders from VA suppliers, referred to herein as 64-1, 64-2, and 64-3, respectively. Also, one PG 58-28 binder, 58, sampled from NC but also commonly used in VA, was used to constitute the reference blends that represent the NCDOT and VDOT specified asphalt mixtures. Both VDOT and NCDOT specify PG 64-22 binders for virgin mixtures and allow PG 64-22 in low RAP mixtures. The current practice for the NCDOT is to use a PG 58-28 virgin binder in RBR mixtures. VDOT also allows the use of PG 58-28 virgin binders in RAP mixes. The 58 binder was also used to prepare some of the extender blends because the use of the PG 64-22 binders resulted in excessive dosages.

Four extenders, denoted E1 through E4 to preserve supplier anonymity were evaluated. E1 and E4 are both re-refined engine oil bottom (REOB) from different sources. E2 also contains an unspecified amount of REOB and E3 is a vacuum gas oil (VGO). Seven RAs were evaluated.

The RAs denoted TF1 through TF4 are all bio-oils derived from triglycerides and fatty acids. The RAs named A and TO are an aromatic extract and tall oil, respectively.

The component materials were used to prepare three reference blends, five extender blends, and 22 RA blends, detailed in Table 17. These binder systems were evaluated as part of research projects sponsored by the NCDOT and VDOT. The dosages are expressed as a percentage of the combined mass of virgin and recycled binder in the blend. The dosage level of the modified blends representing the NC (i.e., R1) mixture were selected to restore the AASHTO M 320-21 high-temperature PG (PGH) of the modified blend to a target of 64°C, as detailed elsewhere (Fried et al. 2022). For the blends representing the VA (i.e., R2, R3, and R4) mixtures, the dosage of RA or extender used to prepare each modified blend was selected based on the manufacturer's recommendation to restore the low-temperature PG (PGL) of the modified blend to -22°C. A maximum additive dosage limit of 10% was also considered when preparing all blends per NCHRP Project 09-58 recommendations (Epps Martin et al. 2020). Correspondingly, the continuous PGH and PGL temperatures reported in Table 7 show that the modified blends for the NC mixture have continuous PGH (PGH_c) values between 64°C and 69°C and the modified blends for the VA mix generally have PGL values between -22°C and -28°C. Notably, the TF4 blends have continuous PGL (PGL_c) values below -28°C. There are also several VA blends that did not achieve the intended minimum PGL of -22°C. Also notable, the NC modified blends have PGL_c values falling below -28°C, the VA modified blends have PGH_c values falling above 70°C in many cases, aligning with reports by Preciado et al. (2023) that restoring target PG properties in one temperature regime leads to notably distinct properties from the PG in the opposite temperature regime. The reference blends have PGH_c values between 70.5°C and 72.9°C and PGL_c values spanning -23.1°C to -27.6°C.

5.3.2 Blend Preparation and Conditioning Procedures

The recycled asphalt binders used to prepare the blends were extracted and recovered from each RAP source in accordance with ASTM D2172, Test Method A, and ASTM D5404. The blends were prepared using the preheating and mixing procedure detailed by Fried et al. (2022). The virgin and RAP binders were preheated to 140°C and then blended using a power drill with a paddle attachment. Finally, the RAs were incorporated using a syringe.

The control binders and blends were subjected to conditioning in the Rolling Thin Film Oven (RTFO) in accordance with AASHTO T 240-21. The RTFO-aged material was subjected

to further conditioning in the Pressurized Aging Vessel (PAV) in accordance with AASHTO R 28-21 at two durations, 20 hours (referred to as PAV-20) and 40 hours (PAV-40) (Haghshenas et al. 2021, Bonaquist et al. 2021, Bennert et al. 2023).

Table 17. Summary of the Binders and Blends Evaluated

Binder/Blend	PGH_c (°C)	PGL_c (°C)	Additive Dose (%)	RBR
64-1	69.0	-25.6	NA	NA
64-1.R1.TF1	66.8	-32.1	5.5	0.35
64-1.R1.TF2	67.7	-32.1	5.5	0.35
64-2	67	-24.6	NA	NA
64-2.R4.TO	71.7	-22.7	2.9	0.35
64-2.R3.E4	69.0	-24.9	10.0	0.3
64-2.R3.A	72.6	-24.9	2.4	0.3
64-2.R3.TO	70.4	-26.3	1.8	0.3
64-2.R2.TF3	74.5	-23.6	3.2	0.29
64-2.R4.TF4	66.7	-30.3	6.0	0.35
64-2.R2.TF4	67.7	-30.1	6.0	0.29
64-2.R4.TF1	71.8	-28.4	3.0	0.35
64-3	68.1	-22.4	NA	NA
64-3.R4.E4	73.6	-19.5	10.0	0.35
64-3.R4.A	75.3	-18.6	2.8	0.35
64-3.R2.A	76.1	-20.2	3.8	0.29
64-3.R3.A	73.2	-22.9	2.6	0.30
64-3.R4.TO	69.6	-20.7	3.8	0.35
64-3.R2.TO	71.8	-23.7	4.0	0.29
64-3.R3.TO	69.6	-23.3	2.9	0.30
64-3.R4.TF3	71.5	-27.5	4.1	0.35
64-3.R2.TF3	73.2	-24.1	4.1	0.29
64-3.R3.TF3	71.9	-27.9	3.1	0.30
64-3.R2.TF4	70.2	-29.4	6.0	0.29
64-3.R3.TF4	64.5	-30.9	6.0	0.30
64-3.R4.TF1	71.1	-25.5	3.7	0.36
64-3.R3.TF1	70.4	-23.9	2.7	0.30
58	60.6	-31.3	NA	NA
58.R1.E1	68.3	-28.9	3.9	0.35
58.R1.E2	68.3	-29.5	7.0	0.35
58.R1.E3	65.7	-31.9	6.7	0.35
58.R1	71.8	-27.6	NA	0.35
58.R3	70.5	-26.2	NA	0.30
58.R4	72.9	-23.1	NA	0.35

NA = not applicable.

5.3.3 Test Methods

The control binders and blends were evaluated using standard Bending Beam Rheometer (BBR) and Dynamic Shear Rheometer (DSR) tests that align with AASHTO M 320-17 at both the PAV-20 and PAV-40 age levels. Low-temperature characterization was conducted using a BBR in accordance with AASHTO T 313-19. Testing was carried out at two temperatures, one meeting the AASHTO M 320-21 PG criteria and another failing. The intermediate-temperature characterization was carried out in the DSR at 25°C in accordance with AASHTO T 315-20 and the corresponding PG criteria specified in AASHTO M 320-21. In addition, temperature-frequency sweep (TFS) testing at the PAV-20 and PAV-40 age levels was conducted using the 8-mm parallel plate geometry with a 2-mm gap on the DSR. Testing at each temperature and frequency combination was done in accordance with AASHTO T 315-20 guidelines. TFS tests were conducted at temperatures of 5°C, 20°C, 35°C, and 50°C over a frequency range of 0.1 to 10 Hz. A strain amplitude of 1.0 percent was applied at 35°C and 50°C while the strain level was 0.1 percent at 5°C and 20°C. These strain levels were verified to yield test results that fell within the linear viscoelastic regime based on strain sweep testing conducted on a subset of the study binders. In the case of all DSR and BBR tests, two replicate tests were conducted for each temperature and age level combination.

DSR testing was carried out at North Carolina State University whereas BBR testing was conducted at the NCDOT Materials and Tests Unit (for 64-1 and R1 blends) or the Virginia Transportation Research Council (VTRC) laboratory (all other binders and blends). Test results were evaluated with respect to established precision limits for repeatability for $|G^*|sin\delta$ in AASHTO T 315-20 and both $S(60)$ and $m(60)$ in AASHTO T 313-19. The test results met repeatability requirements for the NCDOT binders and blends. However, challenges were faced in meeting the AASHTO T 313-19 repeatability requirements for a significant number of the VA binders and blends. The variability in the BBR test results of the VA binders and blends led to counterintuitive trends in the average values of rheological parameters with respect to age level in some cases. Definitive causative factors for this higher-than-normal variability were not identified. Consequently, the BBR test results and associated parameters for the VA binders and blends are omitted from the correlation analysis amongst parameters to provide more clear insight into correlation analysis. It is important to note that the PGL_c values for the VA binders

and blends reported in Table 17 are regarded as approximations given that most did not meet the repeatability requirements.

5.3.4 Statistical Analysis

5.3.4.1 Comparisons of the Blends to the Control Binder

Statistical tests were conducted to compare the blends to a respective control binder. Recall, the control binders are PG 64-22 virgin binders, which are considered to represent the target binder properties. Within the statistical analysis, RA blends were compared to the specific control binder contained within the blend. The same applied to the extender blends that contained a control virgin binder. The extender blends that contained the 58 virgin binder were compared to the 64-1 binder, sourced from the same state. Reference blends were also compared to the respective control binders from the same state. The data was grouped based on the control binder and Bartlett's test (Guthrie 2020) for equal variance was conducted for each group, parameter, and age level combination. If the resultant p-value exceeded 0.05, the assumption of equal variance was accepted and Dunnett's test (Lee et al. 2018) was conducted to compare each blend to the respective control using a significance level of 0.05. Hence, if Bartlett's test resulted in a p-value less than 0.05, then the blends with the highest standard deviations were removed sequentially until a Bartlett's test result with a p-value greater than 0.05 was obtained. Subsequently, Dunnett's test was conducted using the aforementioned approach on the remaining data set. Overall, very few results were omitted due to unequal variance.

If the statistical analysis indicated a blend result was different from the control, the blend was deemed worse or better based on the results and whether a higher or lower parameter is desired as specified in the rheological parameters evaluated.

5.3.4.2 Correlation Analysis

Spearman's rank correlation coefficients (Zaiontz 2023) were calculated for each possible pair of the parameters listed in Chapter 5 to identify groups of durability-related parameters that provide similar insight regarding the relative performance of study binders and blends. Correlation coefficients were calculated separately for results at the PAV-20 and PAV-40 age levels at this stage. Spearman's rank correlation coefficients were also calculated for each parameter at the PAV-20 versus PAV-40 levels to evaluate if the two age levels provide similar or distinct insight regarding the relative performance of the study binders and blends.

Spearman's rank correlation is a nonparametric measure of rank correlation between two variables, defined according to Equation **(29)**. It assesses whether monotonic relationships exist between two variables without the stipulation of a linear relationship. Spearman's rank correlation coefficient ranges from negative one (-1) to one (+1) with negative one (-1) indicating a negative relationship, one (+1) indicating a positive relationship, and values close to zero indicating very weak associations.

$$r = 1 - \frac{6\sum d_i^2}{n(n^2-1)} \quad \textbf{(29)}$$

where r = Spearman's rank correlation coefficient; d_i = difference between the two ranks of each observation; n = number of observations.

5.4 Results

5.4.1 Comparisons of the Blends to the Controls

The comparisons of the virgin binders to that of blends containing recycling agents and additives was performed to provide a direct analysis of the impact of additives on the specific binder used for each blend. These virgin binders were typical for that of 64-22 in NC and VA. Figure 31 through Figure 33 present the comparisons between the 64-1 control virgin binder and respective blends for the low-temperature parameters, intermediate-temperature parameters, and rheological balance parameters, respectively. Recall that the modified R1 blends were all prepared with additive dosages to restore the modified blend PGH to 64°C. In most but not all cases, the statistical comparisons between a given blend and the control for a given parameter are the same at the PAV-20 and PAV-40 age levels (e.g. better or worse at both age levels).

Figure 31 and Figure 32(a) show that the reference blend (58.R1), reflecting the NCDOT's current practice to use a PG 58-28 virgin binder in high RBR mixtures, resulted in statistically equal or better low- and intermediate-temperature PG properties compared to 64-1 (the control binder) at both aging levels. Notably, the 58.R1 blend has lower $S(60)$ but statistically equal $m(60)$ values to the 64-1, indicating a distinct balance of stiffness and relaxation characteristics. However, Figure 32(b) and (c) show that, compared to the control, the 58.R1 blend tends to exhibit inferior $GR_{25°C}$ and $GR_{15°C}$ values. Both 64-1 and 58.R1 fail the $GR_{15°C}$ crack onset limit at the PAV-40 age level. Figure 33 shows that the 58.R1 blend yields statistically equivalent $R_{09\text{-}59}$ and ΔT_c values to 64-1 but generally inferior R_{MC} and T_{45} values.

The TF and 58.R1.E3 (VGO) blends exhibit rheological properties that are better than 64-1 with the exception of the rheological balance parameters. These blends generally have statistically equal ΔT_c values to 64-1 often inferior R_{MC} and $R_{09\text{-}59}$ parameters. The 58.R1.E1 and 58.R1.E2 blends are also generally deemed statistically equal or better than 64-1 with the exception of the rheological balance parameters shown in Figure 33 where they often appear inferior. Notably, these blends reach the ΔT_c limit of -5°C at the PAV-40 age level. Recall that E1 and E2 both contain REOB, which is known to negatively impact the balance of stiffness and relaxation characteristics (Bennert et al. 2023). The 58.R1.E2 and 64-1 binders also fail the $GR_{15°C}$ crack onset limit at the PAV-40 age level.

Also notable, the 64-1 and blends all surpass the warning limit for T_{45} at the PAV-40 age level. Several cases also fail this limit at the PAV-20 age level (58.R1, 58.R1.E1, and 58.R1.E2).

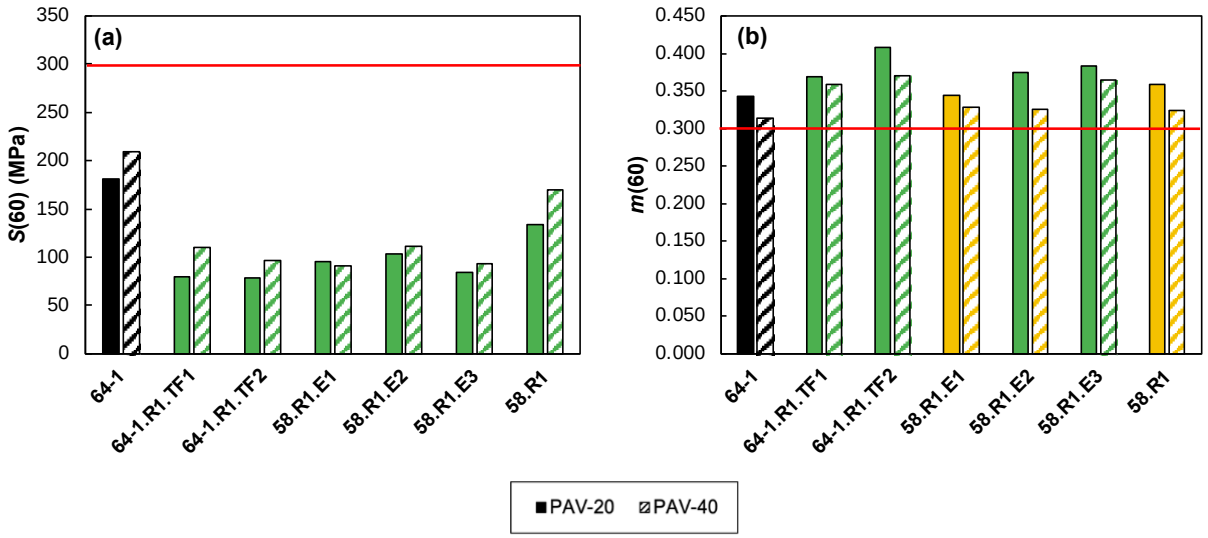

Figure 31. Low-temperature point parameters: (a) *S*(60) and (b) *m*(60). Colors convey Dunnett's test results: green, yellow, and red indicate better, equal, and worse results relative to 64-1, respectively.

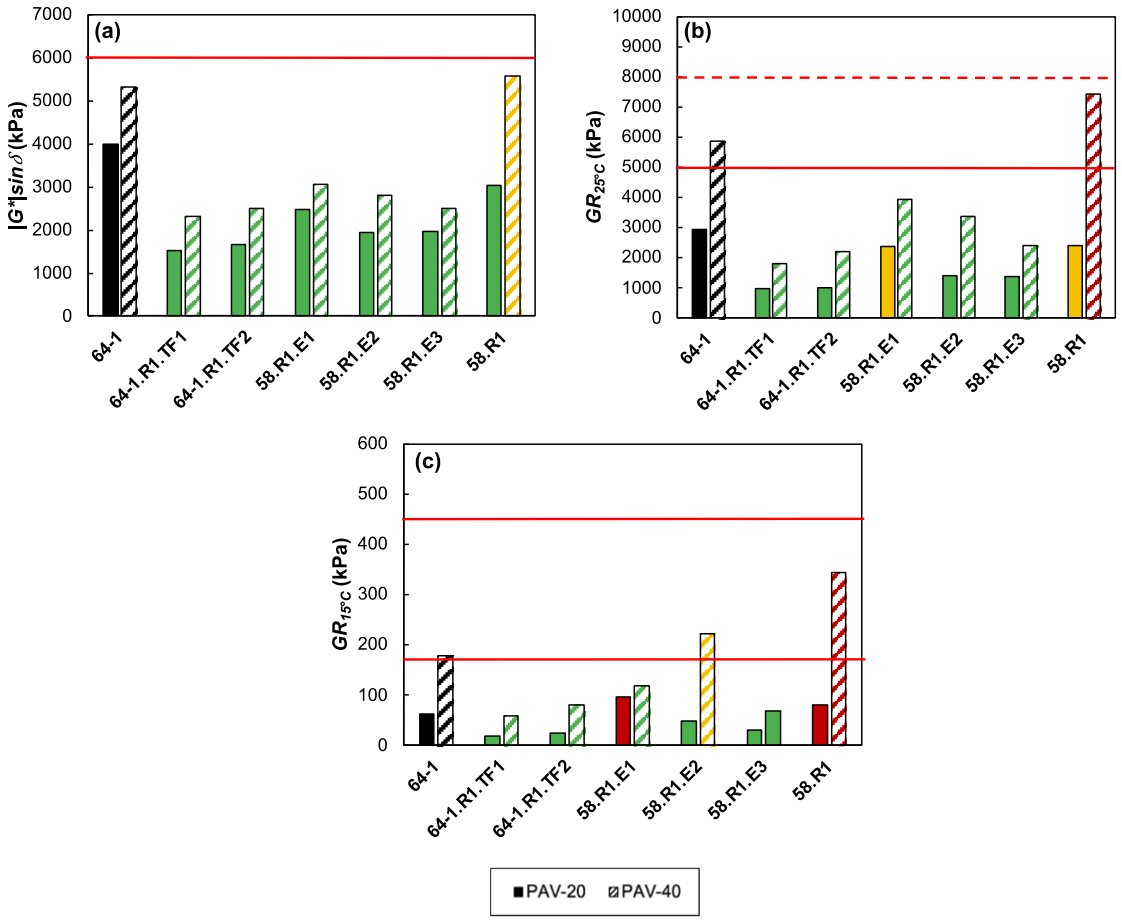

Figure 32. Intermediate temperature point parameters: (a) $|G^*|\sin\delta$, (b) $GR_{25°C}$, and (c) $GR_{15°C}$. Colors convey Dunnett's test results: green, yellow, and red indicate better, equal, and worse results relative to 64-1, respectively.

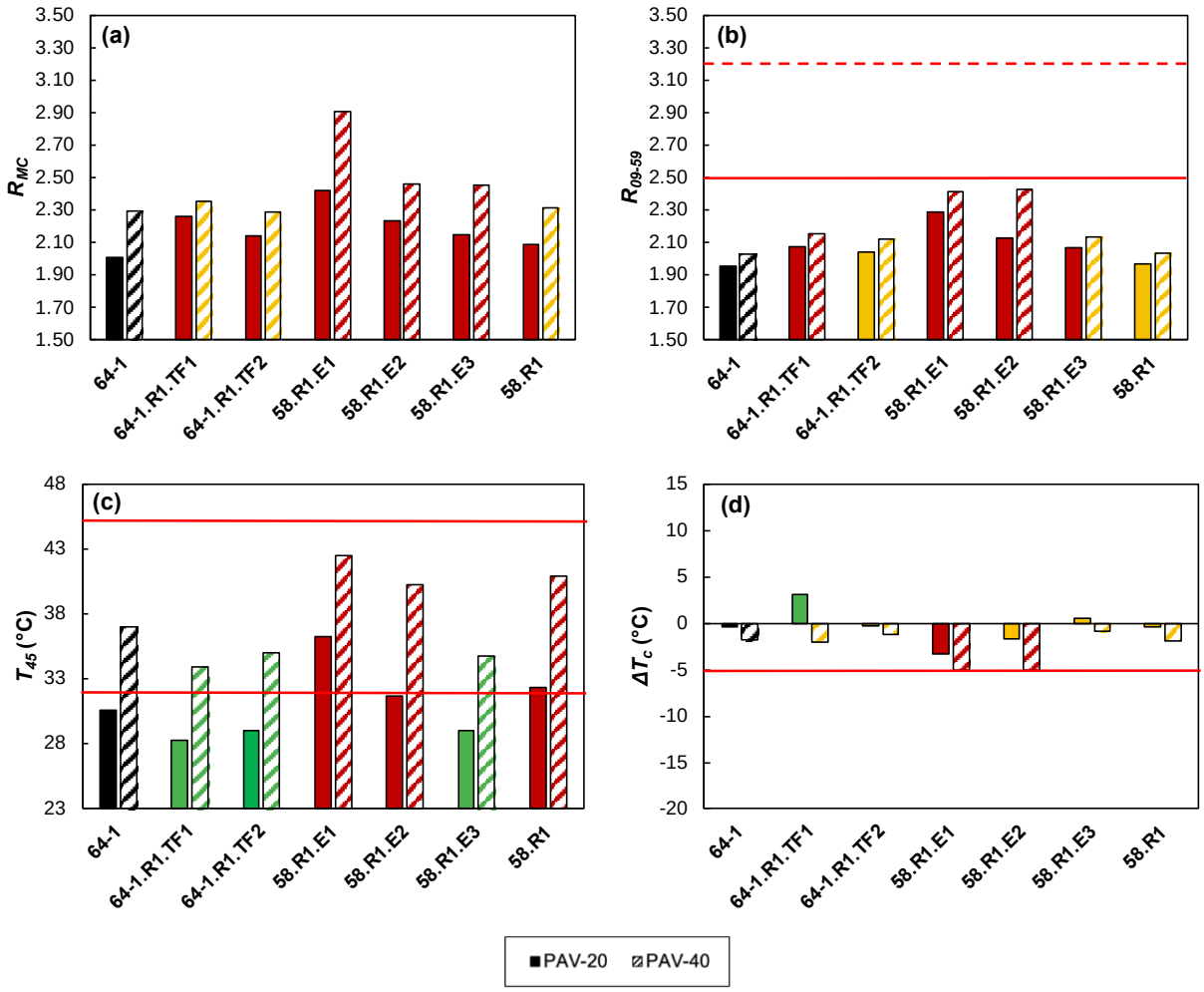

Figure 33. Rheological balance parameters: (a) R_{MC}, (b) $R_{09\text{-}59}$, (c) T_{45}, and (d) ΔT_c. Colors convey Dunnett's test results: green, yellow, and red indicate better, equal, and worse results relative to 64-1, respectively.

5.4.2 Evaluation of the Blends Corresponding to the Virginia Mixtures

Figure 34 and Figure 35 showcase the comparisons for differences in low-temperature point parameters for the 64-2 control virgin binder and the 64-3 control virgin binder respectively. Figure 36 and Figure 38 present the comparisons between the 64-2 control virgin binder and respective blends for the intermediate-temperature parameters and rheological balance parameters, respectively. Figure 37 and Figure 39 present the comparisons between the 64-3 control virgin binder and respective blends for the intermediate-temperature parameters and rheological balance parameters, respectively. Recall that the modified 64-2 and 64-3 blends were

all prepared using additive dosages provided by the manufacturers intended to restore the PGL to -22°C and are discussed collectively.

Similar to the NC blend case, the VDOT reference blends often exhibit equal or better $S(60)$, $m(60)$, $|G^*|sin\delta$ values compared to the 64-2 and 64-3 binders. In some cases, the reference blends also have similar $GR_{25°C}$ values to the controls at the PAV-20 age level but are generally inferior on the basis of the other rheological characteristics evaluated. Despite these inferior characteristics compared to the controls, the reference blends still meet the established criteria with the exception of the $GR_{15°C}$ crack onset limit and the T_{45} warning limit at the PAV-40 age level. Numerous other cases fail the T_{45} warning limit and the 64-2 and 64-3 binders also fail the $GR_{15°C}$ crack onset limit at the PAV-40 age level.

The comparisons between the modified blend and control results are more varied. The TF (triglyceride and fatty acid) and TO (tall oil) blends generally compare most favorably to the controls. These blends generally display equal or better $S(60)$, $m(60)$, $|G^*|sin\delta$ and $GR_{25°C}$ values than their respective controls, with generally more cases of better performance at the PAV-40 than PAV-20 age level. An exception is the 64-3.R2.TO blend. The TF and TO blends exhibit more varied $GR_{15°C}$ comparisons to the controls with many cases indicating an inferior response. However, the TF4 blends consistently exhibit better $GR_{15°C}$ values than the control binders (64-2 and 64-3) and constitute the only modified blends to pass the $GR_{15°C}$ crack onset limit at the PAV-40 age level. Figure 38 and Figure 39 show that the majority of the modified blends have inferior R_{MC}, $R_{09\text{-}59}$, ΔT_c and T_{45} values compared to the respective controls with a few exceptions for select TO and TF4 blends. Additionally, the majority of blends containing 64-2 and 64-3 surpassed the limit for ΔTc of -5.0°C at the PAV-40 age level indicating that these blends would experience worse performance at this age level. Overall, the TF4 blends exhibited the best performance measures of the VA blends. However, while the manufacturer was asked to supply a TF4 dosage to restore the intended PGL, Figure 34 shows an excessive dosage that restored the PGH was provided. Thus, the findings of the TF4 blends tend to align with those for the TF1 and TF2 blend cases where the dosage was selected to restore the PGH.

The A (aromatic extract) blends consistently exhibit inferior properties compared to controls and tend to fail established limits. The E4 (REOB) blends tend to compare favorably to the controls on the basis of $|G^*|sin\delta$ but exhibit instances of worse $GR_{15°C}$ and $GR_{25°C}$ values that exceed recommended limits in some instances. Many modified blends fail the T_{45} warning limit

with one extender blend case (64-3.R4.E4) surpassing the failure limit at the PAV-40 age level. Like the cases for the NC REOB blends, the inferior behavior of the 64-3.R4.E4 is best captured through the rheological balance measures.

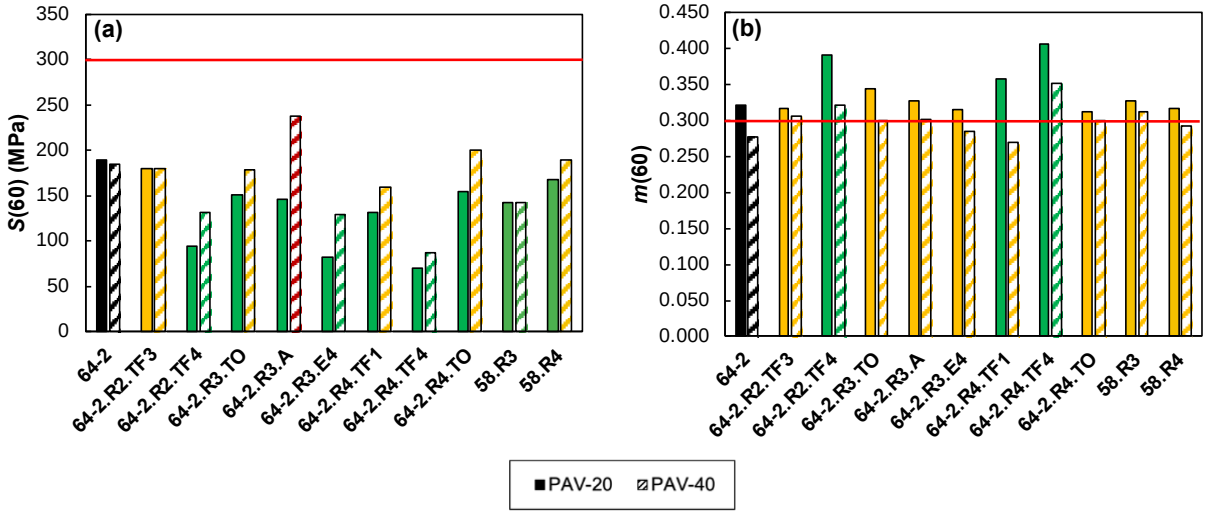

Figure 34. Low-temperature point parameters: (a) *S*(60) and (b) *m*(60). Colors convey Dunnett's test results: green, yellow, and red indicate better, equal, and worse results relative to 64-2, respectively.

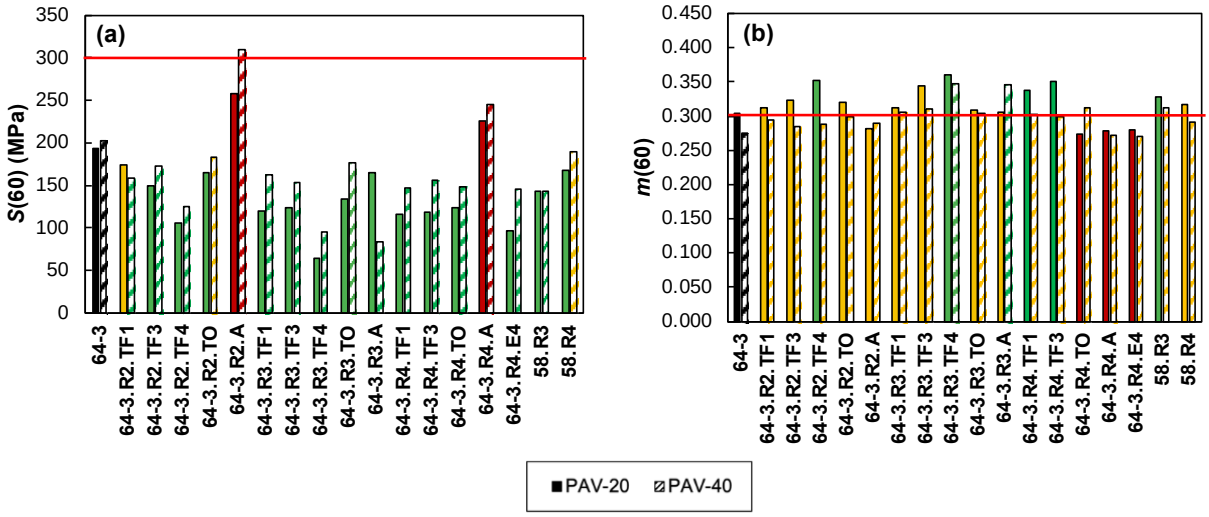

Figure 35. Low-temperature point parameters: (a) *S*(60) and (b) *m*(60). Colors convey Dunnett's test results: green, yellow, and red indicate better, equal, and worse results relative to 64-3, respectively.

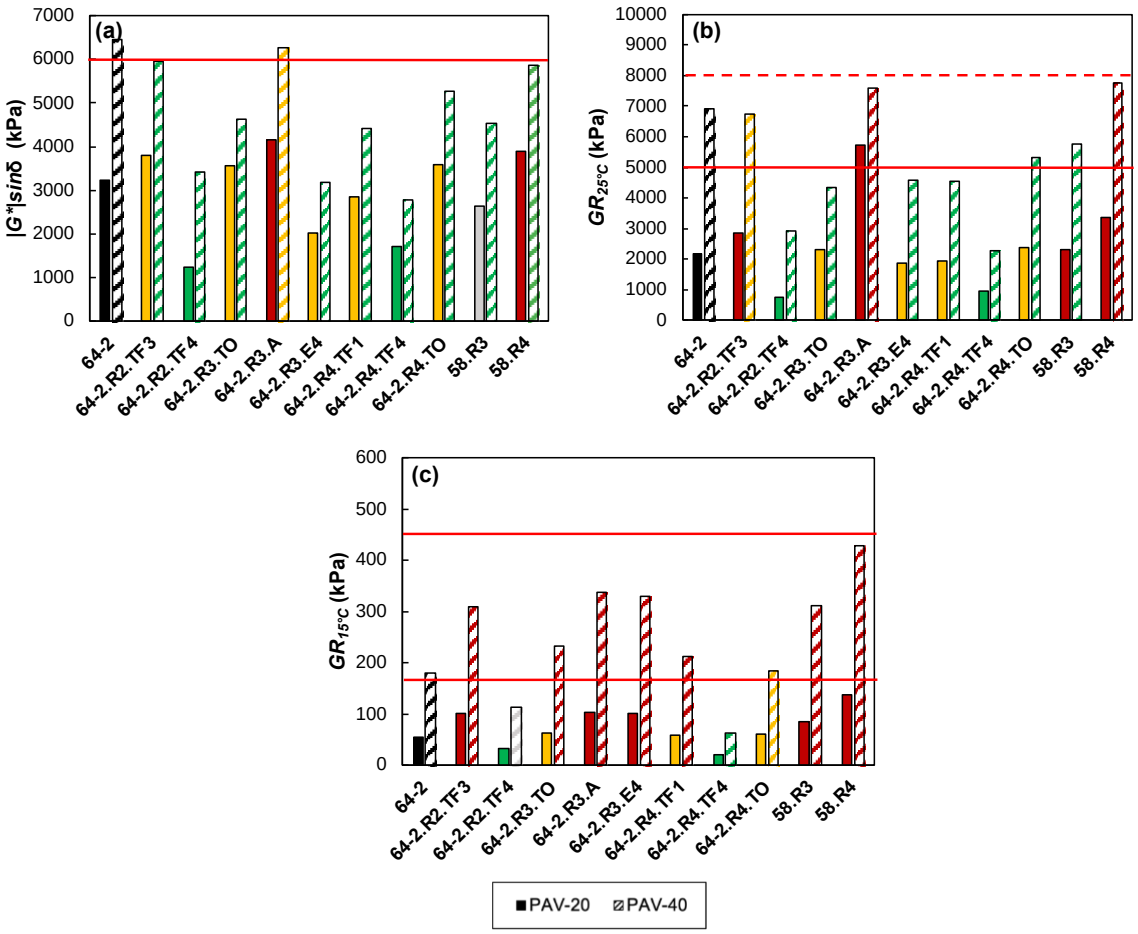

Figure 36. Intermediate temperature point parameters: (a) $|G^*|sin\delta$, (b) $GR_{25°C}$, and (c) $GR_{15°C}$. Colors convey Dunnett's test results: green, yellow, and red indicate better, equal, and worse results relative to 64-2, respectively. Gray indicates Dunnett's test could not be conducted due to unequal variance.

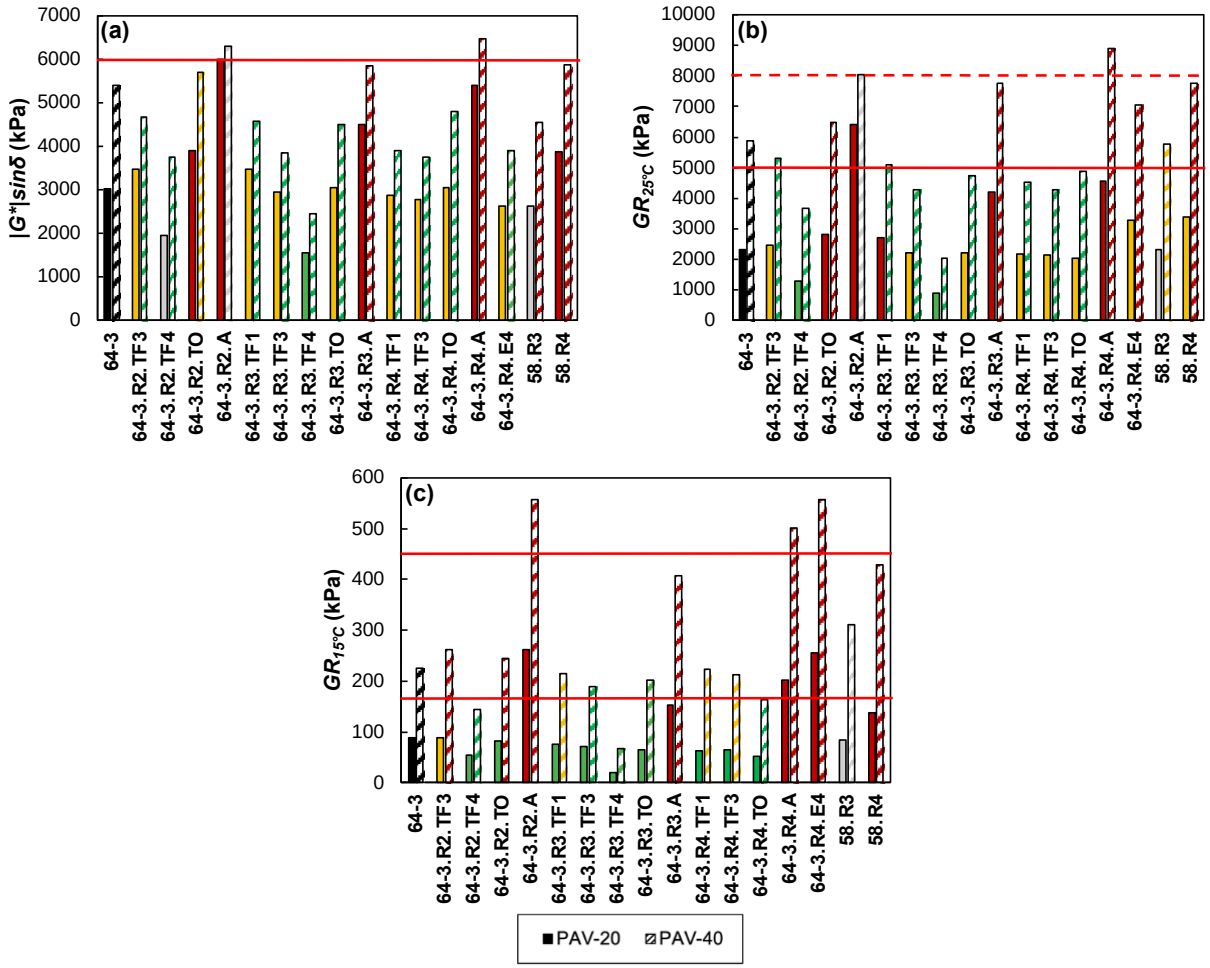

Figure 37. Intermediate temperature point parameters: (a) $|G^*|\sin\delta$, (b) $GR_{25°C}$, and (c) $GR_{15°C}$. Colors convey Dunnett's test results: green, yellow, and red indicate better, equal, and worse results relative to 64-3, respectively. Gray indicates Dunnett's test could not be conducted due to unequal variance.

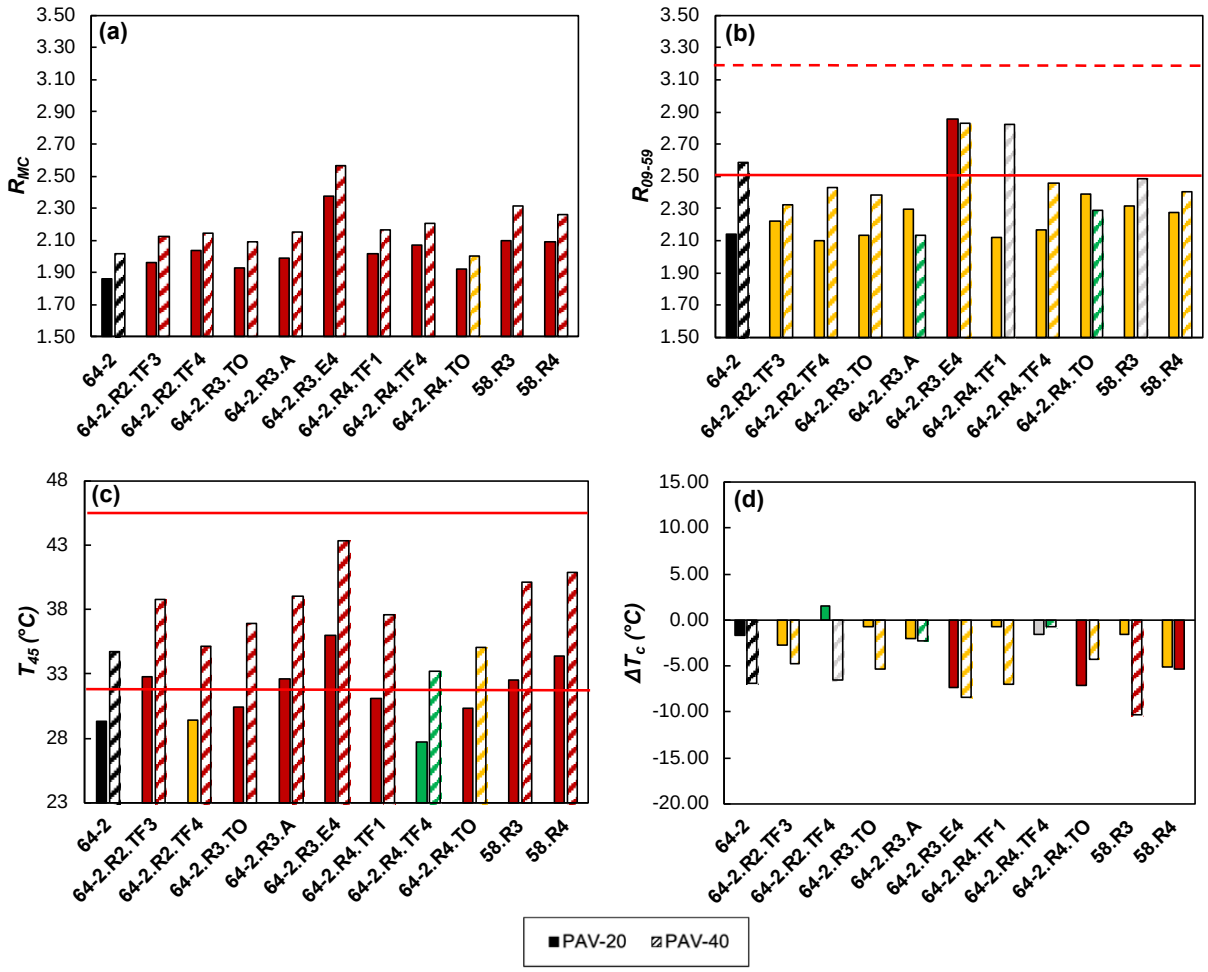

Figure 38. Rheological balance parameters: (a) R_{MC}, (b) $R_{09\text{-}59}$, (c) T_{45}, and (d) ΔT_c.. Colors convey Dunnett's test results: green, yellow, and red indicate better, equal, and worse results relative to 64-2, respectively. Gray indicates Dunnett's test could not be conducted due to unequal variance.

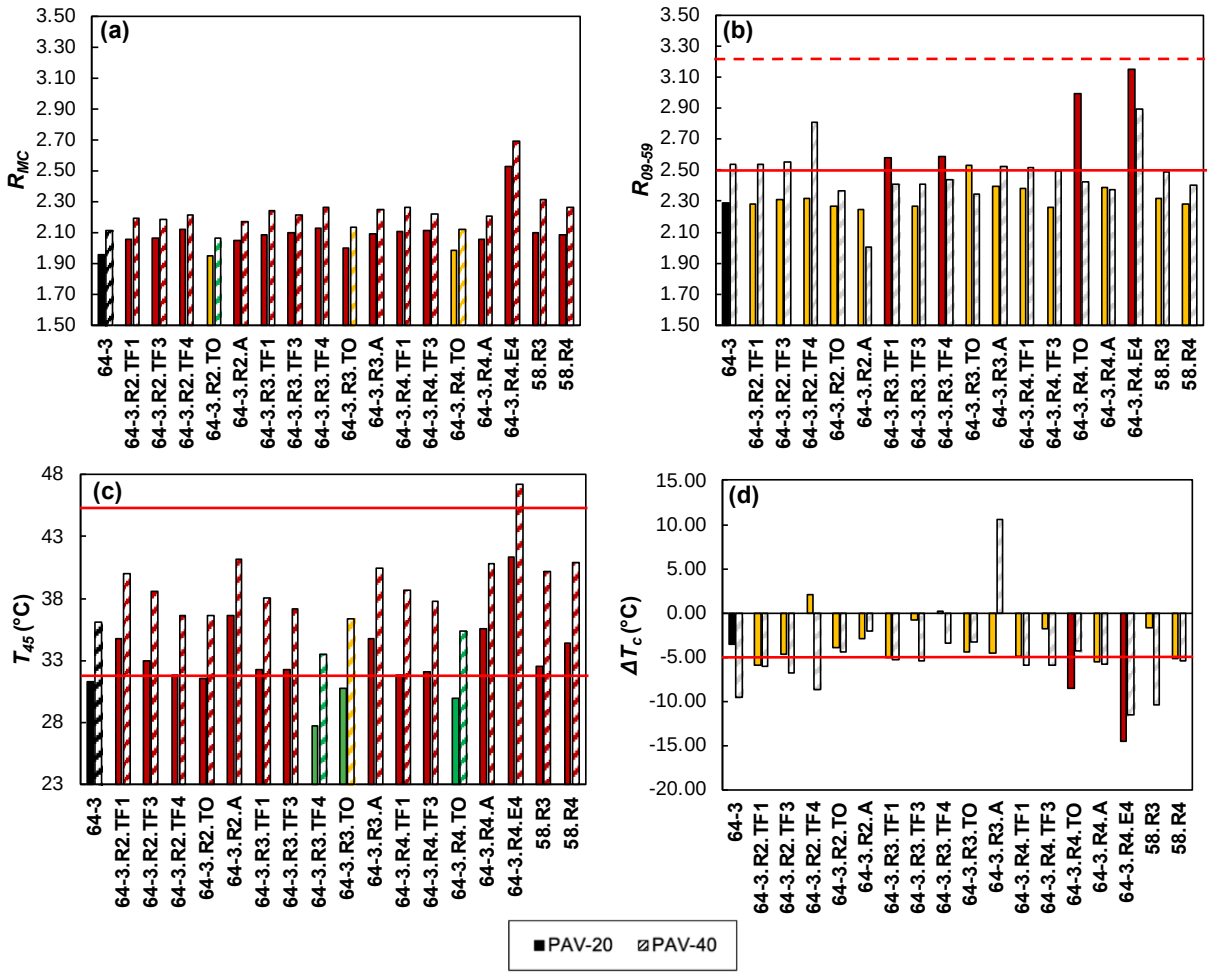

Figure 39. Rheological balance parameters: (a) (a) R_{MC}, (b) $R_{09\text{-}59}$, (c) T_{45}, and (d) ΔT_c. Colors convey Dunnett's test results: green, yellow, and red indicate better, equal, and worse results relative to 64-3, respectively. Grey indicates Dunnett's test could not be conducted due to unequal variance.

5.4.2.1 Correlation Analysis

The values of correlation coefficient (*r*) were calculated for each possible pair of parameters to identify groups of durability-related parameters that provide similar insight regarding the relative behavior of the study binders and blends. For the analysis of all the parameters, the low-temperature correlations were only completed for NCDOT blends and not VDOT blends due to the poor repeatability. Figure 40 and Figure 41 show the Spearman's rank correlation coefficient values among the different pairs of parameters at the PAV-20 and PAV-40 age levels, respectively. The $|G^*|sin\delta$ and $GR_{25°C}$ are highly correlated at both age levels with *r* values near 0.90. The $GR_{25°C}$ and $GR_{15°C}$ also have high correlation coefficients above 0.80 at both age levels.

However, the $GR_{15°C}$ and $|G^*|sin\delta$ are more moderately correlated with r values just below 0.70, which may explain why $GR_{15°C}$ often yielded distinct conclusions regarding the relative performance of the control binders and blends compared to $|G^*|sin\delta$. Interestingly, the intermediate-temperature point parameters are also all moderately correlated with $m(60)$ at both age levels with r values spanning -0.67 to -0.76. The two low-temperature point properties, $S(60)$ and $m(60)$ are more modestly correlated with r values of -0.57 and -0.69 at the PAV-20 and PAV-40 age levels, respectively. While $S(60)$ exhibits modest associations with the intermediate-temperature point parameters at the PAV-20 age level, correlation coefficients with these parameters are very low (below 0.40) at the PAV-40 age level.

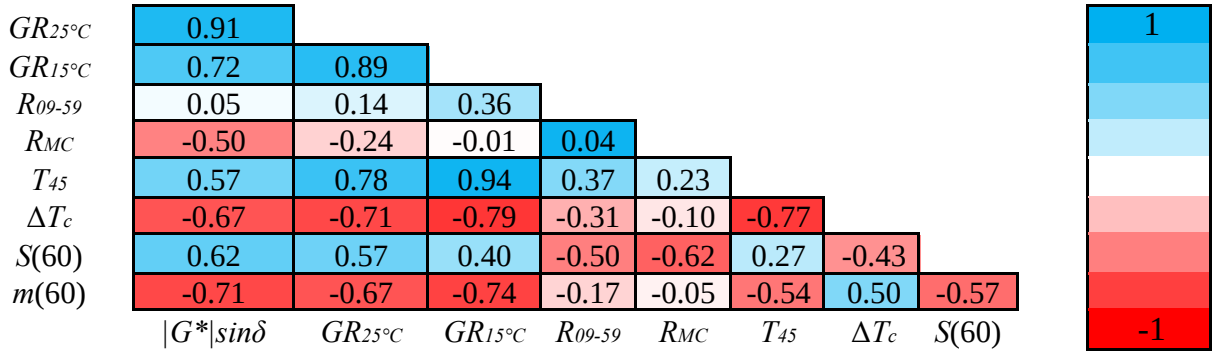

Figure 40. Spearman's Rank Correlation Coefficient Values at the PAV-20 Age Level

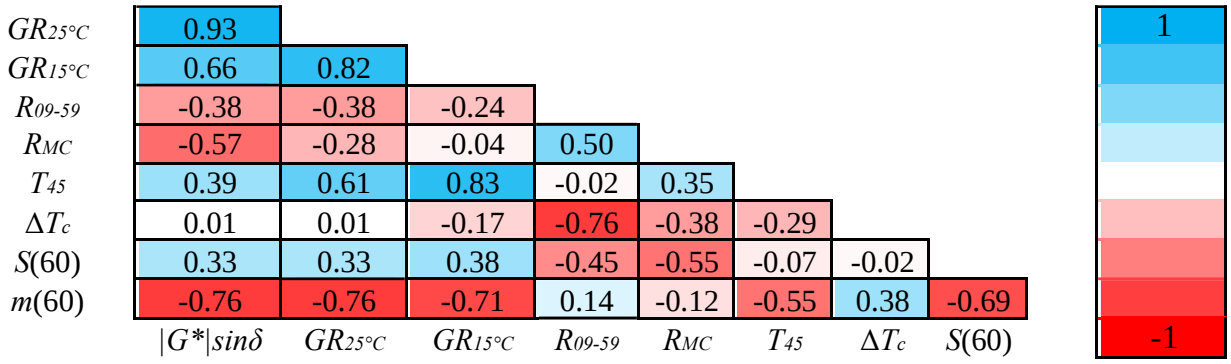

Figure 41. Spearman's Rank Correlation Coefficient Values at the PAV-40 Age Level

The $GR_{25°C}$ and $GR_{15°C}$ exhibit moderate to high correlations with T_{45} with r values consistently above 0.60. However, the other rheological balance parameters do not exhibit any strong associations with the point parameters, suggesting that point and balance parameters bring unique insight to inferences of relative binder performance. While Christensen and Tran (2022) suggested that R_{09-59} and ΔT_c provide redundant information, the two parameters are only highly correlated for the study dataset at the PAV-40 age level. One might also expect the R_{09-59} and

R_{MC} values to be correlated given they are meant to represent the same measure. However, a strong correlation is only apparent at the PAV-20 age level (r = 0.95). The assumption of a glassy modulus may have contributed to the absence of relationships among the $R_{09\text{-}59}$, R_{MC}, and ΔT_c parameters. Lesueur et al. (2021) derived and verified an analytical relationship between ΔT_c and R that included the binder-specific glassy modulus as a variable. Inference of the glassy modulus would have required extrapolation outside of the measurement range, which was why a uniform value was adopted. While weak correlations among $R_{09\text{-}59}$, R_{MC}, and ΔT_c exist in some cases, in many cases, these parameters yielded similar findings regarding the relative properties of the blends compared to the controls. Figure 42 shows that most parameter results are positively correlated at the two age levels with most r values exceeding 0.80, indicating the binders and blends generally aged in a predictable manner. However, there are two cases where moderate correlations falling below 0.70 are evident: $S(60)$ and ΔT_c, suggesting motivation for the PAV-40 age level to evaluate the resistance of binders to extended field aging. The comparatively low correlation for ΔT_c (r = 0.57) is a consequence of the moderate correlation in $S(60)$ at the two age levels and a relatively high but imperfect correlation in $m(60)$. However, $R_{09\text{-}59}$, which is also calculated from $S(60)$ and $m(60)$, displays a very high correlation between the two age levels (r = 0.96).

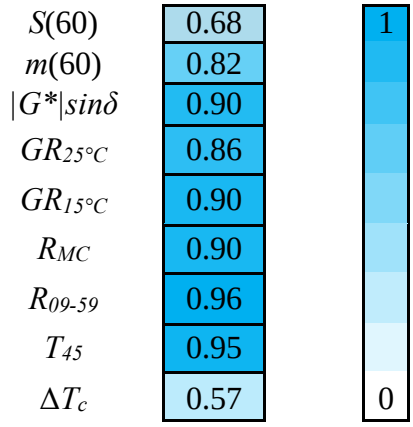

Figure 42. Spearman's Correlation Coefficients Comparing PAV-20 to PAV-40

5.5 Conclusions

The primary findings and conclusions drawn from this study are:

- In most cases evaluated, the reference and RA blends met established rheological property limits. The primary exceptions occurred at the PAV-40 age level for the T_{45} warning limit and the $GR_{15°C}$ crack onset limit. However, even PG 64-22 virgin binders displayed failing cases for these parameters.
- The reference blends often exhibit similar or better performance-graded properties but often exhibit inferior $GR_{15°C}$ and $GR_{25°C}$ and rheological balance parameters compared to the PG 64-22 virgin binders evaluated.
- The rheological characteristics of the RA blends varied with the RA type and dosage.
- The TF blends with dosages that restored the intended PGH generally display superior properties compared to PG 64-22 virgin binder with the exception of certain measures of the rheological balance.
- The parameter of ΔT_c had a suggested limit of -5.0°C that low-temperature restoration blends struggled to meet after undergoing aging at the PAV-40 level
- The TF and TO blends with dosages selected to restore the intended PGL generally show equal or better $|G^*|sin\delta$ and $GR_{25°C}$ values than PG 64-22 binder but exhibit cases of inferior $GR_{15°C}$ results. These blends also generally display inferior rheological balance measures results compared to PG 64-22 binder.
- The A blends with dosage selected to restore the PGL exhibited inferior rheological properties to PG 64-22 binder on the basis of the vast majority of the blends and parameters evaluated. The A blends also tended to fail established limits for the rheological parameters.
- The VGO (E3) extender blend rheological properties are comparable to the TF RA blends that followed the same dosage selection procedure. In contrast, the blends with extenders that contained REOB (E1, E2, E4) generally exhibit inferior rheological balance measures compared to the PG 64-22 binders irrespective of the dosage selection procedure.
- The results of this study suggest that point parameters and balance parameters are generally weakly correlated, suggesting they provide unique insight regarding the rheological behavior of binders. Moreover, the results of this study indicate that recycled binder blends often

exhibit inferior rheological balance parameters, indicating these measures are important to distinguish between virgin and recycled binder blends.

- While correlations exist between the intermediate-temperature point parameters evaluated, the $GR_{15°C}$ and $GR_{25°C}$ identified more cases of potentially inferior performance in the blends compared to the PG 64-22 virgin binders, suggesting they warrant consideration as alternative specification parameters.
- For the majority of the rheological parameters evaluated, the results were highly correlated among the PAV-20 and PAV-40 age levels. However, ΔT_c values were only moderately correlated between the two age levels, suggesting the extended aging duration may be important for screening binders if the parameter is adopted for specification.

5.6 Acknowledgements

This research was financially supported by the North Carolina Department of Transportation, and the Virginia Department of Transportation. The author would like to acknowledge Dr. Ilker Boz, Dr. Jhony Habbouche, Saqib Gulzar, and Jaime Precadio for assisting in sample preparation and data collection. VDOT and NCDOT performed BBR tests on their respective blends for each region.

5.7 References

1. McDaniel, R.S., Soleymani, H.R., Anderson, R.M., Turner, P., Peterson, R. Recommended use of reclaimed asphalt pavement in the Superpave mix design method. *NCHRP Web Doc 30 pp. 1–280.* 2000.
2. Haghshenas, H. F., Rea, R., Reinke, G., & Haghshenas, D. F. Chemical Characterization of Recycling Agents. *Journal of Materials in Civil Engineering, Vol. 32, Issue 5.* 2020.
3. Nogueira, R. L., Soares, J. B., & Soares, S. de A. Rheological evaluation of cotton seed oil fatty amides as a rejuvenating agent for RAP oxidized asphalts. *Construction and Building Materials, Vol. 223, pp. 1145–1153.* 2019.
4. Epps Martin, A., Kasser, F., Mercado, E., Bajaj, A., Cucalon, L., Yin, F., Chowdhury, A., Epps, J., Glover, C., Hajj, E., Morian, N., Daniel, J., Oshone, M., Rastegar, R., Ogbo, C., King, G. The Effects of Recycling Agents on Asphalt Mixtures with High RAS and RAP Binder Ratios, *NCHRP Report 927*, National Academies, Washington, D.C., 2020.
5. Christensen, D. W., and N. Tran. Relationships Between the Fatigue Properties of Asphalt Binders and the Fatigue Performance of Asphalt Mixtures. *NCHRP 982. Transportation Research Board*, Washington, D.C., 2022.
6. NCAT. NCAT Researchers Explore Multiple Uses of Rejuvenators, *Asphalt Technology News, Vol. 26, No. 1.* 2014.
7. Daly, W.H. Relationship between Chemical Makeup of Binders and Engineering Performance. *NCHRP Synthesis 511.* National Academies, Washington, DC, 2017.
8. Preciado, J., Gulzar, S., Fried, A., Castorena, C., Underwood, B. S., Habbouche, J., & Boz, I. Benchmarking Recycled Binder Blends Using Statistical Analysis: A Case Study of Virginia and North Carolina. *Transportation Research Record: Journal of the Transportation Research Board. SAGE Publications*. 2023.
9. Zhang, R., Dave, E. V., Sias, J. E., Tabatabaee, H. A., Sylvester, T., & Wang, Z. Evaluation of the state of practice asphalt binder and mixture tests for assessing the compatibility of complex asphalt materials. *In Road Materials and Pavement Design, Vol. 24 pp. 451–470.* 2023.
10. Bajaj, A., Epps Martin, A., King, G., Glover, C., Kaseer, F., & Arámbula-Mercado, E. Evaluation and classification of recycling agents for asphalt binders. *In Construction and Building Materials Vol. 260.* 2020.

11. Haghshenas, H. F., Rea, R., Reinke, G., Yousefi, A., Haghshenas, D. F., & Ayar, P. Effect of Recycling Agents on the Resistance of Asphalt Binders to Cracking and Moisture Damage. *In Journal of Materials in Civil Engineering, Vol. 33, Issue 10*. 2021.
12. Haghshenas, H., Rea, R., Reinke, G., Haghshenas, D. Chemical Characterization of Recycling Agents. *In Journal of Materials in Civil Engineering.* 2020.
13. Rahbar-Rastegar, R., Sias Daniel, J., & Reinke, G. Comparison of asphalt binder and mixture cracking parameters. *Road Materials and Pavement Design, Vol. 18, Issue sup4, pp. 211–233.* 2017.
14. Zhang, R., Sias, J. E., & Dave, E. V. Comparison and correlation of asphalt binder and mixture cracking parameters incorporating the aging effect. *Construction and Building Materials, Vol. 301*. 2021.
15. Fried, A., Xue, L. G., Gulzar, S., Preciado, J., Underwood, B. S., & Castorena, C. Evaluation of Recycling Agent and Extender Dosage Selection Procedures to Restore the High-Temperature Climatic Performance Grade. *Transportation Research Record, 2676(6), pp. 302–314.* 2022.
16. Bonaquist, R., Adams, J. J., & Anderson, D. A. Asphalt Binder Aging Methods to Accurately Reflect Mixture Aging. *Transportation Research Board.* 2021.
17. Bennert, T., Garg, N., Ericson, C., & Cytowicz, N. Evaluation of Test Methods to Identify Asphalt Binders Prone to Surface-initiated Cracking. *Journal of the Transportation Research Board, Vol. 2677, Issue 3, pp. 897–910.* 2022.
18. Rowe, G. M., and M. J. Sharrock. Alternate Shift Factor Relationships for Describing Temperature Dependency of Viscoelastic Behavior of Asphalt Materials, *Journal of the Transportation Research Board, Vol. 2207.* 2011.
19. Guthrie, W. F. NIST/SEMATECH e-Handbook of Statistical Methods. *National Institute of Standards and Technology, Handbook 151*. 2020.
20. Lee, S., & Lee, D. K. (2018). What is the proper way to apply the multiple comparison test? *In Korean Journal of Anesthesiology, Vol. 71, Issue 5, pp. 353–360.* 2018.
21. Zaiontz, C. Spearman's Rank Correlation, https://real-statistics.com/correlation/spearmans-rank-correlation/, *Real Statistics Resources.* 2023.

22. Bennert, T., Garg, N., Ericson, C., Cytowicz, N. Evaluation of Test Methods to Identify Asphalt Binders Prne to Surface-initiated Cracking. *Transportation Research Record, Vol. 2677(3), pp. 897-910.* 2023.
23. Lesueur, D. L., Elwardany, M. D., Planche, J.-P., Christensen, D., & King, G. N. Impact of the asphalt binder rheological behavior on the value of the δtc parameter. *Construction and Building Materials.* 2021.

Chapter 6 Effects of Recycling Agents and Extenders on the Composition of Recycled Binder Blends

6.1 Introduction

Chapter 5 detailed how different classes of recycling agents (RAs) and extenders (E) affect the rheology of recycled asphalt binder blends. The analysis revealed that RAs derived from triglyceride and fatty acids (TF) and tall oils (TO) and the vacuum gas oil (VGO) extender yielded better rheological outcomes than the aromatic extract (A) RA and extenders containing re-refined engine oil bottoms (REOB). In this chapter, the effects of the different RA and extender types on the composition of recycled asphalt binder blends is evaluated. The goal of the compositional analysis was to complement the rheological testing by providing plausible explanations for the observed trends among the different additive types and further assess oxidative aging susceptibility. The compositional analysis was also leveraged to evaluate methods to detect different additive types within asphalt binder blends.

6.2 Background

Bajaj et al. (2020) proposed that RAs, and by extension, extenders can be classified into three distinct groups based on their function; softeners, replenishers, and emulsifiers. Softeners are products that soften asphalt binders (i.e., decrease the dynamic shear modulus, $|G^*|$, or creep stiffness, S) but do not restore relaxation characteristics (i.e., increase phase angle, δ, or m-value). This imbalance in stiffness and relaxation characteristics is reported to result from colloidal incompatibility, that is an inferior balance of Saturates Aromatics Resins and Asphaltenes (SARA) fractions. It is expected that the additives in the softener group would have the worst performance among the three categories. Bajaj et al. (2020) also report that softeners may not be economical due to requiring a higher dosage than other additive types.

Replenishers and emulsifiers lower the stiffness and improve the relaxation characteristics of asphalt binder blends, although they may not achieve the same characteristics as a virgin asphalt depending on the type and dosage used. Replenishers replace the aromatics in an asphalt lost from oxidative aging. Bajaj et al. (2020) postulated that replenishers help prevent asphaltenes from forming clusters after long-term aging. Replenishers are generally derived from petroleum products to achieve the high concentration of aromatics, which generally yields high compatibility with asphalt blends. However, the Bajaj et al. (2020) report that the properties of

replenished blends are highly dependent on the interactions between the virgin binder and recycled binder in the blend and that high dosages may be required to achieve the desired effect on rheological properties. Emulsifiers, in contrast, are reported to break large asphaltene clusters into smaller clusters that are better stabilized within the maltenes. This emulsification of asphaltene clusters is achieved through highly polar carbonyl groups that act as peptizers, attaching themselves to asphaltene clusters and dispersing them. Emulsifiers are reported to require lower dosages than replenishers and softeners to achieve similar rheological outcomes.

6.3 Objectives

The objectives of this study are to: (1) Leverage the rheological results from Chapter 5 to identify the additives that function as softeners versus replenishers and emulsifiers, and (2) Evaluate the effects of the additives in the NC blends presented in Chapter 5 on composition to identify the mechanisms by which they alter rheology.

6.4 Materials

The NC blends from Chapter 5 were used herein to identify additives that act as softeners versus replenishers and emulsifiers based on the rheological results presented in the previous chapter. The NC blends are further used to evaluate the effects of the additives in those blends on the composition of recycled binder blends. Table 18 summarizes the binders and blends evaluated and experimental methods used. The same dosages used in Chapter 5 were used herein. Recall, E1 and E2 are extenders that contain REOB whereas E3 is a VGO extender. Saturates Aromatics Resins and Asphaltenes (SARA) fractionation was used to evaluate the effects of the additives on the colloidal structure of the blends. Fourier transform infrared (FTIR) spectroscopy testing was used to further identify the presence of polar functional groups in the additives and assess the effects of the additives on carbonyl and sulfoxide growth due to oxidative long-term aging. Additionally, x-ray fluorescence (XRF) spectroscopy was used to detect the presence of heavy metals in additives, which is associated with detrimental rheological effects.

Table 18. Summary of the NC Binders and Blends

Binder/Blend
58
64-1
58.R1
58.R1.E1
58.R1.E2
58.R1.E3
64-1.R1.TF1
64-1.R1.TF2

6.5 Experimental Methods

8.5.1. SARA

SARA analysis was conducted by MTE Services, Inc. on the following binders/blends at both the RTFO and PAV-40 age levels: PG 58-28 (58) and PG 64-22 (64-1) virgin binders, the RAP binder (R1) (at the RTFO age level only), 58.R1, 58.R1.E1, 58.R1.E2, 58.R1.E3, 64-1.R1.TF1, and 64-1.R1.TF2. The asphaltenes content of each binder/blend was determined through precipitation of the binder in a solution of n-heptane. Subsequently, the maltene fraction (that remained in solution) was applied to rods for Iatroscan analysis. The Iatroscan (NTS 2023) was used to determine the breakdown of saturates, aromatics, and resins. Five rods were analyzed in the Iatroscan per binder/blend. However, in a few cases, one rod was lost due to contamination. The SARA results were used to calculate the Colloidal Instability Index (CII), defined in Equation **(30)**.

$$\mathrm{CII} = \frac{\text{Saturates} + \text{Asphaltenes}}{\text{Aromatics} + \text{Resins}} \times 100\% \quad \textbf{(30)}$$

A higher CII indicates less compatible microstructure in the binder, which is often associated with higher age hardening susceptibility and potentially poorer durability (Epps Martin et al. 2020). Tukey's Honest Significant Difference (HSD) tests were used to identify saturates, aromatics, resins, and asphaltenes results with statistically equal means using a 95

percent confidence levels. Results falling in the same group were deemed equivalent whereas results falling in distinct groups were deemed to differ.

An alternative method for determining SARA analysis proposed by Saqib et al. (2018) was also tried. However, reproducing the same results as another lab using the method proved difficult and the thus, the approach was aborted. The details of this method along with the challenges faced are discussed in greater detail in Appendix A.

6.5.1 Fourier Transform Infrared (FTIR)

A Bruker Attenuated Total Reflectance (ATR) FTIR using the OPUS software was used to obtain chemical fingerprints of the NC binders and blends at the RTFO, PAV-20, and PAV-40 age levels. In addition, FTIR analysis was conducted on the additives alone. After absorbance was recorded for a sample a baseline correction was applied within the software using the same approach used by Rad et al. (2018) to reduce the impact of background noise. Each material has two replicates run on two samples, resulting in four measurements for each material at each age level. FTIR spectra were examined to identify if certain peaks corresponding to polar functional groups are present and to evaluate oxidation. In addition, oxidation of the binders and blends was assessed on the basis of carbonyl and sulfoxide peaks and areas. To determine the peak values for sulfoxides the maximum intensity for values between 1005 cm^{-1} and 1040 cm^{-1} are recorded while carbonyls were determined for values between 1650 cm^{-1} and 1820 cm^{-1}.

The changes in carbonyl areas and carbonyl plus sulfoxide areas at the PAV-20 and PAV-40 conditions relative to the RTFO condition were plotted against the rheological properties to evaluate hardening susceptibility due to oxidative aging (Epps et al. 2019, Kim et al. 2021). The existence of carbonyl and sulfoxide components in certain additives complicates such analysis. Therefore, Bajaj et al. (2020) proposed evaluating hardening susceptibility on the basis of carbonyl area growth, equal to the difference in carbonyl area in a long-term aged state to that in a short-term aged state, rather than FTIR indices at a particular age level. This general approach was adopted herein. Given that studies suggest the growth in both carbonyl and sulfoxide components is critical when evaluating oxidative aging as both products contribute to hardening of the binder (Kim et al. 2021), both carbonyl area growth and carbonyl plus sulfoxide area growth were evaluated. The areas were calculated by using the trapezoidal area in Excel. The areas for determining fell into the range of 1005 cm^{-1} and 1040 cm^{-1} for sulfoxides and carbonyls were determined for the area between 1650 cm^{-1} and 1820 cm^{-1}.

Hardening susceptibility is conventionally evaluated on the basis of |*G**| or viscosity. However, these parameters cannot adequately capture potential differences between a softener and replenisher or emulsifier that also restores relaxation characteristics. Therefore, hardening susceptibility was evaluated on the basis of $GR_{15°C}$ and R_{MC} herein. Collective $GR_{15°C}$ and FTIR results were also used to evaluate several Binder Embrittlement Parameters (BEPs). Bajaj et al. (2020) introduced the BEP defined in Equation **(31**) to evaluate the effects of additives on aging susceptibility of recycled binder blends.

$$BEP = \log\left(GR_{RTFO} \times GR_{P40}\right)\left(\frac{\Delta \log\left(GR\right)}{\Delta CA_g}\right)^2 \quad \textbf{(31)}$$

$$BEP = \log\left(GR_{RTFO} \times GR_{P40}\right)\left(\frac{\Delta \log\left(GR\right)}{\Delta \left(CA_g + S_g\right)}\right)^2 \quad \textbf{(32)}$$

$$BEP = \log\left(GR_{RTFO} \times GR_{P40}\right)\left(\Delta \log\left(GR\right)\right)^2 \quad \textbf{(33)}$$

where: GR_{RTFO} is the $GR_{15°C}$ calculated for binder at the RTFO age level and GR_{P40} is $GR_{15°C}$ after PAV-40 aging. The $\Delta\log(GR)$ is the difference in logarithmic distance in $GR_{15°C}$ between the RTFO and PAV-40 age level. ΔCA_g refers the difference in carbonyl area between the RTFO and PAV-40 age level.

The product of the $GR_{15°C}$ at the RTFO and PAV-40 state captures the initial and final rheological properties whereas the ratio between $\Delta\log(GR)$ and ΔCAg represents the hardening susceptibility. Overall, the BEP provides a combined measure of the rheology and compositional changes in a binder. By quantifying the change in ductility and compositional sensitivity of ductility to oxidative aging the parameter can provide insight into both aspects of aging. A lower value of BEP is desirable as it showcases better ductility and resistance to changes in ductility with aging (Bajaj et al. 2020). BEP parameters were also calculated on the basis of change in both carbonyl area and carbonyl plus sulfoxide area for the FTIR results shown in Equation **(32**). Equation **(33)** shows how BEP was determined without accounting for changes in FTIR. This was performed to provide insight into the impact change in carbonyl area had on the overall impact of BEP.

6.5.2 X-ray Fluorescence (XRF)

XRF was conducted by the NCDOT on the NC binders and blends at the RTFO age level as well as the additives alone to identify additives that contained heavy metals. Heavy metals such as zinc and manganese are suspected to cause an increase in oxidation, which could impact long-

term pavement performance (Asphalt Institute 2016). A study by FHWA (2020) was able to determine the presence of REOB due to the amounts of heavy metals present. Heavy metals are found in products containing waste engine oil, such as re-refined engine oil bottoms (REOB) and are generally considered undesirable. Heavy metals can accelerate oxidative aging (Burke and Hesp 2011). The XRF functions by using x-rays to determine the parts per million of different types of inorganic materials present a sample. The sample is placed in-between two polypropylene filters and subjected to high energy x-ray photons (Kaskow et al. 2018). The sample then emits fluorescent photons and the device measures the energy coming off of those photons to determine the amount in count per second (cps) of each inorganic compound that is present. Calcium, copper, and zinc results were examined.

6.6 Results

6.6.1 Identification of Softeners versus and Replenishers from the Rheological Results

The findings in Chapter 5 make it possible to distinguish between additives that function as softeners versus replenishers or emulsifiers. The blends containing E1 and E2 resulted in distinct rheological findings from the blends containing E3, TF1, and TF2. Blends containing E1 and E2 resulted in: (1) lower $S(60)$ values but generally equal $m(60)$ values to the target 64 binder, (2) inferior ΔT_c values compared to the target 64 binder, which is a consequence of the $S(60)$ and $m(60)$ results, and (3) poor crossover temperatures than the target 64 binder. These findings suggest that E1 and E2 are classified as softeners since they soften but do not restore the relaxation characteristics to those of the target virgin binder.

In contrast, E3, TF1, and TF2 are identified as either replenishers or emulsifiers based on the rheological results presented in Chapter 5. Blends containing these additives resulted in: (1) better $S(60)$ and $m(60)$ values compared to the target 64 binder, (2) equal or better ΔT_c to target 64 binder, and (3) superior crossover temperatures to the target 64 binders. It is noted that the blends containing E3, TF1, and TF2 often exhibited inferior R_{MC} and $R_{09\text{-}59}$ values compared to the target virgin binder, suggesting these additives do not fully restore the rheological balance of stiffness and relaxation characteristics to that of a virgin binder. Nevertheless, the collective results do suggest at least partial restoration of both stiffness and relaxation characteristics, rendering them as emulsifiers or replenishers. Rheological characterization alone cannot identify emulsifiers versus replenishers. However, separating the softeners from the emulsifiers and

replenishers helped guide interpretation of the compositional results with respect to rheological impacts.

6.6.2 SARA Results

Figure 43 and Table 19 show the SARA results. An estimate of the SARA composition of a blend of the 64-1 virgin binder and RAP binder at the RTFO age level is included to enable an evaluation of the effect of the TF1 and TF 2 additives on composition. The estimate was obtained using the rule of mixtures (i.e., a weighted average) of the 64-1 virgin binder and RAP binder results. The accuracy of this approach was verified for the 58.R1 blend where 58 virgin binder and RAP binder results as well as the blend result were available. The comparison between the estimates and measurements are shown in

Table 20. The rule of mixtures yields very close agreement to the measured results at the RTFO age level. The rule of mixtures could not be applied to predict the composition of the 64-1.R1 blend at the PAV-40 age level since RAP SARA results at the PAV-40 were not obtained.

Table 19. SARA Results

Binder/Blend	Asphaltenes (%)	Resins (%)	Aromatics (%)	Saturates (%)	CII (%)
58 (RTFO)	18.1	25.6	48.2	8.1	35.5
58 (PAV-40)	23.4	30.6	37.4	8.7	47.2
58.R1 (RTFO)	22.4	30.0	40.9	6.7	41
58.R1 (PAV-40)	27.3	31.6	33.9	7.2	52.7
58.R1.E1 (RTFO)	21.2	34.4	34.5	9.9	45.1
58.R1.E1 (PAV-40)	25.7	34.5	30.0	9.7	54.9
58.R1.E2 (RTFO)	22.4	29.8	39.3	8.4	44.6
58.R1.E2 (PAV-40)	26.5	32.3	33.4	7.9	52.4
58.R1.E3 (RTFO)	21.3	28.9	42.5	7.2	39.9
64-1 (RTFO)	16.7	35.0	42	6.3	29.9
64-1 (PAV-40)	21.2	39.7	34.2	4.9	35.3
64.R1 (RTFO) (Estimate)	21.8	36.6	36.2	5.3	37.2
64-1.R1.TF1 (RTFO)	21.8	39.2	33.1	5.9	38.3
64-1.R1.TF1 (PAV-40)	25.6	41.3	27.0	6.0	46.3
64-1.R1.TF2 (RTFO)	20.7	42.9	32.2	4.2	33.2
64.R1.TF2 (PAV-40)	26.0	44.4	25.3	4.2	43.3
R1	31.0	38.3	27.0	3.6	53.0

Table 20. Comparison of Estimate and Measurement of SARA Fractions for 58.RAP

Determination	Asphaltenes (%)	Resins (%)	Aromatics (%)	Saturates (%)	CII (%)
RTFO Estimated	22.7	30.2	40.6	6.5	41.3
RTFO Measured	22.4	30.0	40.9	6.7	41.0

Figure 43 show that the saturates and resins content of a given binder/blend do not change substantially with age level. Tukey HSD results indicate that differences in saturates content with age level for a given binder/blend are generally statistically insignificant. In contrast, Tukey HSD analysis indicates all binders indicates statistically significant changes in aromatics and asphaltenes contents with aging from the RTFO to PAV-40 condition. For the resins fraction, it was more varied if the content differed significantly at the two age levels for a given binder/blend. The 58.R1, 64.R1, and 58.R1.E1 did not experience a significant change in resins content from the RTFO to PAV-40 age level whereas the other binders/blends did.

The 58.R1.E1 and 58.R1.E2 blends have distinct saturates, resins, and CII values compared to the 58.R1.E3, 64-1.R1.TF1 and 64-1.R1.TF2 blends based on the statistical analysis, suggesting inferior compatibility. However, the 58.R1 blend also has notably poorer compatibility than the 64.R1 blend based on the CII and thus, it is difficult to infer if this a result of differences among the extenders and RAs or due to the differences in the 58 versus 64 virgin binders from Figure 43 and Table 19. The RAP binder has notably higher asphaltenes content than the virgin binders and blends but a statistically similar CII value to the 58.RAP, 58.R1.E1, and 58.R1.E2 blends at the PAV-40 age level. The 58 virgin binder, 58.R1.E1, and 58.R1.E2 exhibited relatively poor ΔT_c values at the PAV-40 age level compared to other binders and blends evaluated, which may be associated with their poor CII values. A similar phenomena was also seen by Bajaj (et al. 2020). The additives that were classified as softeners passed the rheological parameter requirements of the desired grade but exhibited worse performance at T_{45}, ΔT_c, and $GR_{15^\circ C}$ than the additives that were classified as emulsifiers or replenishers. This comparatively worse performance was theorized to be related to incompatibility amongst the SARA fractionizations which was supported by the findings of this dissertation in Table 21.

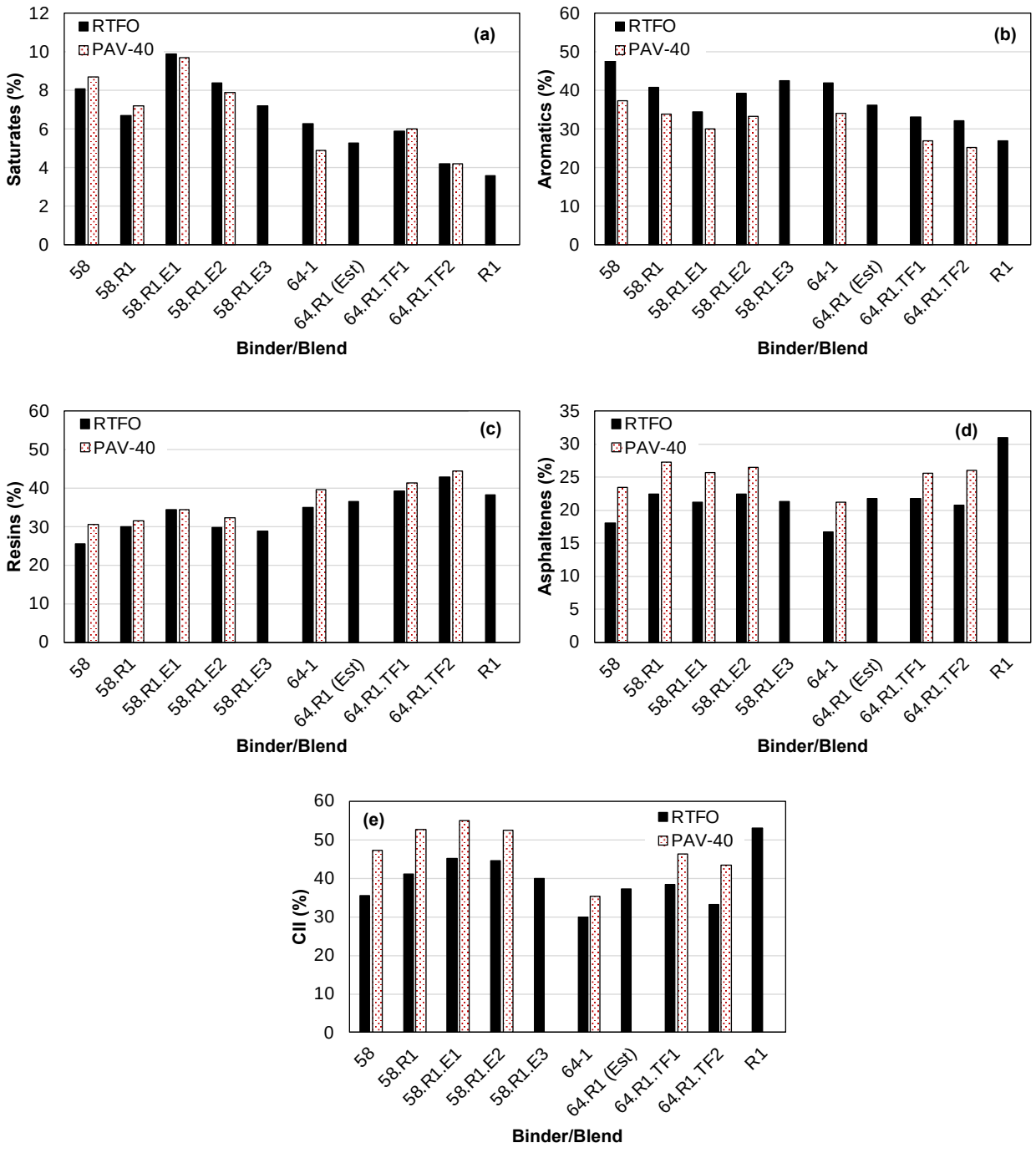

Figure 43. SARA results

To further evaluate the impact of the additives on the SARA composition of binder blends were evaluated. Table 21 and Table 22 show the changes imparted by the additives on the SARA composition of the blends of the 58.R1 and 64-1.R1, respectively. The values in Table 21 and Table 22 were calculated by the taking the content of a given fraction in the blend with the

additive and subtracting the content of that same fraction in the respective reference (58.R1 or 64-1.R1). Cases that reflect statistically significant changes from the respective reference are identified by the * following the reported value. Note that the statistical significance in asphaltene results could not be evaluated since replicate asphaltene content results were not available. Table 21 and Table 22 show that the E1, TF1, and TF2 additives increased the resins content and decreased the aromatics content of the respected reference blend. Additives E1 and E2 also increased the saturates content whereas the TF2 additive decreased the saturates content. Note that Hagshenas et al. (2020) reported that paraffinic oils are almost solely comprised of saturates and TF additives are entirely resins based on SARA analysis of the additives alone. E1 and E2 are classified as paraffinic oils. It is interesting that E1 and E2 impart the increase in resins despite likely consisting primarily of saturates. The effects of E1 and E2 on the SARA composition of the 58.R1 were more pronounced at the RTFO age level compared to the PAV-40 age level. The blend with E3 is the only blend to impart an increase in the percentage of aromatics, suggesting it may be classified as an aromatic extract.

The additives had relatively little effect on the asphaltenes content at the RTFO age level. Some cases indicate a small decrease in asphaltene content due to the addition of the additive. The difference in asphaltenes content between the 58.R1.E1 and 58.R1.E2 blends and the reference 58.R1 were higher at the PAV-40 than PAV-20 age level, indicating the additives may slightly hinder the increase in asphaltene content with long-term aging. However, the differences in asphaltene content at the PAV-40 age level are small and thus may be insignificant.
The E1 and E2 additives increased the CII significantly at the RTFO age level whereas the TF2 additive decreased the CII value relative to the reference blend. The E3 and TF1 additives had insignificant effects on the CII. A higher CII value is associated with poorer chemical compatibility. Notably, the TF1 and TF2 blends performed very similarly rheologically despite their small effect on CII.

Table 21. Change with Respect to Reference 58.R1

Blend	Asphaltenes (%)	Resins (%)	Aromatics (%)	Saturates (%)	CII (%)
58.R1.E1 (RTFO)	-1.2	4.4*	-6.4*	3.2*	4.1*
58.R1.E1 (PAV-40)	-1.6	2.9*	-3.9*	2.5*	2.2*
58.R1.E2 (RTFO)	0.0	-0.2	-1.6	1.7*	3.5*
58.R1.E2 (PAV-40)	-0.8	0.7	-0.5	0.7	-0.3
58.R1.E3 (RTFO)	-1.1	-1.1*	1.6*	0.5*	-1.1

Table 22. Change with Respect to Reference 64-1.R1

Blend	Asphaltenes (%)	Resins (%)	Aromatics (%)	Saturates (%)	CII (%)
64-1.R1.TF1 (RTFO)	0.0	2.6*	-3.1*	0.6	1.1
64-1.R1.TF2 (RTFO)	-1.1	6.3*	-4.0*	-1.1*	-4.0*

Based on the SARA results presented combined with the literature, the E1 and E2 extenders appear akin to paraffinic oils, E3 appears most similar to aromatic extracts, and TF1 and TF2 appear similar to other TF additive types evaluated in the literature. Blends at the RTFO age level containing E1 and E2 both had statistically higher saturates composition when contrasted with the reference material (58.R1). This finding aligns with results by Hagshenas et al. (2020) that conducted SARA analysis on additives alone and found that paraffinic oils are primarily comprised of saturates. Hagshenas et al. (2020) also reported that TF additives are almost entirely composed of resins (99.6%) which was also reflected in the results seen from the binder blends containing TF1 and TF2. Both blends experienced a statistically significant increase in resins present when compared to the reference material (64-1.R1).

6.6.3 FTIR Results

6.6.3.1 Spectra

Figure 44 shows the FTIR spectra of the additives and the virgin binders evaluated. The FTIR results showed a clear distinction between the extenders (E1, E2, E3), RAs (TF1 and TF2), and virgin binders at the RTFO age level (58 and 64-1). The extenders display FTIR spectra that are much more similar to the virgin binders than the TF additives. TF1 and TF2 both exhibit very similar peaks. Specifically, peaks at roughly 720 cm^{-1}, 1162 cm^{-1}, and 1744 cm^{-1} are evident in TF1 and TF2 but were absent or much smaller in the extenders and virgin binders. These peaks

correspond to primary alcohols, dialkyl/aryl sulfones, and aldehydes/esters, respectively, and were also reported in TF additives by Hagshenas et al. (2020). These are polar oxygen-containing species that may have led to the higher resin concentrations in the TF-modified blends within the SARA results. The FTIR results do not provide evidence of such polar components in the extenders. The three extenders exhibit the presence of similar peaks to one another, although not as similar as TF1 and TF2. Some differences between TF1 and TF2 at 1710 cm^{-1}. The virgin binders did not exhibit peaks at 1710 cm^{-1}. Also notable, the virgin binders displayed clear peaks at 1602 cm^{-1} (conjugated carbon-carbon double bonds), which were absent in TF1, TF2, E1, and E2 but a minor peak was evident in E3. In general, E3 displayed more a more similar FTIR spectrum to the two virgin binders than E1 and E2. E3 contained peaks at the same wavenumbers as the virgin binders but often lower absorbance magnitude.

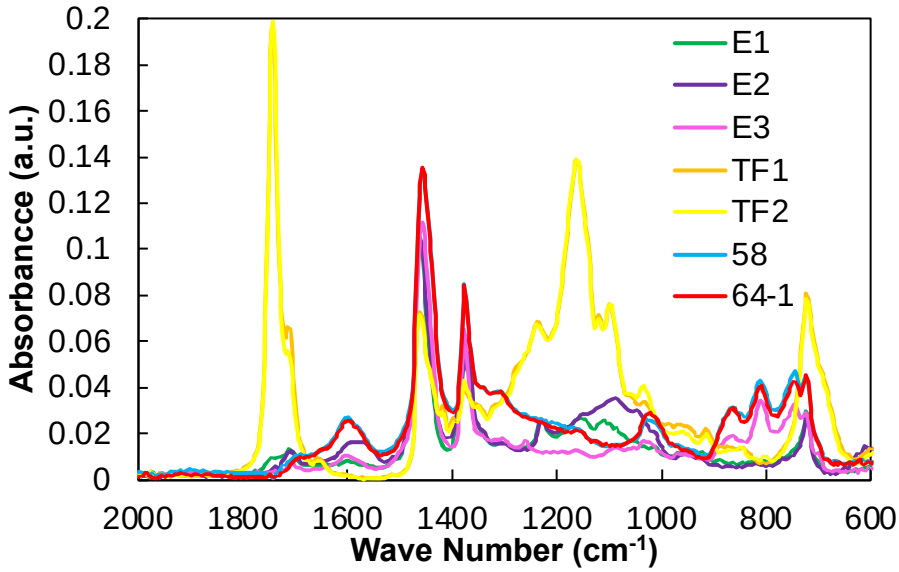

Figure 44. FTIR Results for Additives and virgin binders

Figure 45 shows the FTIR results of the virgin binders and blends at three age levels (a) RTFO, (b) PAV-20, and (c) PAV-40. Note that only wavenumbers spanning 1500 cm^{-1} to 1900 cm^{-1} are shown because this was the region within which distinct peaks were evident in the TF-modified blends (i.e., around 1744 cm^{-1}). Additives could not be identified as clearly through other peaks. In all cases, the virgin binders and blends display peaks around 1700 cm^{-1}, indicating carbonyl components. The peaks are notably higher for the blends compared to the virgin binders, possibly due to the RAP binder (R1) which had undergone prior oxidation and/or the presence of the carbonyl components in the additives themselves evident for the TF additives

in Figure 44. Notably, the blends with the TF additives display peaks around 1744 cm^{-1} whereas the other blends and virgin binders do not. This suggests that FTIR spectra of a binder blend could be examined and used to verify a TF additive was added to the binder on the basis of a peak around 1744 cm^{-1}. The extenders, in contrast, cannot be easily identified in the blends on the basis of the FTIR spectra.

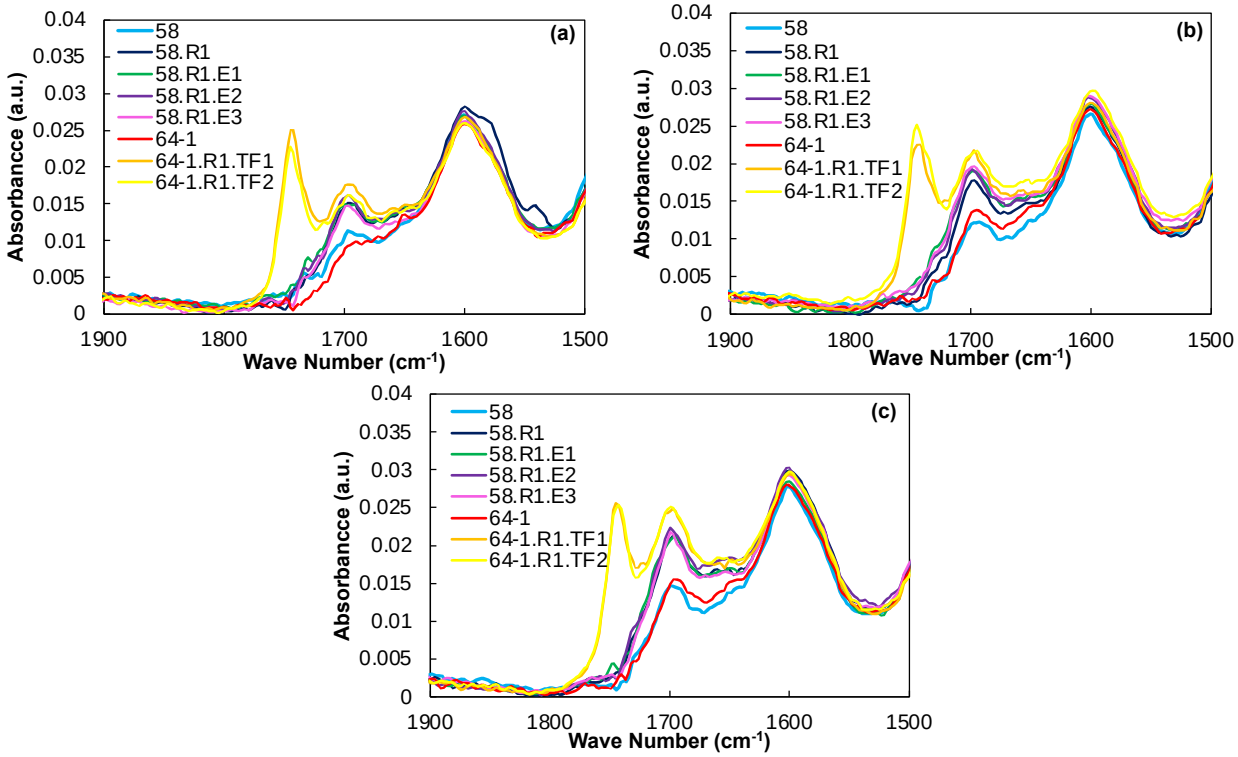

Figure 45. FTIR Results 1900cm^{-1} to 1500 cm^{-1} (a) RTFO (b) PAV-20 (c) PAV-40

When examining the FTIR spectra, it is important to note that the materials can be split into three groups: extenders (E1, E2, E3), recycling agents (TF1, TF2), and the virgin binders. These groupings remained consistent with aging and remained grouped together at RTFO, PAV-20, PAV-40 age levels, but became more noticeable at the PAV-40 age level. Examining the FTIR curves it can be noted that thanks to the peak at 1744 cm^{-1}, blends containing TF additives should be easy to identify utilizing the FTIR.

6.6.3.2 Hardening Susceptibility

The relationship between FTIR and rheological results was assessed to further understand the effects of the additives on aging susceptibility. This analysis was accomplished by contrasting the change in carbonyl area and carbonyl plus sulfoxides area from the RTFO age level to the PAV-20 and PAV-40 level with the corresponding log $GR_{15°C}$ and R_{MC} values. The slope of such

a plot is the ‘hardening susceptibility’, that is a measure of how much a binder hardens relative to the amount of growth in FTIR absorbance areas for oxidation products. Figure 46 shows the hardening susceptibility results. Figure 46 (a) and (c) shows that E3, TF1, and TF2 have similar changes in log $GR_{15°C}$ while having distinct changes in carbonyl and carbonyl plus sulfoxide areas from PAV-20 to PAV-40. Notably, the E3 blend exhibits relatively small changes in carbonyl and carbonyl plus sulfoxide absorbance areas but comparable rheological changes to the other blends. Note that other studies have suggested that aromatic extracts reduce oxidation (Bajaj et al. 2020), which seems to align with the E3 findings and further support that E3 is similar to an aromatic extract RA.

Figure 46 (b) and (d) showcase a clear distinction between E1 and the other additives for both change in carbonyl area and change in carbonyl and sulfoxide area relative to changes in R_{MC}. The E1 blend has the highest change in R_{MC} due to different age levels indicating E1 is providing more rheologically susceptible to the impacts of aging despite E1 experiencing a relatively small increase in carbonyl and carbonyl plus sulfoxide absorbance area when contrasted against other blends. The change in carbonyl plus sulfoxide area for E2 is significantly larger when contrasted against the other blends, indicating it is more susceptible to oxidation based on FTIR measures. However, the blend containing E2 does not experience a larger change in rheological characteristics than all other blends, suggesting a moderate hardening susceptibility. The trends in the hardening susceptibility among the different blends differ depending on whether carbonyl area or carbonyl plus sulfoxide absorbance area is used.

The blends of TF1 and E3 exhibit the smallest changes in carbonyl plus sulfoxide area but do not consistently show the smallest changes in the rheological measures, suggesting they do not have superior hardening susceptibility. TF2 resulted in similar rheological effects compared to TF1 and E3 but displayed higher differences in carbonyl and carbonyl plus sulfoxide absorbance growth. Given the similar rheological results, these findings suggest the practical implications of the FTIR analysis of oxidative aging may be limited. It is further noted that FTIR absorbance areas are not direct measures of the concentration of carbonyl and sulfoxide concentrations in the asphalt as the absorbance peaks and areas in these regions are also contingent upon the remainder of the spectra for that material.

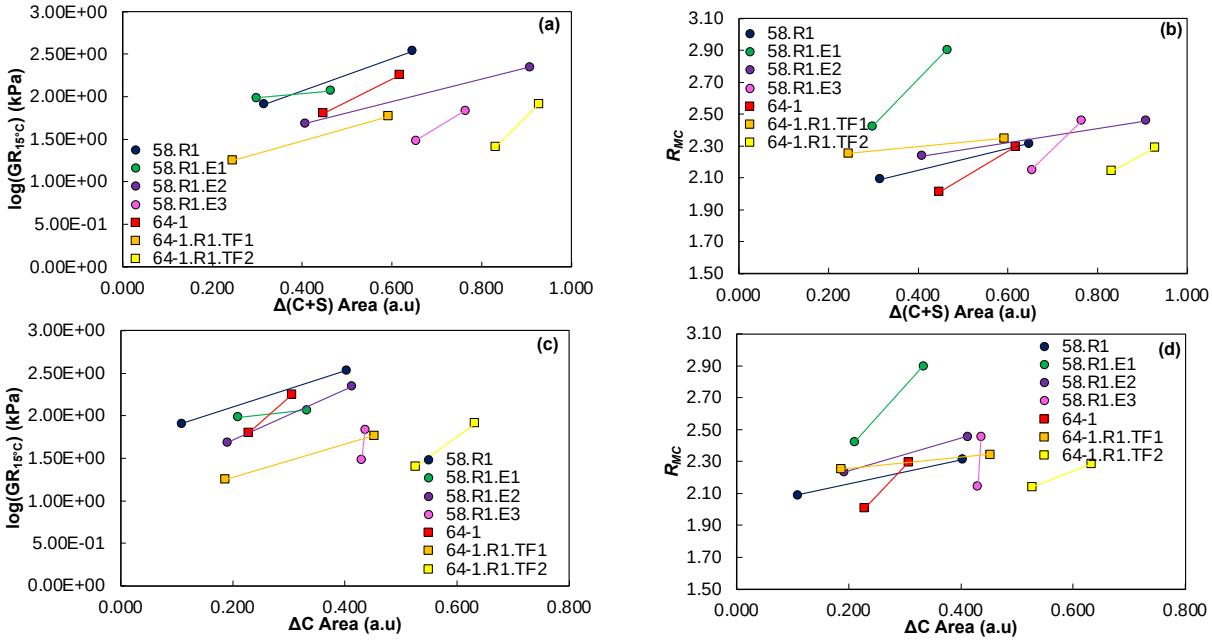

Figure 46. Change in carbonyl and sulfoxide area compared to (a) log($GR_{15°C}$), (b) R_{MC} and change in carbonyl area (c) log($GR_{15°C}$), (d) R_{MC}

6.6.3.3 BEP Parameters

Figure 47 shows the BEP parameter results, which integrate the $GR_{15°C}$ and FTIR results to provide a measure of binder embrittlement. The values support the similarity in rheological performance between the blends containing E3, TF1, and TF2. These blends exhibit lower BEP values than the virgin binders as well as lower than the blends containing E1 and E2, further supporting the prior rheological performance evaluation. It can also be seen that the different methods for determining BEP have a comparatively minor impact on the comparison between the different additive blends. Examining the effect of $GR_{15°C}$ on BEP in Figure 47 (a) and (c) shows that without examining the carbonyl area the intensity of BEP varies, but the overall ranking of the binders is unaffected by including the FTIR measures in the BEP calculation. The comparison of Figure 47 (a) and (b) shows that the change in sulfoxide area has an impact the ranking of 58.R1.E1, 58.R1.E2, and 64-1, while the overall trends are similar in Figure 47 (a) and (b). Overall, the BEP provides support to the idea that the blends containing E1 and E2 yield worse cracking performance compared to blends created with TF1, TF2, or E3. However, the BEP suggests similar performance of the blends containing E1 and E2 to 64-1, the rheological balance measures suggest inferior performance of the E1 and E2 blends. This finding suggests the BEP parameter cannot fully capture rheological performance.

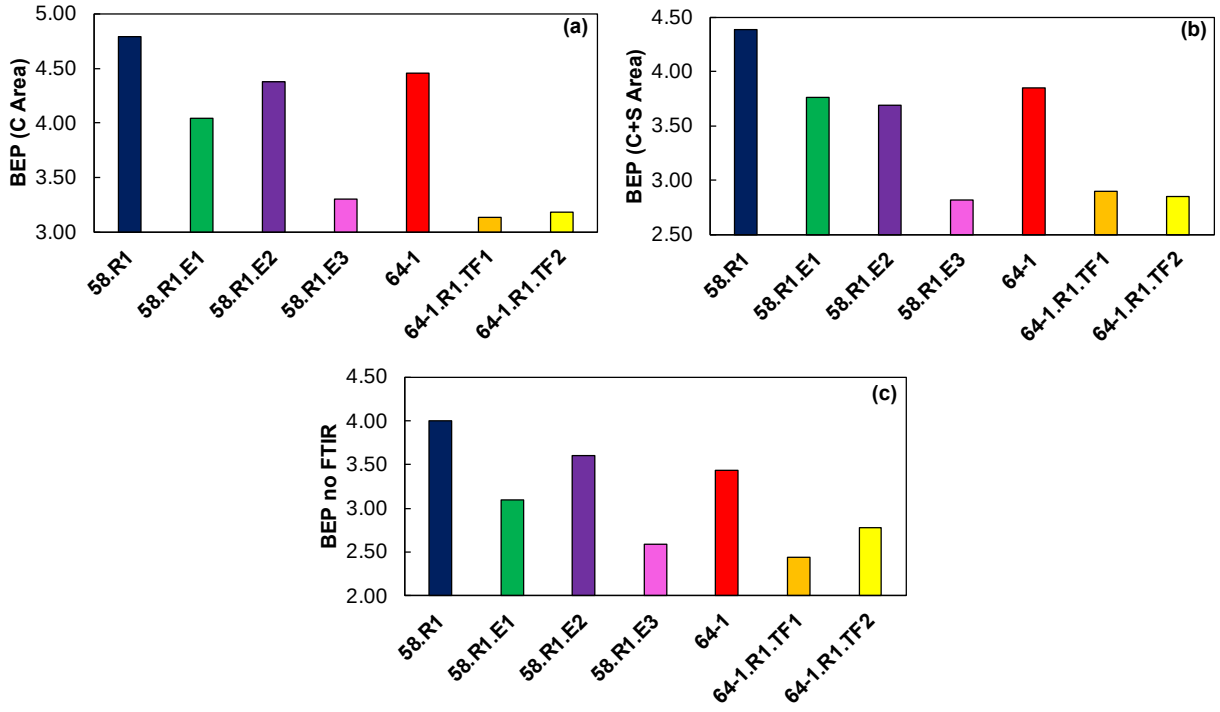

Figure 47. Binder Embrittlement Parameter (a) carbonyl area (b) carbonyl + sulfoxide area (c) BEP without FTIR spectra

6.6.4 XRF Results

FTIR was able to identify TF additives due to the peaks that occur at around 1740 cm^{-1}. However, the blends containing E1, E2, and E3 were more difficult to detect and distinguish between. This prompted prompting the evaluation of XRF results. XRF can detect the presence of inorganic substances in an asphalt blend, including zinc (Zn), copper (Cu), and calcium (Ca) (Kaskow et al. 2018). Figure 48 shows the XRF results of the asphalt binders and blends at the RTFO age level. Copper, zinc, and calcium all showed higher counts per second for blends containing E1 and E2 than those without. This result is expected since E1 and E2 are known to contain REOB. It was also noted that the levels of zinc were slightly higher for the 64-1 than expected, which could indicate a presence of REOB in this binder. It does not appear that the other additives contain REOB or other sources of inorganic components. The XRF results indicate the blend containing E3 had the lowest cps for all three materials of the blended systems, even having lower quantities than TF1 and TF2 suggesting that while E3 is an extender, it does not include potentially detrimental inorganic components and possibly helping explain its superior rheological effects. The elevated levels of Cu, Zn, and Ca in the 64-1 compared to the

58 virgin binder may explain why the E3 blend had lower concentrations of inorganic components compared to the TF additive blends. A potential link between binder performance and XRF results is the BEP. These heavy metals that are present in REOB cause the blends to exhibit higher BEP results than additives without them. This could be due to REOB containing materials are linked with an increase in wax which typically lead to worse binder performance (Kaskow et al. 2018).

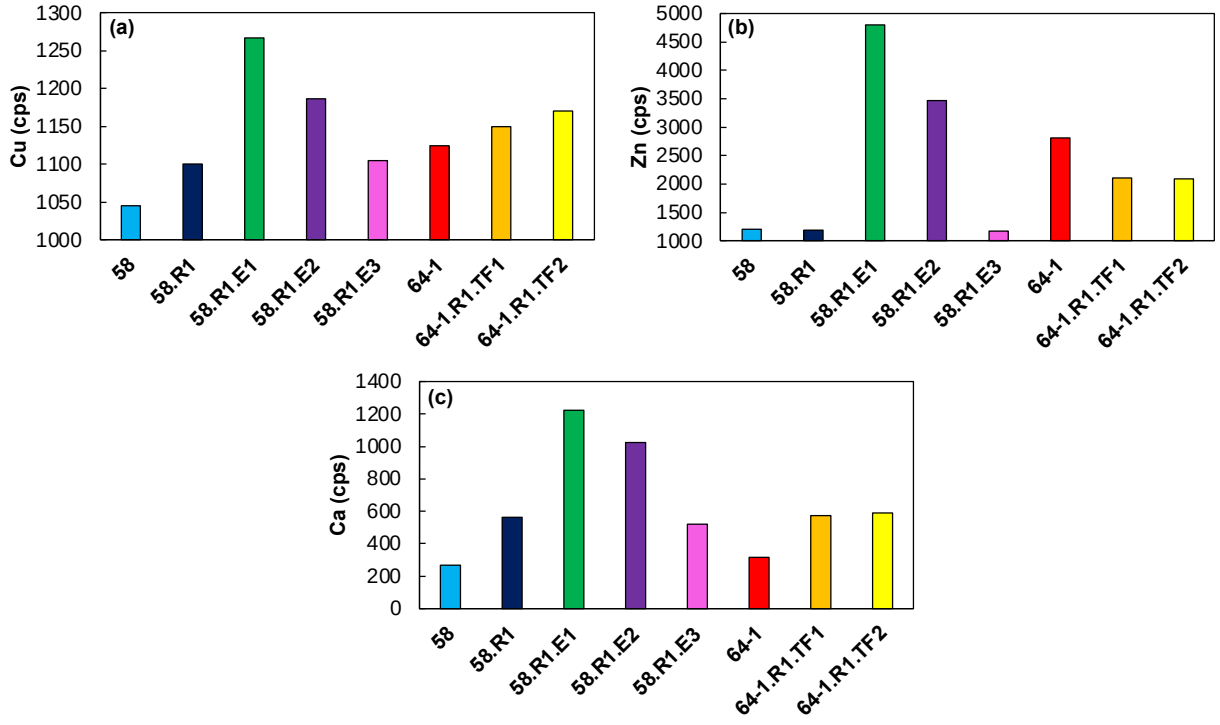

Figure 48. XRF results for inorganic elements: (a) copper, (b) zinc, (c) calcium

6.7 Discussion

Findings from the compositional analysis support that RAs and extenders can be divided into three groups; emulsifiers, replenishers, and softeners as recommended by Bajaj et al. (2020). The rheological properties presented in Chapter 5 demonstrate that E1 and E2 act as softeners whereas E3, TF1, and TF2 restore both relaxation and modulus characteristics, rendering them as replenishers or emulsifiers.

The additives E1 and E2 imparted an increase in the saturates content at the RTFO age level. This increase in saturates imparted a negative effect on the CII when compared to its reference material, 58.R1 as seen in Table 21. As a result, E1 and E2 functioned as softeners that reduced the stiffness but did not comparatively restore the relaxation characteristics of recycled

binder blends. The softeners resulted in worse rheological properties than emulsifiers and replenishers when their dosage was selected to achieve a similar target condition (i.e., restoration of the intended high-temperature grade). E1 and E2 also imparted an increase in the resins content of recycled binder blends. However, it is speculated that the additives themselves do not contain resins based on the SARA composition of paraffinic oils reported by Hagshenas et al. (2020) as well as the FTIR spectra that did not reveal peaks at wavenumbers commonly associated with polar components. The softeners did not have the same peak at around 1744 cm^{-1} that was present for TF1 and TF2. Also noteworthy, XRF showed higher quantities of heavy metals in the blends containing E1 and E2, due to their inclusion of REOB, that were not as evident in the other blends and virgin binders evaluated.

The E3 additive had similar FTIR peaks as E1 and E2. However, due to its effects on rheology, E3 did not fit the classification of softener. Thus, XRF and SARA were important in distinguishing its compositional impacts. E3 was the only additive found to increase the aromatics content of recycled binder blends. Also notable, E3 did not show evidence of polar components in its FTIR spectra and the blend containing E3 exhibited the smallest change in carbonyl and sulfoxide areas due to long-term aging among the blends and binders evaluated. E3 did not contain heavy metals based on the XRF results. Replenishers function by replacing aromatics lost to oxidation and generally impart low oxidative aging susceptibility (Bajaj et al. 2020). Thus, the compositional analysis suggests E3 is a replenisher. Also notable, rheologically, the performance of E3 blends was similar to TF1 and TF2 blends. However, a higher dosage of E3 was required to achieve the same rheological impact as TF1 and TF2, which aligns with reports in the literature for replenishers compared to emulsifiers (Bajaj et al. 2020).

Lastly, TF1 and TF2 are best be classified as emulsifiers. The additives increased the resins content of recycled binder blends. Furthermore, FTIR results demonstrates the TF additives contain polar components, likely explaining the increase in resins content. Resins peptize asphaltenes in asphalt binders and thus, the TF additives are classified as emulsifiers. The emulsifying effect of the TFs was not consistently captured by the CII, but rheologically their performance was consistently better than that of the target virgin binder with the exception of the rheological index R_{MC}. Identifying when TF additives are present in a binder blend can be best be detected through FTIR. As seen in Figure 44, TF additives impart a peak in FTIR spectra around 1744 cm^{-1} that is not present in any other additive or the virgin binder. This makes detection

straightforward as the presence of this peak would indicate the addition of the TF additive to the virgin binder or blend.

Relating the findings between the rheological and compositional, there is a clear benefit of examining both to help classify materials. The rheological performance provides insight into the effectiveness of the additives and the compositional performance can help determine which additives could be more efficient, as well as detecting less desirable additives such as REOB. One parameter that attempts to bridge the gap between compositional and rheological characteristics is the BEP. This parameter utilizes the change from the RTFO to the PAV-40 age level in both $GR_{15°C}$ and in the CA_g measured through the FTIR. The parameter supports the similarities seen between E3, TF1 and TF2, as well as the similarities between E1 and E2. Seen in Figure 47, the BEP provides clear distinction between those blends containing softeners and those with emulsifiers and replenishers. This higher BEP values associated with the softeners would indicate that the material is experiencing more stiffness with aging and is more susceptible to the effects of oxidation on its rheological performance. However, BEP is mostly impacted by the change in rheology by the difference in $GR_{15°C}$ shown in Figure 47 (a) and (c). This shows that while the intensity changes, the overall comparison amongst blends is mostly caused by $GR_{15°C}$ and not change in carbonyl or sulfoxide areaa.

6.8 Conclusions

The primary conclusions drawn from the compositional analysis are:

- SARA, FTIR, or XRF alone are unable to delineate all extender and RA types.
- The FTIR is capable of identifying TF additives in asphalt binder blends through the existence of an absorbance peak at 1744 cm^{-1}. This peak is not evident in extenders or asphalt.
- XRF identified additives with REOB through calcium, copper, and zinc concentrations that exceeded those in other binders and blends.
- TF additives increase the resins content of recycled binder blends due to including polar oxygen-containing functional groups. Consequently, TF additives function as emulsifiers.
- The vacuum gas oil (VGO) extender (E3) evaluated increased the aromatics content of recycled binder blends and did not exhibit clear evidence of oxygen-containing chemical functional groups in FTIR. Consequently, VGO acts a replenisher.

- The extenders containing REOB increased the saturates content and decreased the CII of recycled binder blends, which led them to function as softeners.
- Examination of the parameter BEP showcases that $GR_{15°C}$ has the most significant impact on change in BEP and that omitting the FTIR-based component of the parameter results in little change in the overall trends among the study materials.

6.9 Acknowledgements

The author would like to acknowledge MTE for providing testing for SARA and NCDOT for testing of XRF samples.

6.10 References

1. Bajaj, A., Epps Martin, A., King, G., Glover, C., Kaseer, F., Arambula-Mercado, E. Evaluation and classification of recycling agents for asphalt binders. *Construction and Building Materials Vol. 260*. 2020.
2. Rad, F., Elwardany, M., Castorena, C., Kim, Y. Evaluation of Chemical and Rheological Aging Indices to Track Oxidative Aging and Apshalt Mixtures. *Transportation Research Record Vol. 28.* Washington, D.C., 2018.
3. Epps Martin, A., Kasser, F., Mercado, E., Bajaj, A., Cucalon, L., Yin, F., Chowdhury, A., Epps, J., Glover, C., Hajj, E., Morian, N., Daniel, J., Oshone, M., Rastegar, R., Ogbo, C., King, G.The Effects of Recycling Agents on Asphalt Mixtures with High RAS and RAP Binder Ratios, *NCHRP Report 927*, National Academies, Washington, D.C., 2020.
4. Kim, R, et al. Long-Term Aging of Apshalt Mixtures for Performance Testing and Prediction, *NCHRP Report 871*, National Academies, Washington, D.C., 2021.
5. Asphalt Institute, State of the Knowledge: The Use of REOB/VTAE in Asphalt, *Asphalt Institute Information Series No. 240 (IS-240),* 2016.
6. Burke, K., Hesp, S. Penetration testing of waste engine oil modified asphalt cements. *Conference of Transportation Research Group of India*. 2011.
7. Kaskow, J., Poppelen, S., Hesp, S. Methods for the Quantification of Recycled Engine Oil Bottoms in Performance-Grade Asphalt Cement. *Journal of Materials in Civil Engineering.* 2017.
8. Haghshenas, H., Rea, R., Reinke, G., Haghshenas, D. Chemical Characterization of Recycling Agents. J*ournal of Materials in Civil Engineering, American Society of Civil Engineering. Vol 32.* 2020.

Chapter 7 Conclusions and Recommendations

7.1 Conclusions

This dissertation made four primary contributions; (1) identified the importance of considering uncertainty when selecting RA and extender dosages to restore the high-temperature grade of a blend, (2) developed a readily implementable free shifting procedure, called pairwise interpolation to construct asphalt binder master curves, (3) evaluated the efficacy of different RA and extender additive types at restoring rheological properties, and (4) classified additives based on their mechanism for modifying rheology through compositional analysis. Specific conclusions pertaining to each chapter follow.

7.1.1 Evaluation of Recycling Agent and Extender Dosage Selection Procedures to Restore the High-Temperature Climatic Grade

- Different recycling agent and extender products can yield different rates of change in the asphalt binder continuous AASHTO M 320 high-temperature grade with additive content.
- The rate of change in asphalt binder continuous AASHTO M 320 high-temperature grade with additive content for a given additive was similar for different recycled binder and virgin binder combinations, suggesting that an additive-specific dosage selection procedure could be established using testing of a limited set of recycled and virgin binder blends and then applied to estimate the required additive dose for alternative recycled-virgin binder blends if the high-temperature grade of the virgin-recycled binder blend in the absence of any additive is known.
- Testing of blends containing RAS at the original age level should be avoided as residual agglomerations of RAS may remain. It was found that RTFO aging can be used to achieve a homogenous binder blend with RAS.
- Testing of virgin-recycled binder blends rather than relying on linear blending theory to estimate the high-temperature grade is recommended, especially in the case of RAS binders because conducting high-temperature grading of RAS binders imparts considerable uncertainty.
- The AASHTO M 320 high-temperature grading results of verification blends prepared at selected dosages yielded considerable discrepancies with those predicted from dosage

selection testing in some cases; these results suggest uncertainty in the dosage selection results should be incorporated into the dosage selection procedure.

7.1.2 Practical Methods to Construct Asphalt Binder Master Curves and Calculate Christensen-Anderson Model Parameters

- The pairwise interpolation for constructing asphalt binder master curves developed herein yields good agreement with the Gordon and Shaw (1994) method. The pairwise interpolation method can be more easily implemented than the Gordon and Shaw method but does require that there is overlap in the range of storage and loss moduli in successive isotherms. Furthermore, CA model results obtained using the Gordon and Shaw and pairwise interpolation methods were very similar when using the LR method to obtain *R*, which indicates either method for determining shift factors can be used.
- Rheological measurements where δ increases as the measurement frequency increases should be removed from temperature-frequency sweep data prior to constructing master curves. This finding is limited to the study materials, including unmodified asphalt and conventional polymer-modified asphalt binders. The finding is not applicable to high polymer content asphalt binders that exhibit more complex trends.
- The relationship between reduced frequency and tan δ in logarithmic space over tan δ values spanning from 0.2 to 0.5 is generally linear and can be used to determine the crossover frequency as proposed by Anderson et al. (1994).
- Calculating the CA model *R* value on the basis of measurements at a single temperature-frequency combination as proposed by Christensen and Tran (2022) or the average over a range of temperature-frequency combinations should be avoided because the calculated *R* value can vary with the temperature-frequency combination in long-term aged and polymer-modified asphalts, which leads to poorer $|G^*|$ model predictions than alternative methods.
- Solving for the CA model *R* value using least squares optimization using a previously determined ω_c values on the basis of log storage and log loss moduli values generally yields slightly poorer model accuracy than when computing the squared errors without logarithmic transforms. Least squares optimization to minimize the sum of squared errors for storage and loss moduli was found to yield the highest model accuracy among the methods evaluated.

- The relationship between log (log $|G^*|$) and tan δ is generally linear for tan δ values falling between 0.5 and 2 and can be used to estimate the CA Model *R* value. This approach provided acceptable and comparable model accuracy to least squares optimization in most of the cases evaluated and thus, constitutes a viable alternative to numerical optimization.
- Based on the asphalt binders evaluated in this study, the CA model can accurately reflect asphalt binder rheological behavior when the $|G^*|$ exceeds 10^5 Pa and δ is less than 70° for unmodified asphalts or less than 60° for polymer-modified asphalts.

7.1.3 Evaluation of Alternative Approaches to Restore the Rheology of Recycled Asphalt Binders

- In most cases evaluated, the reference and RA blends met established rheological property limits. The primary exceptions occurred at the PAV-40 age level for the T_{45} warning limit and the $GR_{15°C}$ crack onset limit. However, even PG 64-22 virgin binders displayed failing cases for these parameters.
- The reference blends often exhibit similar or better performance-graded properties but often exhibit inferior $GR_{15°C}$ and $GR_{25°C}$ and rheological balance parameters compared to the PG 64-22 virgin binders evaluated.
- The rheological characteristics of the RA blends varied with the RA type and dosage.
- The TF blends with dosages that restored the intended PGH generally display superior properties compared to PG 64-22 virgin binder with the exception of certain measures of the rheological balance.
- The parameter of ΔT_c had a suggested limit of -5.0°C that low-temperature restoration blends struggled to meet after undergoing aging at the PAV-40 level
- The TF and TO blends with dosages selected to restore the intended PGL generally show equal or better $|G^*|sin\delta$ and $GR_{25°C}$ values than PG 64-22 binder but exhibit cases of inferior $GR_{15°C}$ results. These blends also generally display inferior rheological balance measures results compared to PG 64-22 binder.
- The A blends with dosage selected to restore the PGL exhibited inferior rheological properties to PG 64-22 binder on the basis of the vast majority of the blends and parameters evaluated. The A blends also tended to fail established limits for the rheological parameters.

- The VGO (E3) extender blend rheological properties are comparable to the TF RA blends that followed the same dosage selection procedure. In contrast, the blends with extenders that contained REOB (E1, E2, E4) generally exhibit inferior rheological balance measures compared to the PG 64-22 binders irrespective of the dosage selection procedure.
- The results of this study suggest that point parameters and balance parameters are generally weakly correlated, suggesting they provide unique insight regarding the rheological behavior of binders. Moreover, the results of this study indicate that recycled binder blends often exhibit inferior rheological balance parameters, indicating these measures are important to distinguish between virgin and recycled binder blends.
- While correlations exist between the intermediate-temperature point parameters evaluated, the $GR_{15°C}$ and $GR_{25°C}$ identified more cases of potentially inferior performance in the blends compared to the PG 64-22 virgin binders, suggesting they warrant consideration as alternative specification parameters.

7.1.4 Effects of Recycling Agents and Extenders on the Composition of Recycled Binder Blends

- SARA, FTIR, or XRF alone are unable to delineate all extender and RA types.
- The FTIR is capable of identifying TF additives in asphalt binder blends through the existence of an absorbance peak at 1744 cm^{-1}. This peak is not evident in extenders or asphalt.
- XRF identified additives with REOB through calcium, copper, and zinc concentrations that exceeded those in other binders and blends.
- TF additives increase the resins content of recycled binder blends due to including polar oxygen-containing functional groups. Consequently, TF additives function as emulsifiers.
- The vacuum gas oil (VGO) extender (E3) evaluated increased the aromatics content of recycled binder blends and did not exhibit clear evidence of oxygen-containing chemical functional groups in FTIR. Consequently, VGO acts a replenisher.
- The extenders containing REOB increased the saturates content and decreased the CII of recycled binder blends, which led them to function as softeners.
- Examination of the parameter BEP showcases that $GR_{15°C}$ has the most significant impact on change in BEP and that omitting the FTIR-based component of the parameter results in little change in the overall trends among the study materials.

7.2 Recommendations

This dissertation evaluated the universality of the slope of additive content versus the AASHTO M 320 high-temperature grade of recycled binder blends and found that additives have unique slopes. The results also revealed that that uncertainty should be accounted for when establishing a dosage selection procedure to ensure that the blended binder grade does not fall below the desired value. Subsequent research is recommended to use these findings to establish a standardized procedure for determining optimal additive dosage.

Master curve construction for this dissertation showcased that both methods of shifting; pairwise interpolation and the Gordon-Shaw approach were both effective. These two methods did not differ greatly with their models and determination of parameters. However, there were shortcomings with using the CA model for constructing the master curves. At higher phase angles and lower moduli, the differences between the model and measured increased. This happened at a comparatively lower phase angle when unmodified binder blends were compared with polymer modified blends. Future research should explore alternative master curve models to better represent the full temperature-frequency behavior of asphalt binders. Subsequent research is also needed to develop standardized procedures for temperature-frequency sweep testing.

Results concerning the rheological properties of the binder provided insight into the effects that additives had on binder blends as well as their varying effectiveness under two dosage selection procedures. The additives that exhibited good restoration properties at a dose intended to restore high temperature also performed well when they were utilized to restore low temperature performance. While there were additives that had better performance and effectively restored some properties of the blends to that of the virgin binder, such as the replenishers and emulsifiers, there was no single additive that could simultaneously restore all the rheological properties to that of the target virgin binder. Thus, additional research is suggested to develop new additives that are able to completely restore recycled binder properties, notably the balance in modulus and relaxation characteristics, to those of virgin binders. Furthermore, the research results demonstrate the importance of quantifying the balance in relaxation and modulus characteristics. Additional research is necessary to identify the best parameter to capture this balance and incorporate it into asphalt binder specifications to best address durability.

Classifying the different additives according to the mechanisms used to alter rheology provided insight into their relative effectiveness at restoring rheology. One compositional aspect

of the additives that was not evaluated is the tendency for the additives to cause wax crystalline, which can negatively impact cracking resistance. Future research should evaluate the effects of additives on wax crystallization and glass transition temperature. MDSC testing fell outside the scope of this project. However, it could provide insight into the formation of waxes due to the presence of additives. TF additives were identifiable in asphalt blends through FTIR testing and REOB was detectable in asphalt blends through XRF. However, the limited data set in this dissertation is insufficient to develop thresholds for quantifying whether these additives are present in an asphalt. Future research is warranted to establish such limits.

This dissertation focused solely on binder properties and the impact that the additives had on binder rheology and composition and not their effects at the mixture scale. Future research should examine the effects these additives have on the mixture design and performance.

APPENDICES

Appendix A - SARA Method Evaluation

An alternative method for determining the SARA fractionization was initially tried that was proposed by Bhasin and Sakib (2018). However, after numerous trials, reproducibility and repeatability were unable to be achieved. As a result of these challenges, SARA was performed by an outside testing lab using an Iatroscan instead. The trial results and procedure for the solubility of fractionizations are discussed in this appendix.

The SARA method proposed by Bhasin and Sakib (2018) relies on the solubility of each fractionation and filtering accordingly using a solid phase extraction (SPE) cartridge. A small sample (0.400 g) is placed in 40 mL of n-Heptane with a magnetic stirrer and left for 24 hours. After 24 hours has passed the solution of binder and n-Heptane is placed in four syringes and pulled through a polytetrafluoroethylene (PTFE) syringe filter (0.2µm) which filters out the asphaltenes and into four vials. Two of these vials are then dried in a vacuum oven to determine the amount of maltenes present as well as calculate the amount of asphaltenes that have been filtered out. This is done by measuring the amount of maltenes present after drying the vials as shown by Equation (34).

$$Maltene\,\% = \frac{M_{Maltenes}}{M_{Binder}/\left(30 + V_4\right)} \tag{34}$$

$$Asphaltene\,\% = 1 - Maltene\,\% \tag{35}$$

Where *Asphaltene%* is the percentage of asphaltenes in a sample by mass; *Maltene%* is the percentage of maltenes in a sample by mass; $M_{Maltenes}$ is the average mass of maltenes in vials; M_{Binder} is the mass of binder sample; and V_4 is the volume of binder/n-Heptane solution present in syringe 4 in mL.

Once the percentage of maltenes is determined, the remaining two vials are diluted to have a concentration of 3.33 mg (maltene) per mL of n-Heptane. These vials are then used to determine the percentage of saturates, aromatics, and resins present in each sample. This is done by taking 15 mL of the 3.33mg/mL solution and pulling it through a SPE cartridge. The SPE cartridge is made of a 5 g silica base with a 20 mL capacity meant to adsorb the fractions until the proper solvent washes them through. The first stage pulls through saturates using 10 mL of n-Heptane after the initial 15 mL of binder/n-Heptane solution has been pulled through the SPE

cartridge. Next, the aromatics are separated by using a mixture of 20 mL of toluene and 5 mL of n-Heptane. Finally, the resins are removed by using a mixture of 36 mL dichloromethane and 4 mL of methanol. After this process, the filter should be clear of all binder residue and the three vials are dried in the vacuum oven to determine the mass quantities of each fraction. To properly set up SARA fractionation, binder samples were sent to a second lab to verify reproducibility.

Figure 49. Example of Saturates (X3), Aromatics (X4), and Resins (X5)

While some samples were able to meet the repeatability limits of difference between maltenes of 5% established by Sakib and Bhasin (see Table 24), the results are not reproducible based on multilaboratory comparisons. Table 23 shows the comparison between the NCSU results and results of the outside lab. While efforts were made to identify the sources of variability within and across laboratories, the issues could not be overcome after several attempts to repeat the experiments after making procedural adjustments per guidance from the test developers. Therefore, the use of the method was ultimately aborted. Future research is needed to identify experimental controls to make the procedure repeatable and reproducible. A maltenes check is part of the test where the fraction of a vial containing all maltenes (saturates, aromatics,

resins) is supposed to equal the mass of the three vials individually containing each fraction. This was not met on several samples and attempts to correct this issue proved unsuccessful (including discussions with the developers of the test method). Also, results of a blend of virgin binder and RAP resulted in a higher concentration of saturates than for the two binders contained within the blend. This should not be possible and called into question validity of other results.

Table 23. Comparison of NCSU and Outside Lab

	Outside lab (64-22)	NCSU (64-22)	%Difference	Outside lab (76-16)	NCSU (76-16)	%Difference
Saturates	18.51	35.66	63%	21.73	25.85	17%
Aromatics	56.79	28.80	65%	41.49	38.08	9%
Resins	10.18	21.36	71%	8.66	11.59	29%
Asphaltenes	14.52	14.18	2%	28.12	24.48	14%

Table 24. SARA NCSU Repeatability

	RTFO	RTFO	RTFO	RTFO	NCSU
	58	RAP	58.RAP	B1	64-22 (Y)
Saturates	27.51	27.63	33.37	15.48	25.92
Aromatics	35.27	17.88	23.62	47.47	43.55
Resins	14.20	20.57	18.67	15.37	14.15
Asphaltenes	23.02	33.92	24.33	21.66	16.38
Meet repeatability	Yes	No	Yes	No	No

Appendix B – Fitting Statistics of Chapter 5 Binder Master Curves

Table 25. NCDOT and VDOT RMSE and MAPE

Blend	RMSE |G*|	MAPE Phase Angle
58|PAV-40	3.16%	2.29%
58.R1.E1|PAV-20	3.14%	2.28%
58.R1.E1|PAV-40	2.75%	3.12%
58.R1.E2|PAV-40	3.44%	2.58%
58.R1.E3|PAV-20	2.82%	2.23%
58.R1.E3|PAV-40	2.90%	2.12%
64-1.R1.TF2|PAV-20	2.72%	1.77%
64-1.R1.TF2|PAV-40	3.33%	1.95%
64-2|PAV-20	3.46%	1.60%
64-2|PAV-40	3.97%	2.05%
64-2.R2.TF3|PAV-20	3.90%	1.66%
64-2.R2.TF3|PAV-40	4.30%	1.91%
64-2.R2.TF4|PAV-20	3.10%	1.56%
64-2.R2.TF4|PAV-40	3.72%	1.76%
64-2.R3.A|PAV-20	3.91%	2.02%
64-2.R3.A|PAV-40	4.34%	2.39%
64-2.R3.E4|PAV-20	3.17%	2.41%
64-2.R3.E4|PAV-40	3.61%	3.05%
64-2.R3.TO|PAV-20	3.53%	1.65%
64-2.R3.TO|PAV-40	4.14%	2.06%
64-2.R4.TF1|PAV-20	3.36%	1.63%
64-2.R4.TF1|PAV-40	3.92%	2.02%
64-2.R4.TF4|PAV-20	2.54%	1.41%
64-2.R4.TF4|PAV-40	3.19%	1.82%
64-2.R4.TO|PAV-20	3.47%	1.63%
64-2.R4.TO|PAV-40	4.02%	1.99%
64-3|PAV-20	3.44%	2.31%
64-3|PAV-40	3.84%	2.47%
64-3.R2.A|PAV-20	4.22%	2.09%
64-3.R2.A|PAV-40	4.60%	2.36%
64-3.R2.TF1|PAV-20	3.82%	1.84%
64-3.R2.TF1|PAV-40	4.13%	2.15%
64-3.R2.TF3|PAV-20	3.56%	1.77%
64-3.R2.TF3|PAV-40	4.03%	2.10%

64-3.R2.TF4|PAV-20	3.23%	1.71%
64-3.R2.TF4|PAV-40	3.61%	1.98%
64-3.R2.TO|PAV-20	3.80%	1.83%
64-3.R2.TO|PAV-40	4.08%	2.08%
64-3.R3.A|PAV-20	3.76%	2.16%
64-3.R3.A|PAV-40	4.13%	2.52%
64-3.R3.TF1|PAV-20	3.36%	1.91%
64-3.R3.TF1|PAV-40	3.75%	2.26%
64-3.R3.TF3|PAV-20	3.36%	1.89%
64-3.R3.TF3|PAV-40	3.78%	2.28%
64-3.R3.TF4|PAV-20	2.43%	1.55%
64-3.R3.TF4|PAV-40	3.10%	1.99%
64-3.R3.TO|PAV-20	3.31%	1.87%
64-3.R3.TO|PAV-40	3.63%	2.00%
64-3.R4.A|PAV-20	4.00%	2.27%
64-3.R4.A|PAV-40	4.34%	2.58%
64-3.R4.E4|PAV-20	3.81%	3.41%
64-3.R4.E4|PAV-40	4.37%	3.92%
64-3.R4.TF1|PAV-20	3.18%	1.84%
64-3.R4.TF1|PAV-40	3.82%	2.32%
64-3.R4.TF3|PAV-20	3.26%	1.89%
64-3.R4.TF3|PAV-40	3.77%	2.28%
64-3.R4.TO|PAV-20	3.19%	1.86%
64-3.R4.TO|PAV-40	3.72%	2.29%
58.R3|PAV-20	3.51%	2.17%
58.R3|PAV-40	3.90%	2.57%
58.R4|PAV-20	3.74%	2.23%
58.R4|PAV-40	4.09%	2.63%
58.R2.TF3|PAV-20	3.93%	2.05%
58.R2.TF3|PAV-40	4.12%	2.38%
Average	**3.62%**	**2.14%**
Min	**2.43%**	**1.41%**
Max	**4.60%**	**3.92%**

Appendix C - Black Space Graphs

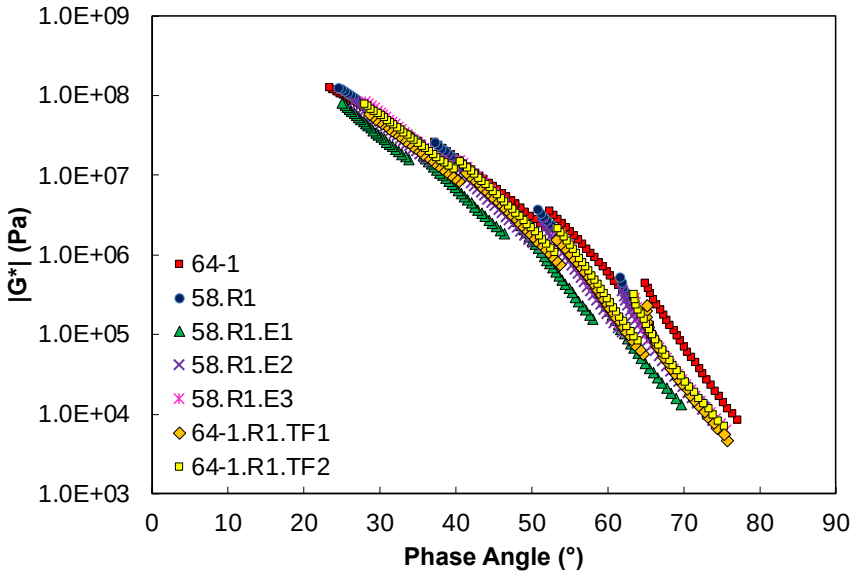

Figure 50. NCDOT all blends black space graph

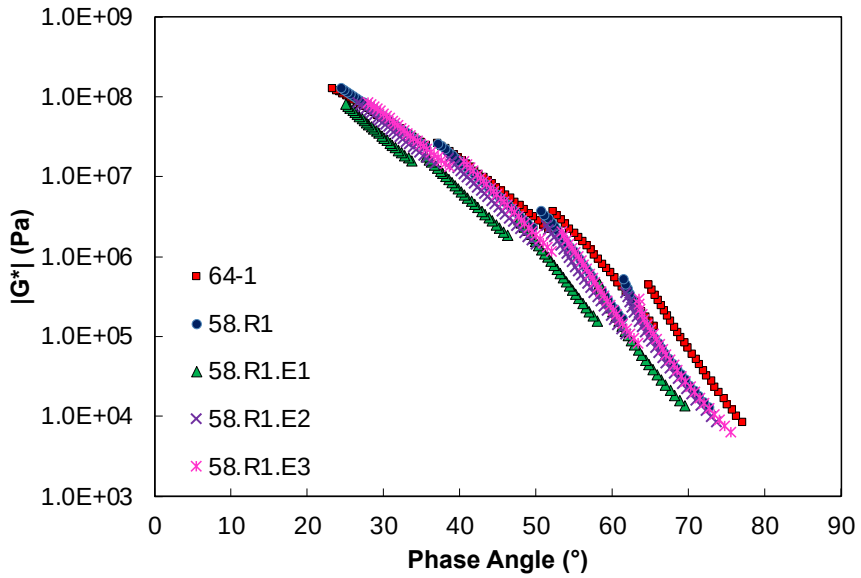

Figure 51. NCDOT 58 blends black space graph

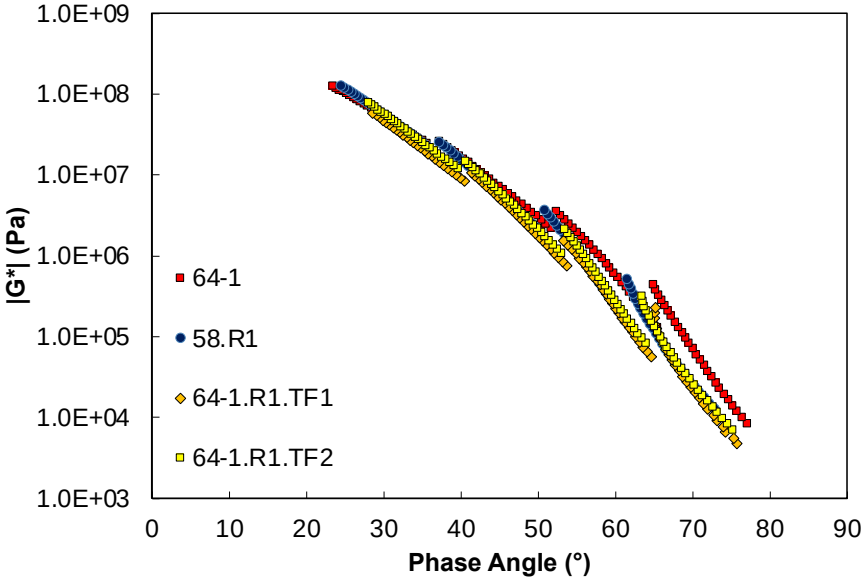

Figure 52. NCDOT 64-1 blends black space graph

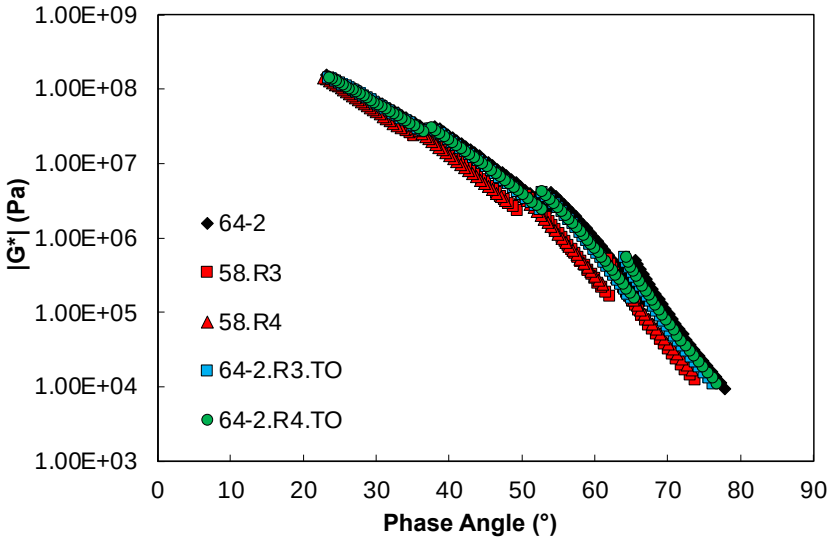

Figure 53. VDOT 64-2 TO blends black space graph

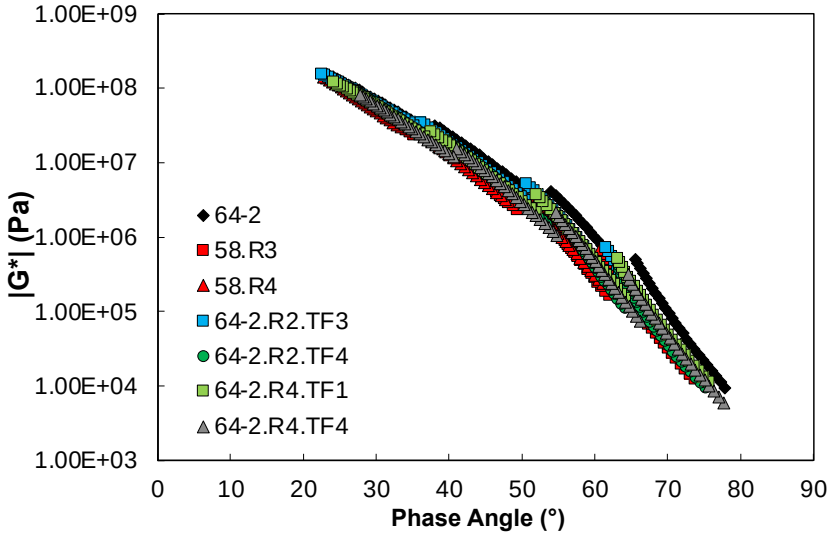

Figure 54. VDOT 64-2 TF blends black space graph

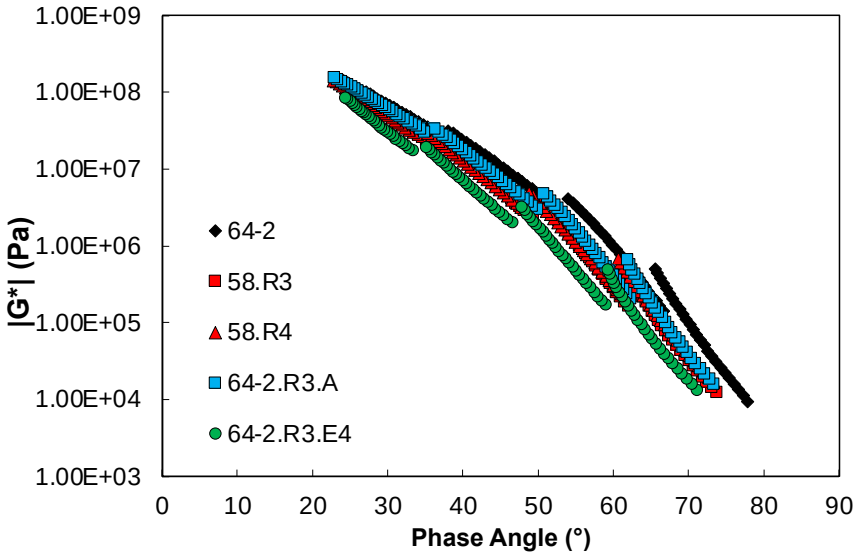

Figure 55. VDOT 64-2 A and E blends black space graph

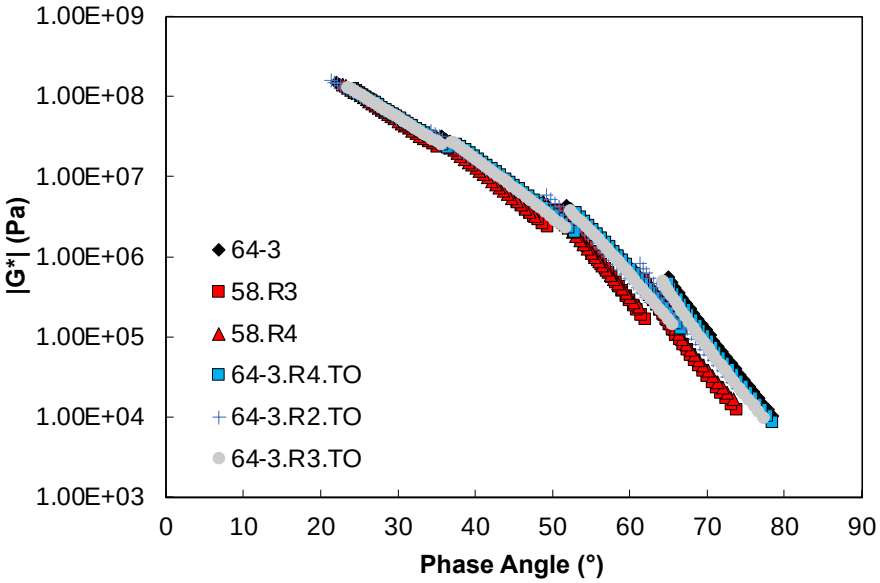

Figure 56. VDOT 64-3 TO blends black space graph

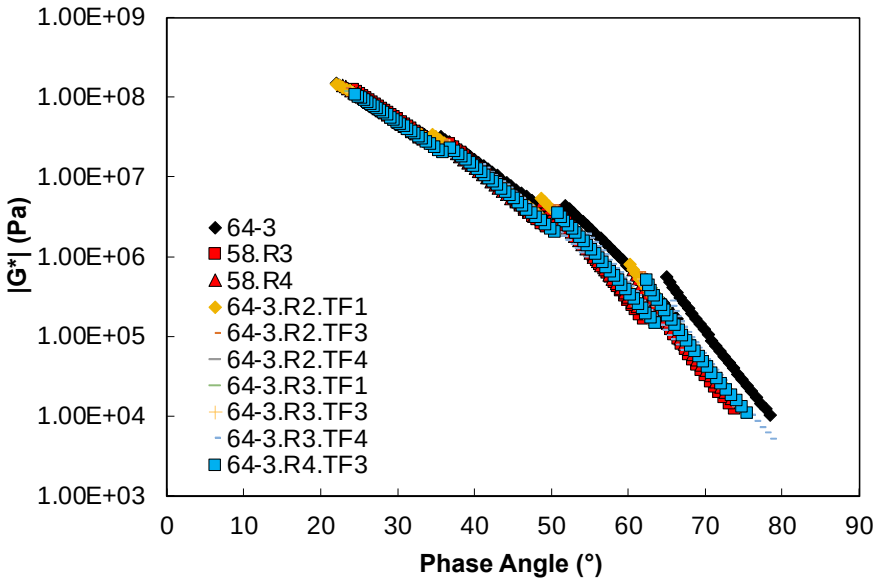

Figure 57. VDOT 64-3 TF blends black space graph

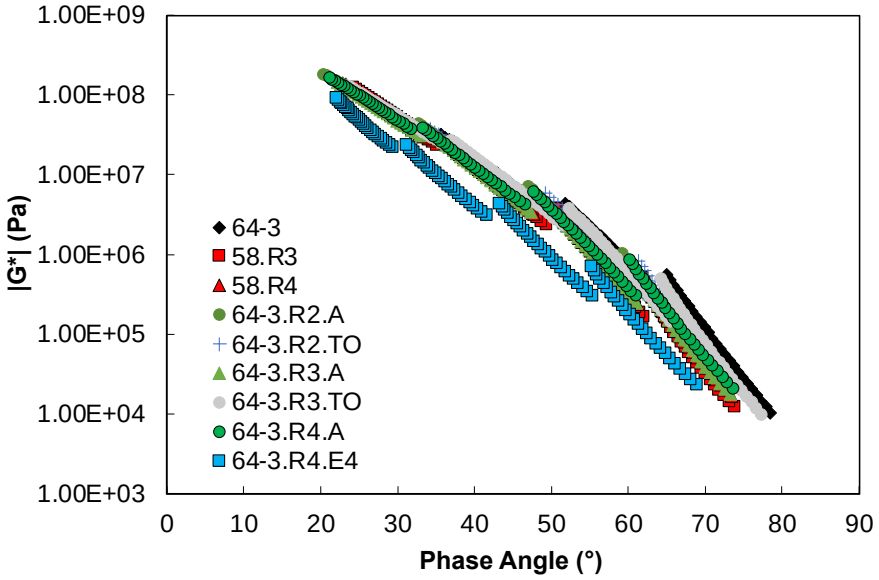

Figure 58. VDOT 64-3 TO and A blends black space graph